MONTHLY WEATHER REVIEW

A NOTE ON FREEZING NUCLEI ANOMALIES

DWIGHT B. KLINE AND GLENN W. BRIER

U. S. Weather Bureau, Washington, D. C.

[Manuscript Received May 7, 1958; Revised July 29, 1958]

ABSTRACT

Daily freezing nuclei observations taken in the Washington, D. C., area during the first 3 months of 1958 showed large fluctuations in time relative to probable observational uncertainties. Anomalous values were detected around the January dates predicted by the meteoritic dust hypothesis. However, subsequent "peaks" do not appear to be associable with any known major meteor streams. A composite analysis of the dates of dominant peaks in similar observations at a number of other locations since 1954 tends to confirm the existence of singularities in January which are statistically highly significant.

1. INTRODUCTION

Information regarding the sources, physical properties, and natural variability of freezing nuclei in the atmosphere is relatively meager. Most current observational techniques are tedious and subject to uncertainties and differences in interpretation. Few systematic or routine observations over extended periods have been attempted in the United States. The most extensive series is that summarized by Schaefer [20].

The intriguing hypothesis that significant anomalies in the freezing nuclei content of the lower atmosphere during January may be attributable to dust from meteor streams intercepted by the earth's atmosphere some 30 days earlier has been advanced by Bowen [4]. Direct physical confirmation is lacking, and both favorable and inconclusive evidence have appeared in the literature. It is generally felt that serious meteorological as well as astronomical difficulties exist and remain to be resolved.

The purpose of this note is to present a preliminary summary of the results of a series of nuclei observations taken during January, February, and March 1958, near Washington, D. C. (about 8 miles west of the metropolitan area). Also, the question is considered whether these observations and similar ones made elsewhere over the past few years during the month of January lend any support to the hypothesis that there is some common factor producing worldwide variations in freezing nuclei.

2. OBSERVATIONAL PROCEDURES

This program was undertaken by the Weather Bureau in cooperation with the Radiophysics Division of the Australian Commonwealth Scientific and Industrial Research Organization, which kindly provided observational equipment of the type described by Warner [24]. Practical considerations required using the 10-liter cold box as a "mixing chamber" rather than as an expansion chamber as originally intended. The procedure adopted was essentially that described by Schaefer [20]. In addition, efforts were made to prevent frost formation by coating all interior surfaces with glycerin. This precaution was found to be of crucial importance, since the occurrence of frost was observed to produce highly erratic readings, sometimes increasing the number of observed ice crystals by 1 or 2 orders of magnitude over a 2-minute observational period. The refrigeration system was thermostatically regulated to maintain a wall temperature of about $-21°$ C. In practice, however, the wall temperature fluctuated between $-19°$ and $-23°$ C., due to the cycling of the compressor. Since there were measurement uncertainties including sampling volume, moisture control, temperature variations, time-dependency of nucleation effects, and other observational factors, it was felt essential to introduce some degree of replication in the observational program. The usual procedure was to observe a series of six samples at each observational period which,
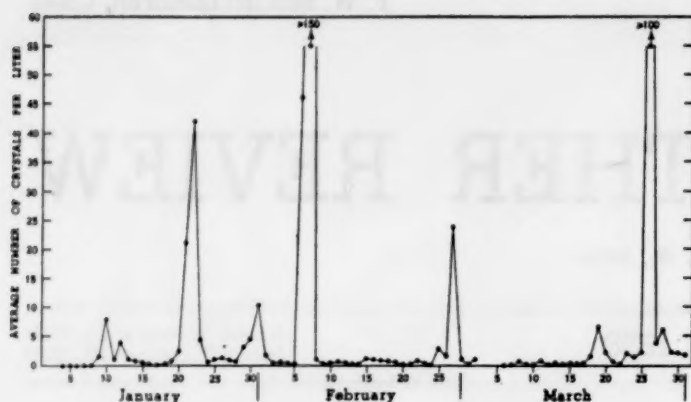
FIGURE 1.—Daily observations of ice nuclei at a mean temperature of −21° C., Washington, D. C., January 4–March 31, 1958.

during the first 2 months, was both morning and evening. The March program was confined mainly to evening observations. Ordinarily one series of six samples was examined. On a number of occasions, however, several additional series were obtained during periods of interest in order to evaluate the consistency of the observations. Data for March 3 and 4 are missing due to equipment malfunction.

3. ANALYSIS OF WASHINGTON, D. C., DATA

The results of observations near Washington, D. C., are summarized in graphical form in figure 1. The plotted values are the arithmetic averages of all individual samples taken each day, omitting, however, the relatively few observations when frost was detected inside the cold box. Since no absolute measuring technique exists in this field, a quantitative interpretation of the observed numbers of nuclei seems impracticable at this stage. However, the relative variations obtained appear to be of interest since they exhibit a reasonable degree of internal consistency.

One or more series of observations during a particular observation period will be defined as a "set" in the following discussion of the statistical analysis of the data. During the 87-day period from January 4 through March 31, a total of 146 sets was obtained, 93 in the evening and 52 in the morning. In all, a total of 1,074 individual samples was observed. The values ranged between 0 and more than 400 per liter. Since these numbers were far from normally distributed the Freeman-Tukey [12] transformation

$$T=\sqrt{x}+\sqrt{x+1}$$

was made on the data where x was the observed nuclei count. The statistical analysis was then performed on the variable T.

An analysis of variance indicated that, for the data as a whole, there was no consistent difference between the morning and the evening observations. The variation between series within a set was usually quite small but was statistically significant due to the contribution of a few periods such as January 29–30, February 6–7, and February 27 when the counts were fairly high. When average counts are high or increasing rapidly, this behavior might be expected from statistical sampling considerations. Physically, it probably indicates that the air is not completely mixed by turbulent diffusion and that the distribution of nuclei in the free air is not uniform. In addition, it appears that these variations are due to sampling different parcels of air and not a result of appreciable errors in counting.

The variation of mean nuclei counts between sets of observations was very large and statistically highly significant. Table 1 shows the analysis of variance of the 1,074 samples. The variance between sets is 20 times the "experimental error," based on the variability between samples within the sets. To be significant at the 1 percent level a variance ratio F of only 1.43 would be required as compared with the observed F=20.1. Clearly, these variations of nuclei counts with time represent some real physical phenomenon, regardless of the explanation.

Efforts to relate these freezing nuclei anomalies to synoptic weather features or local sources of contamination have so far proved inconclusive. All of the "peaks" occurred during high humidity conditions and situations in which the air flow was such as to indicate at least a limited marine trajectory during the preceding 24-hour period. Nevertheless, low values also occurred during similar situations, and the interpretation of the results is complicated by uncertainties regarding "washout" mechanisms due to precipitation, and possibly other factors such as strength and duration of air movement over the ocean and resulting salt particles produced from the ocean surface. In this connection evidence has been reported by Birstein and Anderson [3] that sea salt may act as a freezing nucleus at a threshold temperature of about −15° C. There were no instances of anomalous freezing nuclei concentrations active in the observed temperature range in airmasses with a definite continental trajectory. Considered alone, these results therefore cannot be dissociated from terrestrial influences.

The January anomalies in the Washington, D. C., data appear to be of interest in that they occurred on or near the dates predicted by the meteoritic dust hypothesis, that is, around January 12, 22, and 31 (or February 1). On the other hand, the subsequent "peaks" during February and March, two of which were quite pronounced, do not appear to be associable with any well-recognized meteor streams reported in the literature. It should be pointed out, however, that this period is not devoid of meteoritic activity, and that improved observational techniques in this field may eventually reveal the presence of meteor showers.

TABLE 1.—*Analysis of variance of nuclei counts (transformed data)*

Source of variance	Degrees freedom	Mean square	F
Between sets	144	6,703	20.1
Within sets, "error"	929	334	
Total	1,073		

4. STATISTICAL ANALYSIS OF SUPPLEMENTARY DATA

In view of the difficulties of interpreting the variations in a single series of nuclei observations, and the implications if corresponding anomalies occur elsewhere at widely scattered locations, it is appropriate to examine all available data bearing on the point. In following up his meteoritic dust hypothesis, Bowen has encouraged a number of groups to obtain ice nuclei measurements during the month of January and the first few days of February since 1954. Comparatively few observations exist for other months.

A number of pertinent observations have been made, some by aircraft and some at the surface. Table 2 presents a summary of January observations known to the authors at this date which were available in conveniently usable form. The dates shown as dominant peaks in the table represent the day of the month in which the nuclei counts were highest. In cases where the original data were reported in terms of the threshold temperature at which nuclei were detected, the day on which the warmest temperature was observed was selected. In all cases, however, the peaks listed as dominant were very pronounced with the actual values departing by several standard deviations above the background "noise" level for the month. The other peaks listed were less pronounced, on the average, than the dominant peaks and were determined by selecting those dates on which the values were higher than the adjacent days and above the monthly average. Although in a few cases the selection
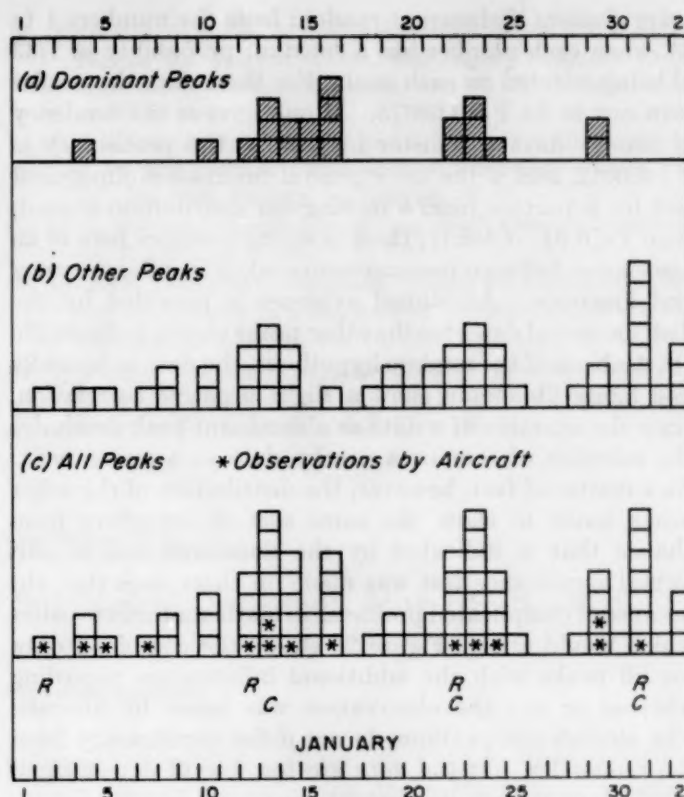

FIGURE 2.—Dates of high ice nuclei counts, January 1954–1958 and dates of rainfall singularities (R) reported by Bowen [7] and cirrus cloud singularities (C) reported by Bigg [2].

TABLE 2.—*Dates of high freezing nuclei counts, January 1954–58*

Year	Location	Reference	Day of month		Remarks
			Dominant peak	Other peaks	
1954	Sydney, Australia	21	22	4, 12, 14, 31	Aircraft.
1955	Sydney, Australia	21	23	13, 29	Aircraft.
	Tucson, Ariz.	21, 16	16	7, 24	Aircraft—7 and 24 somewhat questionable.
	Panama	11, 6	13	18, 31	
	Haleakala, T. H.	5, 6	29	10, 23	
1956	Sydney, Australia	5			No peaks.
	Pretoria, South Africa	17	29	2, 13	Aircraft.
	Southern England	19	4		Aircraft—sampling did not include all days.
	Western Australia	1	23	13, 21, Feb. 1	
	Palo Alto, Calif.	8	13	21	
1957	Swakopmund, South West Africa.	10	10	12, 24	
	West Palm Beach, Fla.	15	16	13	
	Palo Alto, Calif.	15	16	23, 31	
	Australia	6	15	22, 25, Feb. 2	Data used were mean daily values from 6 stations.
	Frankfurt/Main, Germany.	14	23	8, 14, 30	
1958	San Juan, P. R.		24	14, 19	
	Washington, D. C.		22	10, 12, 31	
	West Palm Beach, Fla.			28, Feb. 2	Blowing dust at critical dates.
	Mauna Loa Obser., T. H.			12, 24, 29	Equipment difficulties—missing data during month.
	Palo Alto, Calif.	9	14	8, 19, 24	Sampling did not include all days.
	Kleiner Feldberg, Germany.	13	16	23, 29	
	Pretoria, South Africa	18	14	23, 31	
	Swakopmund, South West Africa.	18	12	16, Feb. 2	
	Australia	6	15	5, 22, 31	Data used were mean daily values from 6 stations.

of these minor peaks might be questioned, it seemed desirable to include them in the list for the information of the reader rather than to take the chance of introducing a bias by arbitrarily omitting them.

Figure 2 gives a graphical presentation of these data. Figure 2a shows how the dominant peaks were distributed during the first 33 days of the year. The 22 dominant peaks are distributed among 11 dates and 5 groups or clusters. It would be possible for the 22 peaks to be distributed among as many as 22 dates instead of 11, and it would be possible for the 11 dates observed to be separated into as many as 11 groups instead of the 5 clusters observed. If these 22 peaks are not related to any common physical phenomenon, one would expect them to be distributed randomly throughout the period more or less uniformly. On the other hand, an alternative hypothesis is suggested by the singularity concept to the effect that the 22 peaks should tend to cluster around a relatively few dates or periods during the month. A relatively simple statistical test can then be made by asking whether the dates of the 22 peaks observed show a significant departure from a random selection of dates, each date between January 1 and February 2 being equally likely. This question can be answered making use of the work of Stevens [22] and Swed and Eisenhart [23]. This is equivalent to determining the probability that in 22 trials, 11 or fewer numbers will be selected and grouped in 5 or

fewer clusters if chosen at random from the numbers 1 to 33, when each number has a constant probability of 1/33 of being selected on each trial. For these data the results turn out to be $P = 0.00075$. If one ignores the tendency of the 11 days to cluster in groups, the probability is $P = 0.0012$, and if the more general Smirnoff-Kolmogoroff test for departure from a rectangular distribution is used, then $P < 0.01$. Clearly, there is strong evidence here of an association between measurements taken in different years and locations. Additional evidence is provided by the distribution of dates for the other peaks shown in figure 2b. On the basis of the random hypothesis, the data in figure 2a and figure 2b should show a slight negative correlation, since the selection of a date as a dominant peak precludes the selection of that or a nearby date as a minor peak. As a matter of fact, however, the distribution of the other peaks tends to show the same sort of departure from chance that is indicated by the dominant peaks. No formal significance test was made on these data (fig. 2b) because of complicated problems in mathematical statistics which would arise. Figure 2c shows the combined data for all peaks with the additional information regarding whether or not the observation was made by aircraft. The aircraft observations do not differ significantly from the remainder, but the data are too few to detect small effects even though they might exist.

At the bottom of figure 2 are shown the dates, R, of worldwide rainfall singularity reported by Bowen [7]. The letter C indicates the dates of cirrus cloud singularities reported by Bigg [2]. They are presented here as a matter of interest and information without comment or interpretation since they are discussed in the referenced papers.

5. CONCLUDING REMARKS

Although there is considerable uncertainty at this stage regarding the physical and quantitative significance of available data, there seems little doubt that the variability of freezing nuclei is a real phenomenon. Taking the data at face value, there is good statistical evidence to support the hypothesis that there is a temporal association in anomalous counts at widely separated locations over the earth during the month of January. Whether or not these singularities are attributable to meteoritic debris is a question that cannot be resolved at this time. Close inspection of available data indicates that many of the anomalies appear to be relatively sudden and shortlived. It is difficult to reconcile this with existing meteorological concepts of dispersal and diffusion mechanisms in the atmosphere. It therefore seems reasonable to consider other possible mechanisms that could contribute to these variations. One might speculate on the possible effect of solar variations. Although the association may be entirely coincidental, it is of interest to note that the major peaks of February 7 and March 26 in the Washington, D. C., data corresponded with the occurrence of unusual bursts of solar radio noise in the 10,000-mc. band. In any case, the empirical evidence now accumulated suggests that

efforts are warranted in obtaining further observations on the variations and physical nature of freezing nuclei and their meteorological (and geophysical) significance.

ACKNOWLEDGMENTS

REFERENCES

1. E. K. Bigg, "Counts of Atmospheric Freezing Nuclei at Carnarvon, Western Australia, January 1956," *Australian Journal of Physics*, vol. 9, No. 4, 1956, pp. 561–565.
2. E. K. Bigg, "January Anomalies in Cirriform Cloud Coverage over Australia," *Journal of Meteorology*, vol. 14, No. 6, Dec. 1957, pp. 524–526.
3. Seymour J. Birstein and Charles E. Anderson, "Preliminary Report on Sea Salt as an Ice Nucleus," *Journal of Meteorology*, vol. 10, No. 2, April 1953, p. 166.
4. E. G. Bowen, "The Influence of Meteoritic Dust on Rainfall," *Australian Journal of Physics*, vol. 6, No. 4, 1953, pp. 490–497.
5. E. G. Bowen, "January Freezing Nucleus Measurements," *Australian Journal of Physics*, vol. 9, No. 4, 1956, pp. 552–555.
6. E. G. Bowen, private communication, 1958. (1957 data for Australia given in this communication have recently been published by E. G. Bowen in "Freezing Nucleus Measurements in January 1957", *Australian Journal of Physics*, vol. 11, No. 3, Sept. 1958, pp. 452–455.)
7. E. G. Bowen, "The Relation Between Rainfall and Meteor Showers," *Journal of Meteorology*, vol. 13, No. 2, April 1956, pp. 142–151.
8. R. N. Bracewell, "Counts of Atmospheric Freezing Nuclei at Palo Alto, California, January 1956," *Australian Journal of Physics*, vol. 9, No. 4, 1956, pp. 566–568.
9. R. N. Bracewell, private communication, 1958.
10. A. E. Carte and S. E. Mossop, "Daily Counts of Atmospheric Ice-Forming Nuclei near Swakopmund, South West Africa, during Summer 1956–57," *Geofisica Pura e Applicata*, vol. 38, 1957/III, pp. 208–214.
11. B. M. Cwilong, "Abnormal Freezing Nuclei in the Atmosphere," *Nature*, vol. 176, No. 4472, July 16, 1955, pp. 129–130.
12. Murray F. Freeman and John W. Tukey, "Transformations Related to the Angular and the Square Root," *Annals of Mathematical Statistics*, vol. 21, 1950, pp. 607–611.
13. H.-W. Georgii, private communication, 1958.
14. H.-W. Georgii, "Relations between Ice Nuclei and Particles of Atmospheric Aerosols," Technical Note, Contract AF 61(514)–927, Johann Wolfgang Goethe Universität, Institut für Meteorologie und Geophysik, Frankfurt/Main, May 1957.

15. K. J. Heffernan, "A Preliminary Report to the U. S. Weather Bureau on Natural Freezing Nuclei Measurements at West Palm Beach, Florida, 1956–1957" (Manuscript, USWB Library).

16. A. R. Kassander, L. L. Sims, and James E. McDonald, "Observations of Freezing Nuclei over the Southwestern U. S.," *Scientific Report No. 3*, University of Arizona, Institute of Atmospheric Physics, November 1, 1956. 18 pp.

17. S. C. Mossop, A. E. Carte, and K. J. Heffernan, "Counts of Atmospheric Freezing Nuclei at Pretoria, January 1956," *Australian Journal of Physics*, vol. 9, No. 4, 1956, pp. 556–560.

18. S. C. Mossop, private communication, 1958.

19. R. J. Murgatroyd and M. P. Garrod, "Some Recent Airborne Measurements of Freezing Nuclei Over Southern England," *Quarterly Journal of the Royal Meteorological Society*, vol. 83, No. 358, October 1957, pp. 528–533.

20. Vincent J. Schaefer, "The Concentration of Ice Nuclei in Air Passing the Summit of Mt. Washington," *Bulletin of the American Meteorological Society*, vol. 35, No. 7, Sept. 1954, pp. 310–314.

21. E. J. Smith, A. R. Kassander, and S. Twomey, "Measurements of Natural Freezing Nuclei at High Altitudes," *Nature*, vol. 177, No. 4498, January 14, 1956, pp. 82–83.

22. W. L. Stevens, "Significance of Grouping," *Annals of Eugenics*, vol. 7, 1937, pp. 57–69.

23. Frieda S. Swed and C. Eisenhart, "Tables for Testing Randomness of Grouping in a Sequence of Alternatives," *Annals of Mathematical Statistics*, vol. 14, 1943, pp. 66–87.

24. J. Warner, "An Instrument for the Measurement of Freezing Nucleus Concentration," *Bulletin de L'Observatoire du Puy de Dome*, No. 2, April/June 1957, pp. 33–46.

CORRESPONDENCE

Comments on "Some Interesting Aspects of a Subtropical Depression, May 18–28, 1958"

EUGENE W. HOOVER

District Forecast Office, U. S. Weather Bureau, Washington, D. C.
October 1, 1958

In a recent article Clark and French [1] referred to forecast rules used at the District Forecast Office at Washington to forecast the movement of both tropical and extratropical cyclones. They briefly explained these rules as follows (see second column, p. 191, of their article): "When 12-hour pressure *rises* are in the path of a storm the Low will tend to turn to the left. Alternatively, when 12-hour pressure *falls* are in the path, the Low will tend
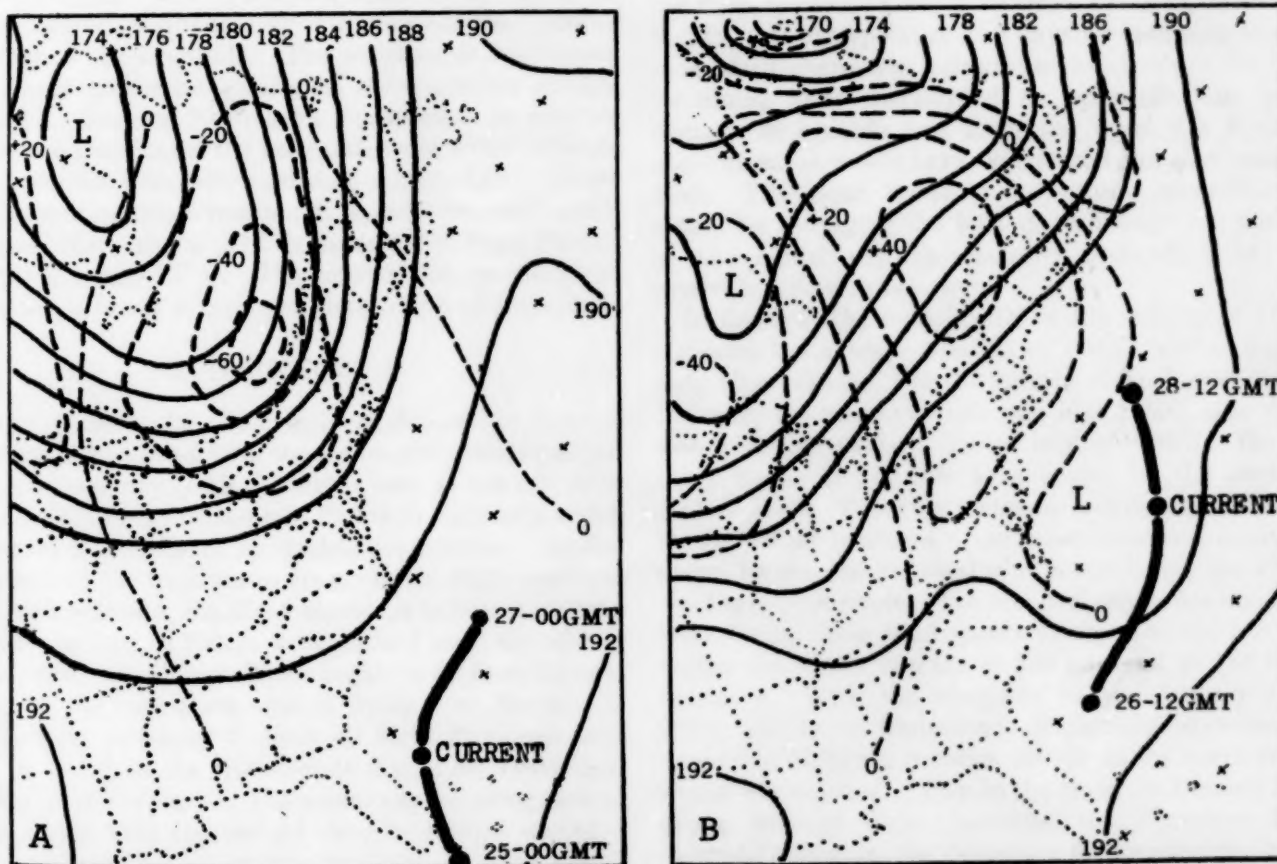

FIGURE 1.—500-mb. contours (solid) in hundreds of feet, and their 24-hour height changes (dashed) in tens of feet for (A) 0000 GMT, May 26, and (B) 0000 GMT May 27, 1958. Track of the subtropical depression is shown on each chart for the 24 hours before and after map time.

to run to the right." Actually these rules apply to 24-hour, 500-mb. height rises and falls and not to 12-hour surface pressure changes as stated in their article.

The rules they were discussing are stated in an unpublished manuscript by this writer [2]. These rules for forecasting the movement of low pressure centers are: When 24-hour height rises at 500-mb. are in the path of a Low, it will tend to turn to the left of the indicated steering. Alternatively, when 24-hour height falls are in the path of the Low, it will temporarily turn to the right of the indicated steering.

Surface pressure changes for 12-hour periods are plotted at the Washington District Forecast Office and used in many ways. To take the latest information into account, surface pressure changes are sometimes used to estimate 500-mb. height changes. The indicated thickness advection between sea level and the 500-mb. level must be subtracted from surface pressure changes to estimate height change at 500 mb.

The error in the first forecast issued by the District Forecast Office at 0315 EST, May 26, is attributed not to a failure of the rules but to some erroneous calculations in estimating changes at the 500-mb. level from late surface and thickness advection indications. The 500-mb. chart for 0000 GMT, May 26, (fig. 1A) indicates the Low should turn northeastward.

The 500-mb. charts with the contours and 24-hour, 500-mb. height changes for 0000 GMT, May 26, and 1200 GMT, May 27, are shown in figure 1. The reader might like to compare the observed movement of the Low, shown by the tracks in figure 1, with that suggested by the rules discussed above and illustrated in figure 12, page 196, of Clark and French's article. The caption of this figure should read: "Forecast rule using 24-hour, 500-mb. height changes."

The radius of curvature of the track in the upper left side of their illustration should be less than in the upper right side. The height changes should not be used independently of the steering indicated by contours. The deflection or acceleration of the low center depends upon the height changes and their relationship to the contours.

REFERENCES

1. J. R. Clark and W. O. French, "Some Interesting Aspects of a Subtropical Depression May 18–28, 1958" *Monthly Weather Review*, vol. 86, No. 5, May 1958, pp. 186–196.
2. E. W. Hoover, Devices for Forecasting the Movement of Hurricanes, U. S. Weather Bureau, Washington, D. C., Sept. 1956. (Unpublished manuscript.)

AN ANALYSIS OF ROUTINE 300-MB. TRANSOSONDE FLIGHTS FROM JAPAN[1]

J. K. ANGELL

U. S. Weather Bureau, Washington, D. C.

ABSTRACT

Routine Navy-sponsored 300-mb. transosonde flights from Japan for the months September 1957–February 1958 are analyzed. Statistics on the wind velocity, acceleration, and power spectra for the flights are indicated. With the aid of radiosonde data, the mean vertical motions and mean horizontal divergences along the flights are evaluated. Comparisons of transosonde velocities with geostrophic velocities obtained from National Weather Analysis Center maps are presented.

1. INTRODUCTION

Under the auspices of the United States Navy, routine 300-mb. transosonde flights, or constant level balloon flights, were initiated from Iwakuni, Japan, in the summer of 1957. Details concerning the transosonde system may be found in papers by Mastenbrook [1] and Mastenbrook and Anderson [2]. On these routine flights the balloons were positioned at 2-hourly intervals by Navy radio-direction-finding stations while the balloons were west of 135° W. longitude and by Federal Communications Commission radio-direction-finding stations while the balloons were east of this longitude. The positions so determined were placed on the meteorological teletypewriter circuits in Pearl Harbor and Norfolk for transmission to analysis centers and constituted the basic data from which 300-mb. wind velocities were estimated on a routine basis. More accurate and complete position data, however, were available from Navy and FCC logs made up in Pearl Harbor and Washington, D. C. The information presented in this paper is based solely upon data obtained from these logs.

2. TRAJECTORIES

Figure 1 shows, for the months of September through February, the trajectories of the flights which were tracked for at least one day. All the flights were at 300 mb. with the exception of a few 150-mb. flights in February which are shown in the figure by dashed trajectories. At the end points of the trajectories are given the flight numbers and, in parentheses, the flight durations in hours. Flight durations as long as 7 days were realized until the middle of November when the balloons began to fly over Europe. Owing to the restriction against flying over Eurasia, it then became necessary to limit all flight durations to 5 days, as noted in the transosonde flights for December, January, and February. The average speed along several of the flights that approached close to Europe exceeded

100 knots. For example, in November, flight 44 reached Ireland only 4 days after release from Japan, having traveled a distance exceeding 10,000 nautical miles.

Figure 2 gives mean 300-mb. transosonde trajectories for each of the five months September through January, and two mean trajectories for the month of February, one for the balloon flights at 300 mb. and one for the balloon flights at 150 mb. In order to keep some "memory" of the short-duration flights in the mean trajectories and to reduce the irregularity in mean trajectories resulting from the loss of flights of short duration, these short flights were extrapolated to 5 days by assuming that the mean daily changes in latitude and longitude of the flights remaining aloft represented an approximation to the changes in latitude and longitude which the flights of short duration would have experienced had they remained aloft. The mean monthly trajectories were then obtained by averaging the latitude and longitude positions of the actual and extrapolated trajectories at daily intervals following release.

In figure 2, the notation D_3 in the vicinity of Oregon indicates the average position of the December flights 3 days after release. For the months of November through February the mean monthly positions 3 days after release were over the western United States, even for the February flights at 150 mb. as indicated by the circled F_3 near El Paso. From the distances and directions between the daily mean positions, mean velocities were computed, as shown by the conventional wind barbs giving the average wind speeds in knots. For the first day following release from Japan, these wind speeds averaged about 110 knots during the winter months at 300 mb. and at 150 mb. in February. With the exception of the January trajectories, the mean transosonde trajectories traversed the west coast of North America farther to the north as midwinter was reached. Thus in the mean the October flights passed through Baja California, the November flights through California, the December flights through Oregon, and the February 300-mb. flights near the U.S.-Canadian border.
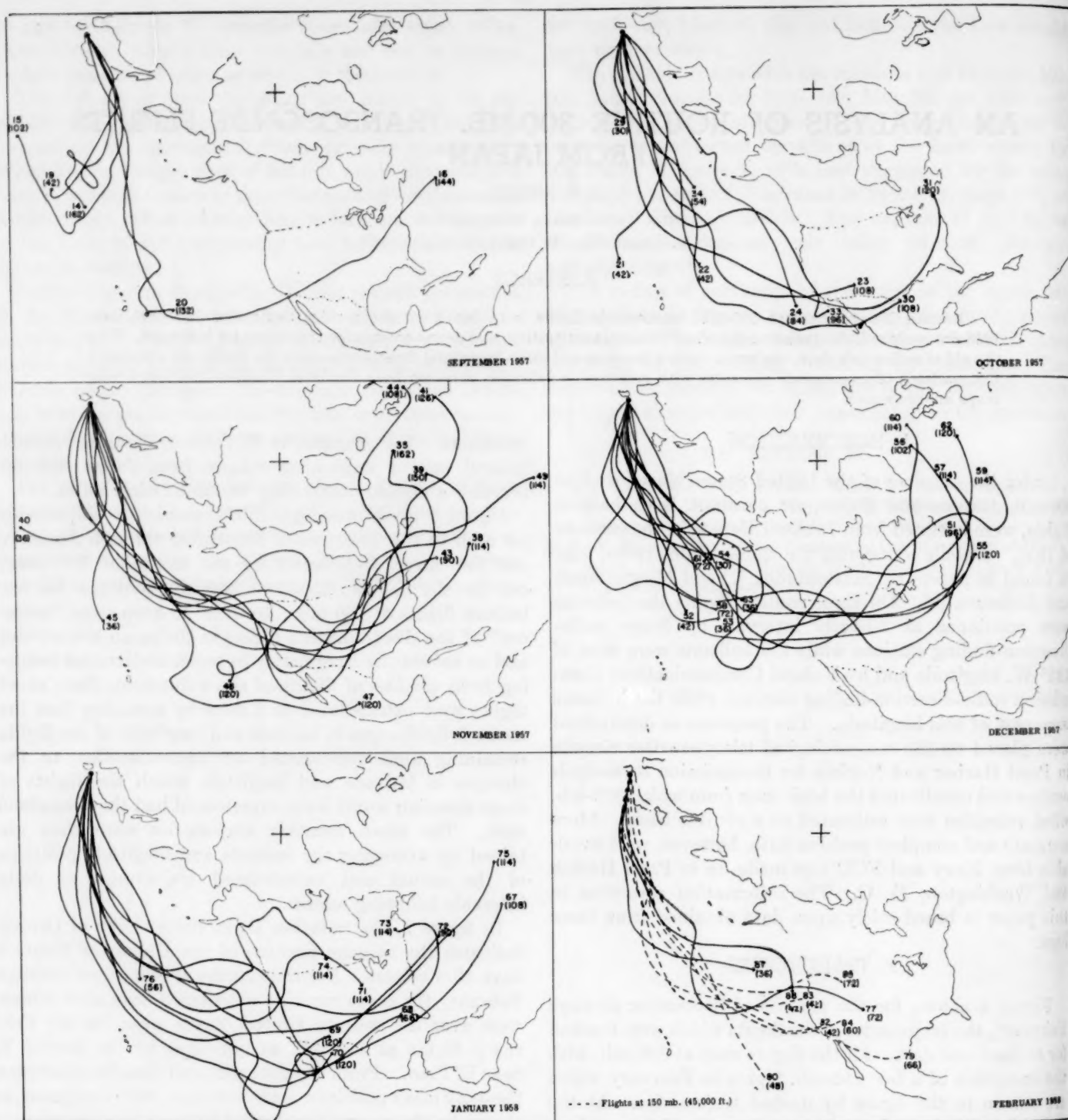
FIGURE 1.—Transosonde trajectories at 300 mb. (solid lines) and 150 mb. (dashed lines) for the months September 1957–February 1958 with the flight number and flight duration in hours (in parentheses) indicated at the end of each trajectory.

Figure 3 shows the mean trajectory for all flights during the 6-month period, determined in the manner indicated above. For all the flights the mean balloon position after 1 day was near the 180th meridian, after 3 days near the west coast of the United States, and after 5 days near the east coast of the United States. This mean trajectory remained very close to latitude 36° N. throughout, traversing the Pacific in a region where conventional upper-air data are lacking, as shown by the dots which represent the radiosonde stations in the Pacific area. The winds derived from the distances between daily positions along this mean trajectory indicate that in the mean for all 6 months the balloons moved eastward at an average speed of about 95 knots during the first day after release from Japan, whereas over the eastern Pacific and the United States the eastward movement averaged about half this value.
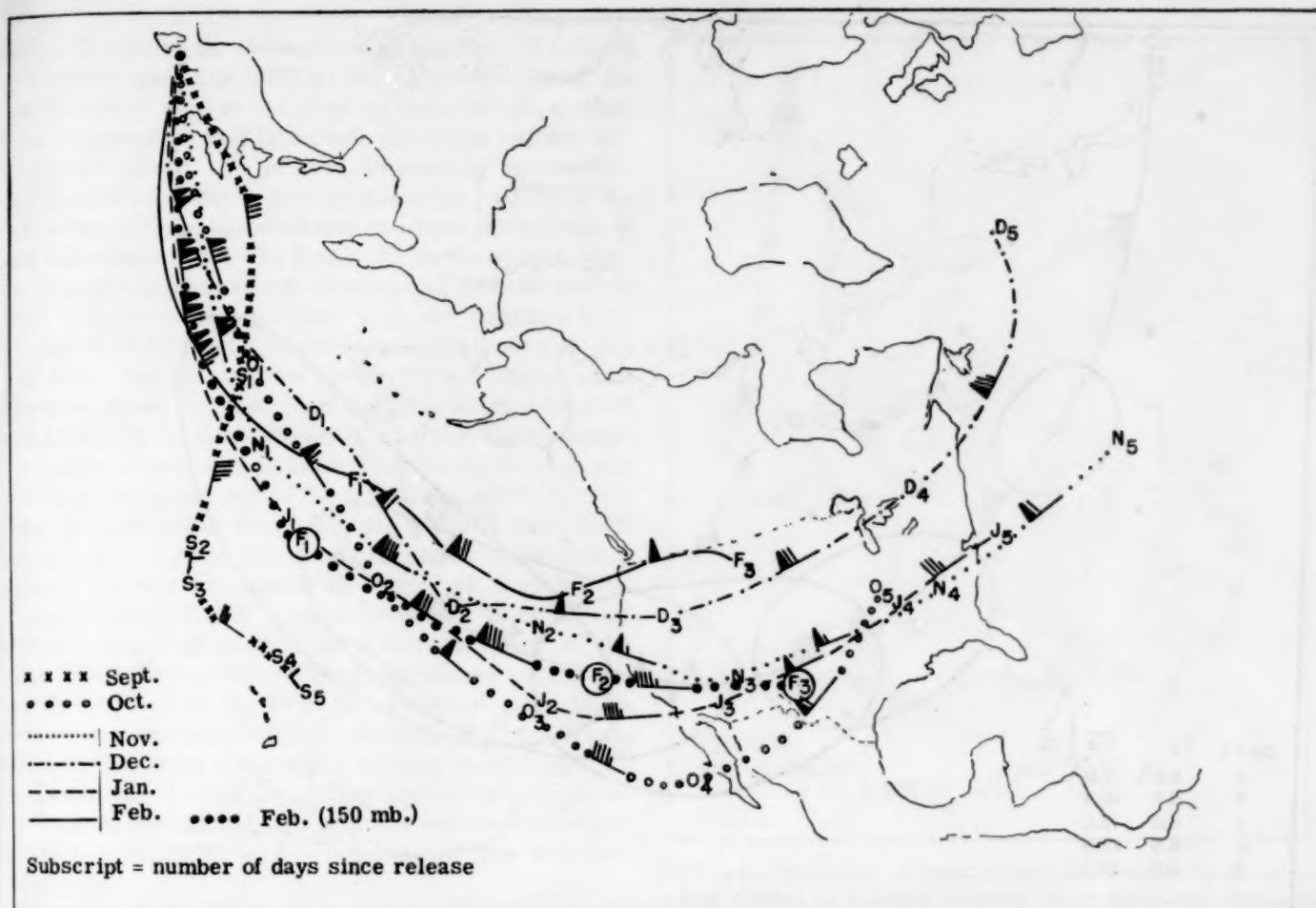
FIGURE 2.—Mean monthly transosonde trajectories for September 1957–February 1958 with the letters along the trajectories indicating the mean monthly transosonde positions at daily intervals following release (S=Sept., etc.); the numerical subscripts, the number of days since release; and the customary wind shaft and barbs, the derived 24-hour average velocities.

The ellipses centered on the daily positions along the mean trajectory represent the mean of the monthly standard deviations of position at daily intervals, obtained by finding the standard deviations of latitude and longitude positions. It is difficult to obtain reliable values for these mean monthly standard deviations of position owing to the tendency for the tracking networks to lose contact with balloons which go far south or far north—the very flights which would yield a large meridional standard deviation of position. Since the short duration trajectories had been extrapolated to 5 days by the technique described above, it seemed logical to obtain estimates of the standard deviations of position from the combination of actual and extrapolated trajectories. In the lower left-hand corner of figure 3 are given, in the left-hand sigma column, the mean standard deviations of the meridional positions, in degrees latitude, after a certain number of days, and in the right-hand column the mean standard deviations of the longitudinal positions, in degrees latitude, after a certain number of days. It may be noted that the longitudinal standard deviation increases nearly linearly with time, whereas the meridional standard deviation actually decreases slightly after 3 days. This

implies that for these flights the balloons tended to be more widely dispersed latitudinally over the west coast of North America than over the east coast of North America. However, because of the difficulty in obtaining reliable standard deviations of position from flights of varying duration, this result may not be conclusive.

3. STATISTICS ON VELOCITY AND ACCELERATION

Owing to the difficulty of obtaining accurate balloon positions over the Pacific, some smoothing was necessary to obtain reliable velocities from the transosonde data. The smoothing involved averaging three latitude and longitude positions, each 2 hours apart, and replacement of the latitude and longitude position at the middle time by the average value. This was done so as to yield an averaged position every 6 hours, as shown in figure 4 by the dots. The numbers along the trajectory in this figure give the number of days since balloon release. The 6-hour average velocity was then determined from the distance and direction between the averaged 6-hourly positions. The acceleration was determined from changes in velocities 12 hours apart.
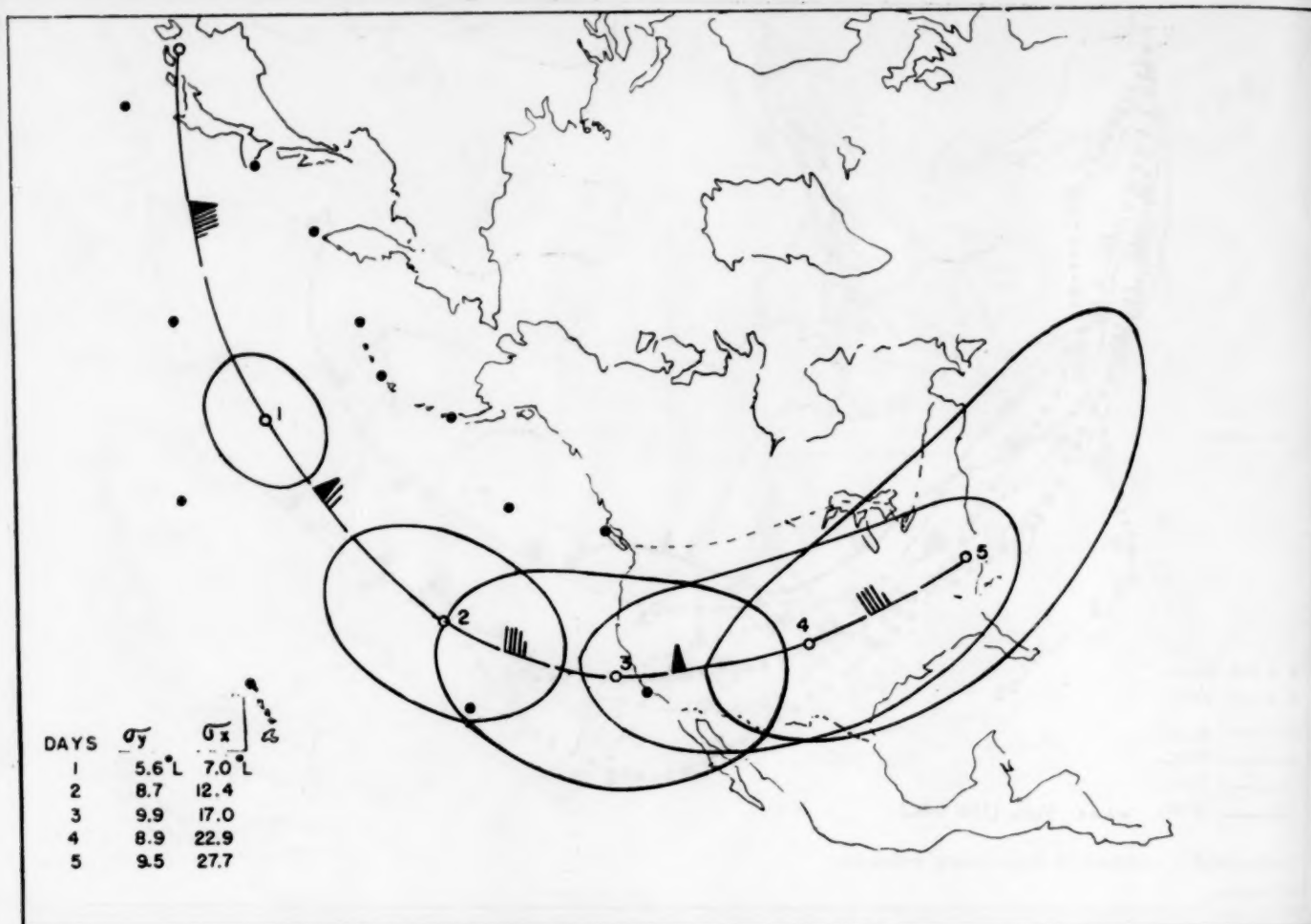
Tables 1 and 2 give some statistics on the 6-hour

FIGURE 3.—Mean transosonde trajectory, September 1957–February 1958, with the numbers along the trajectory indicating the mean transosonde position at daily intervals following release; the wind symbols, the derived 24-hour average velocities; the ellipses, the mean-monthly standard deviations of position; and the dots, the adjacent upper-air stations in the Pacific.

average velocity and 12-hour average acceleration obtained in this way. It is seen that in this quadrant during November, December, and February, more than one-third of the winds at 300-mb. exceeded 100 knots, and that in February at 150 mb. about half the winds exceeded this value. It also may be noted that the average value

for the products of the velocity components is 258 knots², a value close to that obtained by integrating around the hemisphere using synoptic data. The average correlation between the velocity components is +0.14, with only the month of January yielding a negative correlation.

In table 2 it is seen that for all months the tangential acceleration was less than the normal acceleration, in the average about 60 percent of the normal acceleration. It may also be noted that there was no strong correlation between tangential and normal acceleration, in other words, there was no obvious tendency for wind speeds to increase, say, in the troughs rather than on the crests of the trajectories. However, the positive correlation of 0.08 between tangential acceleration and meridional flow, suggests that the speed and kinetic energy of the balloons and air parcels tended to increase as they passed through the pretrough southerlies.

4. VERTICAL MOTION AND DIVERGENCE ALONG TRAJECTORIES

The constant level balloon is constrained to remain near a surface of constant height or pressure and thus gives no

TABLE 1.—*Monthly statistics of 6-hour average 300-mb. wind velocities obtained from transosonde flights for September 1957 to February 1958*

Month 1957-58	Percentage of cases in which wind speed exceeded the given value (kt.)						Average wind speed (kt.)	Average product of zonal-meridional velocity components (kt.²)	Corr. coeff. between zonal-meridional velocity components	Cases
	25	50	75	100	125	150				
Sept..........	72	47	22	9	1	1	47	33	0.03	97
Oct...........	97	72	46	19	4	1	67	98	.16	113
Nov..........	96	80	59	35	12	3	81	443	.25	197
Dec..........	97	91	65	39	9	4	87	595	.22	161
Jan...........	95	78	53	32	15	7	80	−53	−.04	168
Feb..........	100	96	72	40	28	12	107	358	.21	25
Mean........	93	77	53	30	10	4	77	258	.14	761
Feb. (150 mb.).	96	87	78	51	29	5	98	113	.15	55

direct information on the vertical air motion. As shown by Neiburger and Angell [3], an indirect indication of the vertical motion may be obtained by the adiabatic method if the temperature and lapse rate along the balloon trajectory are known. At present, to estimate the vertical motions, it is necessary to extrapolate to the position of the balloon the 300-mb. temperatures and lapse rates obtained from radiosonde data. In figure 5B we show, as a function of longitude, the average elevations of those air parcels which initially were associated with the constant level balloons at 30,000 feet. These mean elevations were derived from vertical motions obtained from temperature differences along the individual trajectories as estimated from 12-hourly National Weather Analysis Center maps. The number of evaluations utilized per 10-degree longitude sector is given at the top of the figure, and at the bottom topographic features along latitude 36° N. have been sketched in. During this 6-month period there was a tendency for the air parcels to ascend as they moved eastward toward North America, reaching their highest point near the crest of the Sierra Nevada. East of the Rocky Mountains a rather strong descending motion apparently occurred on the average. Computing the mean products between adiabatically determined vertical motions and horizontal transosonde velocity-components we find, based on 315 cases (fig. 5B), a positive correlation of 0.48 between meridional flow and vertical motion and a positive correlation of 0.17 between zonal flow and vertical motion.

Figure 5A shows the mean horizontal divergence as a function of longitude, obtained by computing the geostrophic vorticity from NAWAC maps at 12-hourly intervals along the trajectories and applying the simplified vorticity equation. During this period there are indications of horizontal convergence over and to the west of the North American continent at 300 mb., with a maximum of convergence to the east of the Rocky Mountains and a minimum of convergence just to the west of the Sierra Nevada.

5. POWER SPECTRA FOR TRANSOSONDE FLIGHTS

For each transosonde flight, the contributions of oscillations with various frequencies to the variance of the series were determined for the speed (V) and the zonal (u') and meridional (v') velocity components in the

FLIGHT 35

2200 GMT Oct. 31 - 1600 GMT Nov. 6, 1957
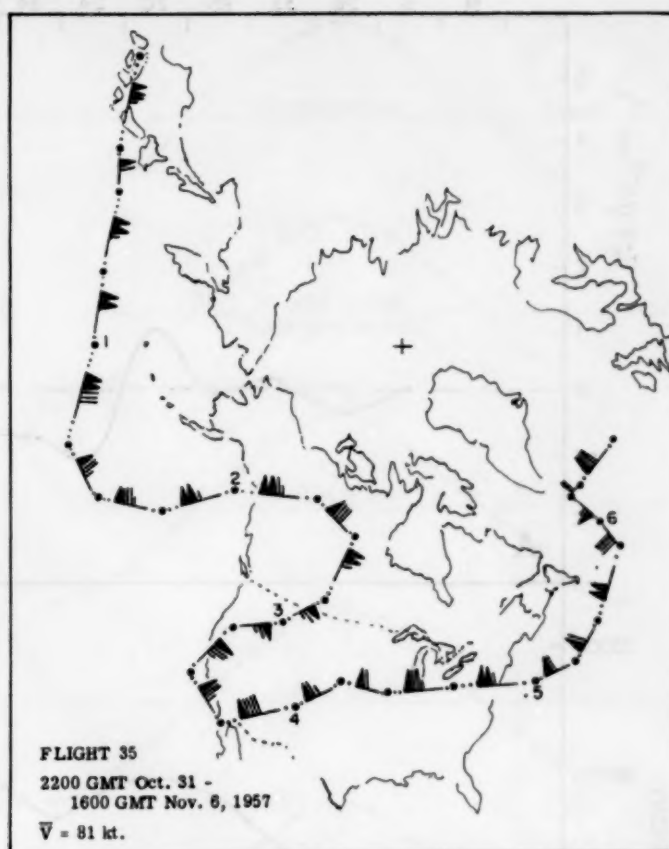
$\overline{V} = 81$ kt.

FIGURE 4.—Trajectory of Flight 35 with the 6-hour average velocities plotted at 6-hourly intervals along the path. Numbers along the trajectory indicate number of days since balloon release.

manner indicated by Tukey [4]. Also computed were the variations with frequency of the inphase-outphase relationships (cospectrum) and 90-degree phase lag relationships (quadrature spectrum) between the zonal and meridional velocity components. Figure 6 shows the average variation with frequency of these parameters for the 30 flights of at least 4 days duration. A peak in the variance as a function of frequency means that fluctuations at that frequency are more pronounced than fluctuations at adjacent frequencies, and from this it is usually assumed that there are "predominant eddies" through which the air parcels and constant level balloons are streaming. However, Gifford [3] and others believe

[3] Private communication.

TABLE 2.—*Monthly statistics of 12-hour average 300-mb. accelerations obtained from transosonde flights for September 1957–February 1958*

| Month 1957-58	Percentage of cases in which tan. acc., $\dot{V}$, and normal acc., $(V\dot{\theta})$, exceed the given value (kt./hr.)							Average tan. acc. (kt./hr.)	Average normal acc. (kt./hr.)	Corr. coeff. between tan. and normal acc.	Corr. coeff. between tan. acc. and meridional flow	Cases
	1	2	3	4	6	8	10					
September	79 (73)	39 (52)	20 (33)	12 (21)	6 (15)	2 (7)	2 (2)	2.2	2.7	0.13	0.15	87
October	72 (80)	44 (57)	15 (36)	10 (29)	2 (14)	0 (8)	0 (6)	1.8	3.1	−.15	.29	95
November	83 (92)	51 (73)	29 (52)	16 (42)	5 (26)	1 (17)	0 (11)	2.3	4.5	.15	.11	174
December	84 (89)	53 (72)	31 (50)	19 (41)	5 (29)	1 (17)	1 (11)	2.4	4.4	.04	.02	151
January	73 (87)	51 (60)	25 (46)	18 (38)	6 (18)	1 (9)	0 (5)	2.2	3.6	−.13	−.03	148
February	95 (95)	58 (85)	42 (69)	26 (63)	10 (53)	5 (26)	0 (11)	3.0	5.7	.05	−.31	19
Mean	79 (86)	49 (65)	26 (46)	16 (37)	5 (22)	1 (13)	0 (8)	2.3	3.9	.02	.08	674
Feb. (150 mb.)	84 (79)	51 (56)	23 (37)	14 (19)	0 (5)	0 (2)	0 (0)	2.2	2.5	−.18	.08	43
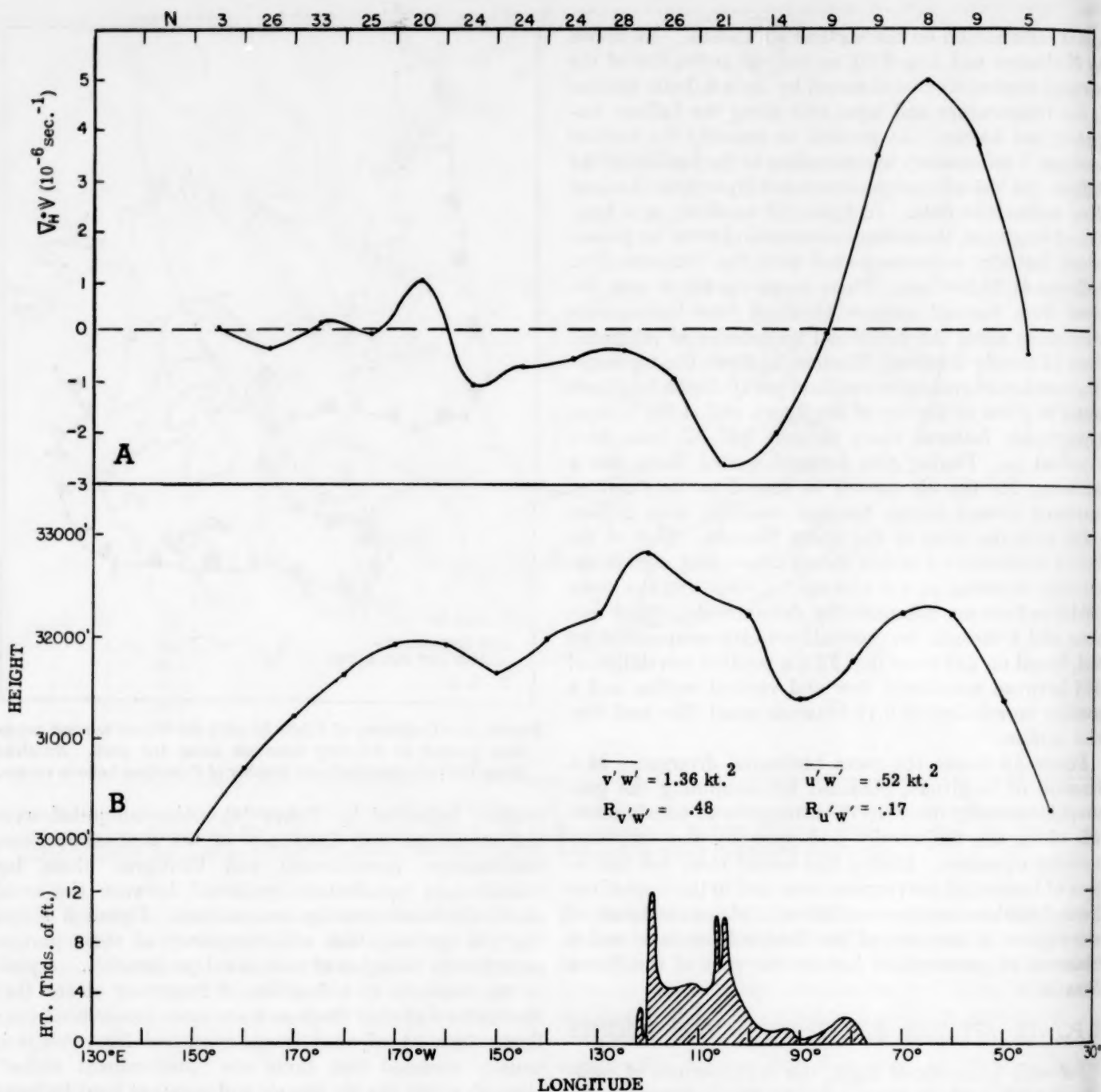
FIGURE 5.—Mean variation with longitude of horizontal divergence (A), and average elevation of air parcels initially located at the 30,000-foot positions of the balloons (B), based on transosonde flights for September 1957–February 1958. Correlation between vertical motion and zonal-meridional velocity components is inserted in B; topography along latitude 36° N. is sketched at bottom of figure; and number of evaluations per 10° longitude sector is given along the top.

that peaks in the one-dimensional spectral curves do not necessarily represent the passage of air parcels through physical cartwheel-type eddies. Bearing in mind that there is some doubt as to the interpretation and significance of one-dimensional spectral peaks, note that in figure 6A the speed and zonal components of velocity have peaks in the variance at a period near 5 days. This peak is probably the result of strong

winds over Japan followed by rather strong winds off the east coast of North America, a distance the average transosonde traverses in about 5 days. The variance of the meridional wind component, however, shows a peak at a period of somewhat more than 2 days. This peak may correspond to the average time it takes a balloon or air parcel at 300 mb. to pass through a typical long wave in the westerlies. In the upper right-hand corner of
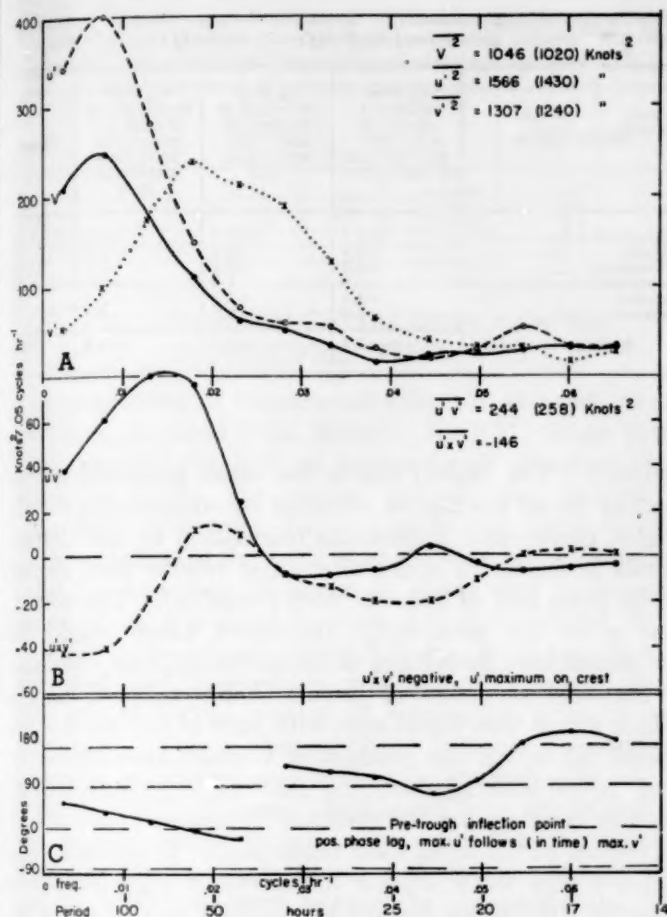
FIGURE 6.—Variation with frequency and mean values of the variance of velocity and zonal and meridional velocity components (top), the cospectrum and quadrature spectrum between zonal-meridional velocity components (middle), and the phase lag between zonal-meridional velocity components (bottom) for the 30 transosonde flights (September 1957–February 1958) of at least 4 days' duration.

FIGURE 7.—Positions of maximum zonal wind (u') shown by dots along schematic wave-shaped trajectories of different period for all transosonde flights, September 1957–February 1958. Letters indicate mean positions of u' for the individual months, and arrows the means for all months.

figure 6A are given the average variances obtained by summing the variances per unit frequency interval, and, in parentheses, the average values obtained by summing the no-lag products obtained from individual flights. For these flights the variance of the zonal wind component was slightly greater than that of the meridional component.

The middle diagram of figure 6B shows that apparently the maximum contribution to the positive correlation between zonal and meridional velocity components (solid line) occurred for fluctuations at a period near 3 days. Most fluctuations at periods shorter than 36 hours yielded a negative correlation between these components. The quadrature spectrum (dashed line) suggests that in the mean the zonal wind component was greater on the ridges (quadrature variance negative) than in the troughs for fluctuations at all periods except those near 2 days and 17 hours.

The phase lag between zonal and meridional velocity components as a function of frequency can be obtained by finding the arctangent of the ratio of the quadrature spectrum to cospectrum, as shown in figure 6C. A phase lag of zero degrees means that the two components are exactly in phase (zonal wind component at a maximum at the pretrough inflection point) while a phase lag of 90 degrees means that the zonal wind component is at a maximum on the crest of the trajectory. We see that for fluctuations at periods of 2 days or greater the zonal wind component reached a maximum at, or slightly downstream from, the pretrough inflection point, but that for shorter period oscillations it was at the maximum somewhat downstream from the trajectory crest.

In order to make this concept somewhat clearer, in figure 7 are shown schematic wave-shaped trajectories for different periods of oscillation; namely, a 120-hour period, a 60-hour period (mean long-wave period?), a 36-hour period, a diurnal period, and an inertial period. The dots along the schematic trajectories indicate the positions of maximum zonal wind (u') for the individual flights. The letters along the trajectories indicate the mean positions of u' for the various months (S=September, etc.) and

FIGURE 8.—Mean transosonde trajectory (solid line), mean geostrophic trajectory (dashed line), and mean trajectory derived from equation of motion and change in zonal wind speed with time (dotted line) for flights from September 1957–February 1958.

the arrows indicate the means for all months. It is seen that, in the case of long-period oscillations, for the great majority of flights u' reached a maximum in the pretrough southerlies, but as the periods of oscillation get smaller the positions of maximum u' become more evenly distributed or even tend to congregate in the posttrough northerlies. There is no indication of a grouping of the maximum u' values on the trajectory crest for oscillations with inertial period, as might be expected of pure inertial oscillations.

6. AGEOSTROPHIC MERIDIONAL MOTIONS DERIVED FROM TRANSOSONDE TRAJECTORIES

If the transosondes were allowed to float completely around the hemisphere, then a comparison of their mean termination latitude with the latitude of their launching point would furnish information on mean meridional ageostrophic motions. Thus, if at 30,000 feet there was a mean equatorward drift of air with a speed of 1 knot all around the hemisphere, a balloon circumnavigating the hemisphere in 10 days would find itself (assuming a steady state pressure field) 240 nautical miles south of its release point. However, since the transosondes at most circumnavigate two-thirds of the hemisphere, complications arise owing to the mean decrease of speed east of Japan (see fig. 3). Because of this decrease in speed in passing from Japan over the North American continent, ageostrophic meridional flow toward high pressure is certain to occur in this particular sector of the hemisphere. Therefore, in order to detect a hemispheric meridional drift of air, one must first subtract the above tendency. In figure 8, the solid line is the mean trajectory for all the flights, as copied from

TABLE 3.—*Mean monthly meridional ageostrophic motions determined by 3 different methods*

Month 1957–58	v_{ag} from temporal change in zonal wind and equation of motion (kt.)	v_{ag} from difference in geostrophic and actual trajectories (kt.)	v_{ag} from measurements of wind and geostrophic wind along trajectories (kt.)	Cases
September	−1.5	−10.0	−9.0	22
October	−1.9	−6.3	−1.5	45
November	−1.3	−2.7	−4.7	58
December	−.9	1.8	−1.6	82
January	−3.1	−3.0	−2.1	82
February	−5.8	1.8	5.0	11
Mean	−1.9	−2.5	−2.8	300

figure 3. The dashed line is the mean geostrophic trajectory for all the flights, obtained by constructing for all flights geostrophic trajectories originating at the transosonde positions 12 hours after their release from Japan (only front half of 300-mb. map available). The dotted line gives the geostrophic trajectory which would be estimated from knowledge of the actual trajectory and use of the zonal component of the simplified equation of motion which states that the change with time of the zonal wind speed ($\dot{u}$) equals the product of Coriolis acceleration(f) and meridional ageostrophic flow (v_{ag}). Neglected in such an equation are the effects of friction and the vertical advection of the zonal wind component. It appears from figure 8 that there is some indication of a greater ageostrophic drift of air toward the equator in this sector of the hemisphere than would be assumed from the change in zonal wind speed. The vertical advection term (from the vertical motion pattern in figure 5 and the knowledge that the zonal wind is usually increasing with height at 300 mb.) would enhance the evidence for unexplained equatorward drift to the west of the Sierra Nevada and decrease the evidence to the east, but its effect should nearly cancel out in the mean.

Because of uncertainties in the above procedure, an alternate method for estimating the deviation of meridional wind from meridional geostrophic wind was utilized. This involved simply the measurement, from 300-mb. NAWAC maps, of the meridional component of the geostrophic wind at all points where transosonde winds were available. In table 3 are shown, by month, the estimates of ageostrophic meridional wind (v_{ag}) obtained by the three techniques. The measurements of the geostrophic winds along the trajectories confirm, in the mean, the evidence for ageostrophic equatorward drift of air at 300 mb. which is not accounted for by decrease in zonal wind speed. However, it is also apparent from the table that it is the fall months that bring about this mean result; if only the winter months are used, they indicate a slight unexplained poleward ageostrophic drift of air at midlatitudes. It is hoped that the study of further transosonde flights will clarify the situation; nevertheless, it is possible that the techniques proposed here are not sufficiently reliable for the purpose at hand.

TABLE 4.—*Mean angles of indraft (i) and mean ageostrophic wind speeds (V−V_g) obtained from comparison of 300-mb. NAWAC analysis and transosonde velocities, September–November, 1957*

		Pacific Ocean area	North America
i	degrees	−2.6	−1.1
|i|	do	12.6	13.3
V−V_g	knots	9.0	5.1
|V−V_g|	do	21.4	20.3
Cases		107	61

7. COMPARISON OF TRANSOSONDE AND GEOSTROPHIC VELOCITIES

A comparison of transosonde velocities and geostrophic velocities obtained from 300-mb. NAWAC maps shows that, despite the lack of conventional upper-air data over the Pacific, the routine 300-mb. map analysis is reasonably accurate. Table 4 gives the algebraic and absolute values of the angle between wind and geostrophic wind (i) and the difference in speed and geostrophic speed $(V-V_g)$ over the Pacific and over the United States obtained from comparisons of 6-hour average transosonde velocities and geostrophic velocities. The comparison was limited to the months of September, October, and November, since in December the transosonde positions began to be plotted and utilized as analysis aids on the 300-mb. NAWAC maps. It is noted from the table that the average absolute angle between the transosonde wind and geostrophic wind over the Pacific was only 12.6 degrees, about the same as over the United States. The average algebraic value of i over the Pacific was −2.6 degrees (flow toward high pressure), in agreement with the decrease in wind speed between Japan and North America. The transosonde winds, however, averaged about 9 knots greater than the geostrophic winds over the Pacific while over North America the difference was only 5 knots, this despite the fact that on the average balloons were flying at 280 mb. over North America and at 290 mb. over the Pacific. It is believed that this 9-knot difference is significant and is due to the tendency

to linearize contour spacing over the Pacific and thus underestimate the wind strength near the jet cores where the majority of the balloons fly. The general accuracy of the Pacific analysis in regions of little data may be due to the relative smoothness of the 300-mb. flow east of Japan and the scarcity of small-scale oscillations— oscillations which could pass undetected through the sparse observational network.

8. CONCLUSION

In conclusion, these routine transosonde flights offer a wealth of material for research, and can be of considerable use in weather analysis and forecasting, particularly in the forecasting of jet-stream conditions for high-flying aircraft. However, beginning in September 1958, the transosonde flights will take place at 150 mb., forced to this higher elevation by commercial jet aircraft. It remains to be seen whether transosonde observations at this new level are of the same utility as the flights at 300 mb.

ACKNOWLEDGMENT

REFERENCES

1. H. J. Mastenbrook, "Transosonde Flights for January and February 1956," Memo. Rep. 632, Naval Research Laboratory, Washington, D. C., 1956.
2. H. J. Mastenbrook and A. D. Anderson, "Evaluation of the Transosonde System, Data Report for Period April 1953 to August 1953," Memo. Rep. 240, Naval Research Laboratory, Washington, D. C., 1953.
3. M. Neiburger and J. K. Angell, "Meteorological Applications of Constant-Pressure Balloon Trajectories," *Journal of Meteorology*, vol. 13, No. 2, April 1956, pp. 166–194.
4. J. W. Tukey, "The Sampling Theory of Power Spectrum Estimates," Woods Hole Symposium, Application of Autocorrelations to Physical Problems (NAVEXOS-P-735), Office of Naval Research, Washington, D. C., 1950, pp. 47–67.

GEOGRAPHICAL FREQUENCY OF TROUGHS AND RIDGES ON MEAN 700-MB. CHARTS

WILLIAM H. KLEIN AND JAY S. WINSTON

Extended Forecast Section, U. S. Weather Bureau, Washington, D. C.

[Manuscript Received July 7, 1958; Revised July 30, 1958]

ABSTRACT

The geographical frequencies of occurrence of troughs and ridges on both 5-day and 30-day mean 700-mb. charts for the Northern Hemisphere during a long period of record are presented for individual months. Many regions of maximum and minimum frequency show a close relationship to trough and ridge positions on long-period mean, or normal 700-mb. charts. However, even a cursory inspection of these frequency charts shows that they yield considerably more information for both the practicing forecaster and the research worker than can be derived solely from normal maps. Preferred trough and ridge locations and their seasonal changes appear to be related largely to land-sea boundaries with their associated thermal influences and also to prominent orography.

1. INTRODUCTION

It is generally recognized that the major troughs and ridges of the planetary wave pattern have climatologically preferred regions of occurrence. These regions are directly or indirectly related to the geographical distribution of prominent mountain barriers as well as to thermal and frictional influences associated with land and water surfaces. The preference for these regions is so pronounced that in many areas the trough and ridge locations are clearly delineated on long-period mean, or "normal," charts of height at mid-tropospheric levels.

However, the normal chart can only begin to answer the question as to the likelihood of a trough or ridge occurring in a given geographical area, for mean heights do not uniquely define the actual frequency distribution of troughs and ridges. This distribution can be obtained only by summarizing the observed frequencies from the historical file of upper-air charts. The value of such information in supplementing long-period normal maps at the 700-mb. level has been demonstrated by one of the authors for both monthly mean [8] and daily [9] charts. Some work along these lines has also been published for daily 500-mb. charts by Austin et al. [1], Dammann [6], and Essenwanger [7].

The scope of all previous studies, however, has been limited to either a small part of the hemisphere, a short period of record, or a few months of the year. A project was therefore initiated a few years ago to extend the previous work on trough-ridge frequency to each month of the year, and also to as large a portion of the Northern Hemisphere and as long a period of record as the availability of data would permit.

The principal results of this project are presented in figures 1–48, which are grouped by months. These frequency charts are consulted regularly as climatological background information in the preparation of extended forecasts for both 5- and 30-day periods [12]. In addition, they can furnish valuable clues for the short-range forecaster, and for the theoretician in his attempts to explain the dynamics of the general circulation.

2. DERIVATION AND PRESENTATION OF DATA

The charts used in this project were 5-day mean maps (prepared twice a week) and 30-day mean maps (prepared once a month) at the 700-mb. level, obtained from the files of the Extended Forecast Section of the U. S. Weather Bureau. The starting point for the 5-day mean data was chosen as September 1946, when a reasonably complete coverage of good data for most of the hemisphere became available. To obtain as many cases as possible, 30-day mean maps were included which have been extended back to October 1932 by judicious extrapolation of surface observations in North America, the Atlantic, and the Pacific [12]. In all cases the latest date used was August 31, 1955. Thus in areas with complete and uninterrupted data coverage, such as the United States, this study is based upon 9 years of record for the 5-day means and 23 years for the 30-day means (except 22 in September). The exact period of record is indicated in the lower right-hand corner of each chart. In most other regions, however, less data were available, and the approximate number of years used in each area is given in table 1.

TABLE 1.—*Number of years used in various areas for compiling data on frequencies of mean troughs and ridges*

Area	5-day mean	30-day mean
North America	9	20–23
Atlantic and western Europe	9	19–23
Eastern Pacific	9	19–23
Western Pacific and northeastern Asia	8–9	15–20
Central and eastern Europe	7–8	8–19
North Africa	6–9	6–21
Asia (except northeast)	6–8	6–9

In general the results of this report are quite reliable in the region from the east coast of Asia eastward to the west coast of Europe and Africa. In the remainder of the Northern Hemisphere, however, the results (particularly for 30-day means) should be interpreted with caution since complete hemispheric analyses have been available only since 1949. Of course, it is always possible that secular trends or climatic fluctuations in the general circulation, as well as additional data, may modify these results at some future period.

As in previous studies [8, 13], troughs were defined as lines connecting the points of minimum latitude reached by the contours (maximum latitude in easterly flow) or, in equivalent form, as lines connecting points of minimum height along latitude circles.[1] In similar fashion, ridges were defined in terms of maximum height or latitude (minimum latitude in easterly flow). Definition in terms of axes of maximum curvature or vorticity was not attempted because of the difficulties of objective determination. Anyway, on mean maps such axes usually coincide with trough or ridge lines defined in the simple objective manner given above. Trough or ridge lines of all intensities were considered without differentiation, except that minor troughs or ridges, with both intensity (height gradient from trough to ridge along latitude circle) less than 10 feet and lateral extent less than 10° of latitude, were omitted. The positions of all other troughs and ridges on each 5- and 30-day mean map (regardless of whether in westerly or easterly flow) were recorded to the nearest 10° of longitude (except 20° at 70° N.) along each 10° latitude circle from 30° N. to 70° N. (and also 20° N. for the 30-day means). The total number of mean charts with troughs or ridges at each standard intersection (e. g., 30° N.–140° W., 30° N.–150° W., 40° N.–140° W., 40° N.–150° W., etc.) was then tabulated separately for 5- and 30-day means for all Januarys, all Februarys, etc.

Due to the difference in length of 10° longitude intervals at high and low latitudes, the frequencies were adjusted to an equivalent basis (unit of 10° longitude at 50° N.) by multiplying by the ratio of the cosine of 50° to the cosine of each latitude. The coefficients used are given in table 2. These adjusted frequencies[2] were divided by the total number of cases available during each month and then expressed as percentages.

Interpretation of the analyzed fields of trough or ridge frequencies for each month, which are given in figures 1–48, is relatively straightforward. For example, figure 1 shows the percent of time that troughs were present on 5-day mean maps within equivalent 10° arcs of longitude during the 9 Januarys of record. It does not necessarily indicate the number of different troughs that traversed

[1] The physical significance of troughs defined in this fashion is that they separate areas with southerly geostrophic flow components from areas with northerly flow. The importance of meridional flow components in relation to vertical motion and weather has been demonstrated in numerous studies by Miller and others (e. g., [11]).

[2] The adjusted frequencies may be somewhat inaccurate at latitudes where the adjusting coefficient of table 2 differs considerably from 1 in regions where the zonal gradient of trough or ridge frequency is nonlinear. A discussion of these errors has been presented elsewhere [2, 10].

TABLE 2.—*Size of unit areas in which frequencies of troughs and ridges were tabulated, and coefficients used for adjusting these frequencies to an equal-area basis*

Latitude (° N.)	Width (° long.)	Adjusting coefficient
20	10	0.68
30	10	.74
40	10	.84
50	10	1.00
60	10	1.29
70	20	.94

each area, since some troughs may have been located for several weeks within the same 10° longitude zone. Likewise figure 3 shows the percent of all 5-day periods in which ridges were located in each longitudinal zone along each latitude circle during January.

Climatological interpretation of the trough and ridge frequencies derived in this study is facilitated by comparison with trough and ridge locations on "normal," or long-period mean maps. For this reason the appropriate monthly normal 700-mb. contours [17] have been superimposed on figures 1–48 as light dotted lines. Although the normal troughs and ridges have not been explicitly delineated, they can be readily located by noting where the contours attain minimum and maximum latitudes.

General inspection of figures 1–48 at once reveals that geographical preferences are more pronounced on the part of 30-day mean troughs and ridges than in the case of their 5-day mean counterparts. This is indicated by the fact that on the 30-day mean charts areas of zero frequency are much more extensive, and centers of maximum frequency are more sharply delineated. As a result the spatial gradients of trough and ridge frequency are considerably stronger in the case of 30-day mean charts. These frequencies were therefore uniformly analyzed at intervals of 10 percent, whereas the 5-day mean frequencies were analyzed at 5 percent intervals (except 10 percent intervals for frequencies greater than 20 percent). Likewise, shading to emphasize areas of high frequency was started at 20 percent for the 30-day means, but at only 15 percent for the 5-day means.

Aside from these differences, the frequency charts for 5- and 30-day means are generally similar, despite the fact that they were derived from different periods of record. The centers of maximum and minimum frequency are usually located in the same areas on both sets of charts, although the magnitude of the extremes is larger for the 30-day means. Furthermore, the location and orientation of the axes of maximum and minimum frequency correspond closely on the two sets of charts. This lends support to the belief that the large-scale aspects of the frequency charts may be considered as generally stable and reliable features of the general circulation.

For this reason the 5- and 30-day means are discussed jointly in the following summary of the principal features of figures 1–48. For ease of presentation, however, troughs and ridges are considered separately. In the discussion to follow only the highlights are pointed out,

small-scale features are neglected, and only a few attempts at explaining the reasons for the climatological features are made. Likewise, no effort has been made to relate the trough-ridge frequencies to climatological frequencies of cyclones and anticyclones at sea level [10], although many obvious parallels could be pointed out.

3. DISCUSSION OF RESULTS

TROUGHS

From a hemispheric point of view, the outstanding feature of the charts for trough frequency is the extensive area of maximum frequency in the normal trough in eastern Canada during each month of the year. This area of high frequency extends southward to a position along or off the east coast of the United States in every month except November (also October for the 5-day troughs). However, in the United States another pronounced maximum of troughs is found over the Mississippi Valley and Plains States during many of the non-summer months. In winter the western maximum is in general agreement with calculated positions of orographically produced troughiness (e. g., Charney and Eliassen [5] and Bolin [3]), while the maximum off the east coast appears to be mainly the result of non-adiabatic heating and baroclinic instability (e. g., as suggested by Sutcliffe [16] and Smagorinsky [15]). The locations of maximum trough frequency in eastern Canada and off the east coast of the United States in summer, on the other hand, are not so readily explained, particularly in view of reversals of thermal gradients and weakening of the westerlies. It is probable that these high trough frequencies may be largely quasi-barotropic, downstream consequences of high frequencies of ridges over western Canada and the central United States in summer (to be discussed below).

Between the two trough maxima in the United States region in the cold season there is a relative minimum in trough frequency along the Appalachians or the east coastal plain. This is especially pronounced during the first 4 months of the year and could not have been readily anticipated from the normal contours alone.

The east coast of Asia, like the east coast of North America, is characterized by a trough in the normal contours and a high frequency of troughs observed on 5- and 30-day mean maps. High frequencies are most pronounced between November and April when the maximum area is located over or east of Japan. During the warmer months there is a tendency for the axis of maximum frequency to split, with one branch retreating westward to east Asia and the other appearing in the western Pacific. The latter branch merges with a center of maximum frequency in the Bering Sea, where troughs are frequent all year long, but with highest frequencies in summer.

Another preferred area for troughs throughout the year is the southeastern Pacific, just west of Lower California, where a trough in the normal contours is also present each month. This area of maximum trough frequency is confined to low latitudes during the colder months of the year, but during the warmer season it extends northward along the west coast of the United States. Maximum trough concentration in this region is observed during June, and the maximum of 57 percent in figure 21 is the highest frequency of 5-day mean troughs observed in any portion of the Northern Hemisphere during any month of the year. The quasi-permanent trough along the west coast of North America in summertime has been attributed by Wexler [18] to the marked thermal contrast between cool air over the eastern North Pacific Ocean and heated air over the western plateau.

The west coast of Africa resembles the west coast of Mexico in many respects. During each month a normal trough is present in this region, and observed trough frequency is high. Furthermore, the axis of maximum trough frequency tends to be confined to low latitudes during winter and to extend northward along the coast of Europe during summer. The greatest frequency is reached during July in the case of 30-day mean troughs (fig. 26) and August for 5-day mean troughs (fig. 29).

Another region where low-latitude troughs concentrate throughout the year is India-Burma. This is visible chiefly on the 30-day frequencies since they extend southward to 20° N. However, a definite duality exists in this maximum frequency area; from February through May the maximum is over the Burma-South China area, while from June through January it is over India-Pakistan. The extension of this trough northward across the Tibetan Plateau is notable on both 5-day and 30-day frequency charts during the summer months and is probably associated with the maximum strength of the Asiatic summer monsoon. Other areas of local trough preference during most of the year are the Black Sea and the Hawaiian Islands. The former displays a pronounced maximum frequency in summer, which tends to be on the east side of the sea.

Several areas exhibit very marked seasonal differences. A striking example is the Mediterranean, where troughs are infrequent during the summer months but abundant during the rest of the year. A similar characteristic applies to Alaska, the Gulf of Alaska, Japan, and the Near East. Likewise, in the Great Plains of the United States troughs frequently occur in the lee of the Rocky Mountains during winter and spring, but seldom in summer. The opposite is true in the northern Plateau region of the United States and in Siberia east of Lake Baikal, where troughs are frequent in summer but scarce in winter. Most of these differences can be explained on the basis of thermal reversals and seasonal variations in the latitude and strength of westerlies crossing mountain barriers.

The transition from winter to summer conditions occurs at different times in different areas. For example, the frequency of troughs declines sharply from April to May in Alaska and the Gulf of Alaska, from May to June in central portions of the United States and the Mediterranean, and from June to July over the Japanese Islands
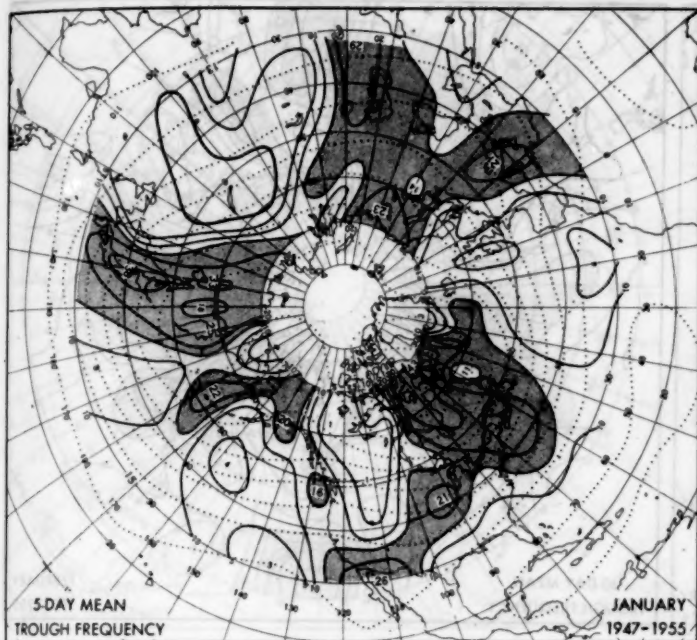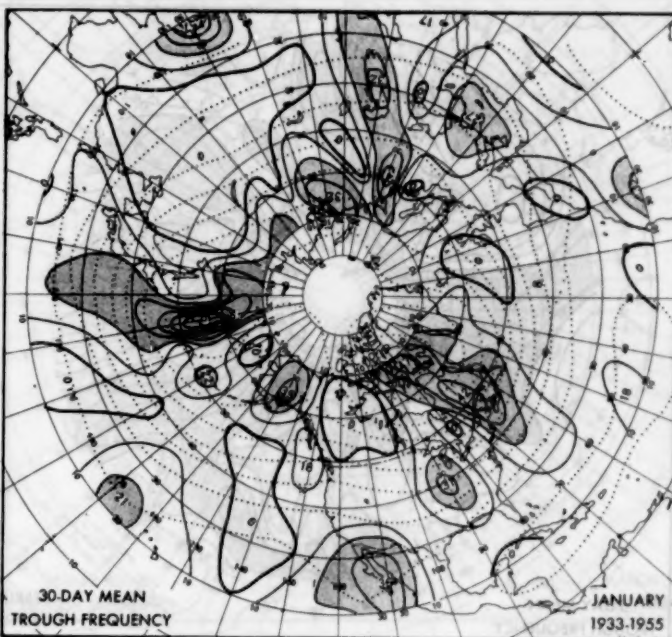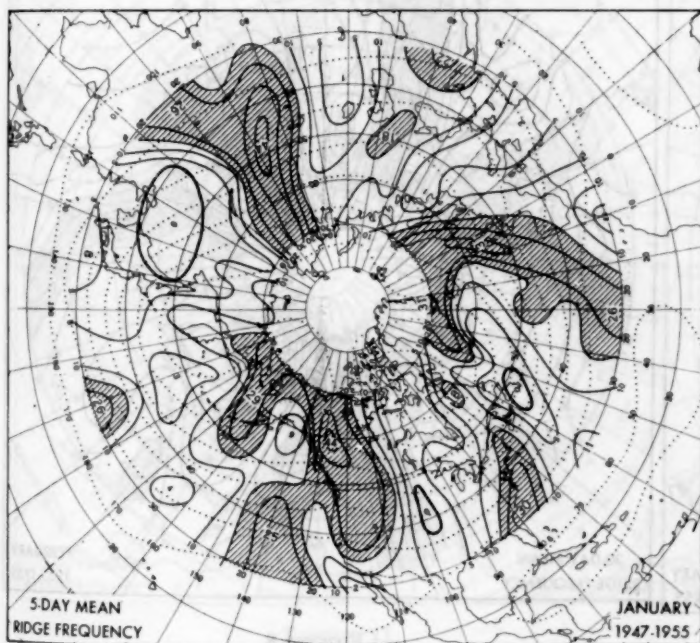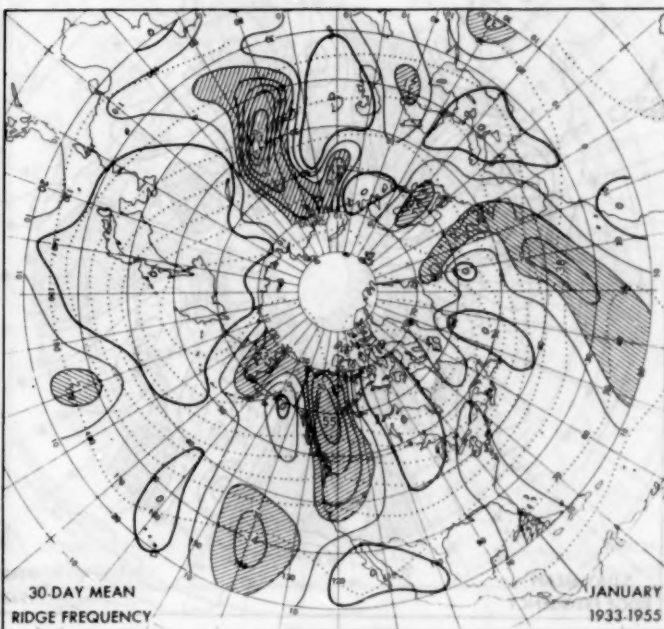
FIGURE 1.

FIGURE 2.

FIGURE 3.

FIGURE 4.

FIGURES 1–48.—Percent of time that troughs (ridges) on 5-day and 30-day mean 700-mb. charts were located within 10° longitude intervals at latitudes from 30° N. (20° N. for 30-day charts) to 70° N. for the month and period of record indicated in the lower right-hand corner of each chart and also in table 1. The data were adjusted to an equivalent basis with 10° of longitude at 50° N. as the unit by use of the coefficients listed in table 2. The lines of equal frequency are drawn at intervals of 5 percent for 5-day charts (except 10 percent for frequencies above 20 percent) and at 10-percent intervals on 30-day charts, with the zero line heavier. Areas with frequency greater than 15 percent (20 percent for 30-day charts) are shaded. Centers of maximum frequency are labeled in large numerals; centers of minimum frequency in small numerals. The unlabeled dotted lines are the normal 700-mb. contours [17] for the month, drawn at intervals of 200 ft.
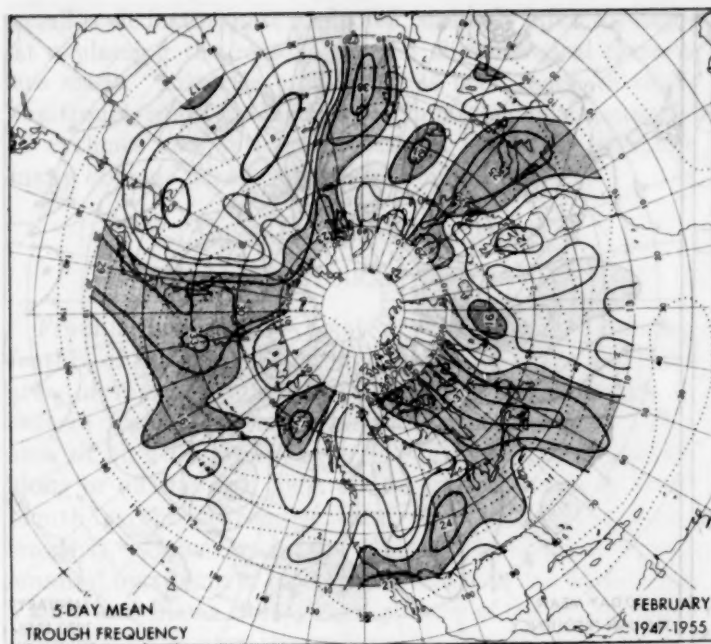
FIGURE 5.
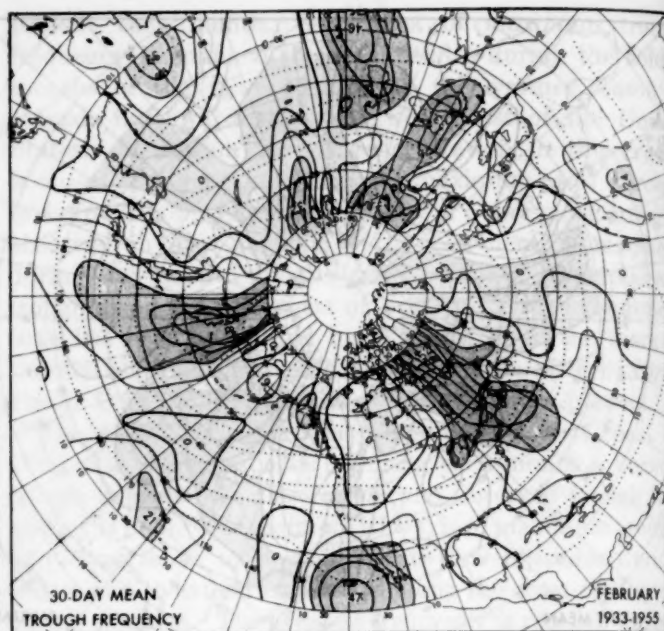
FIGURE 6.
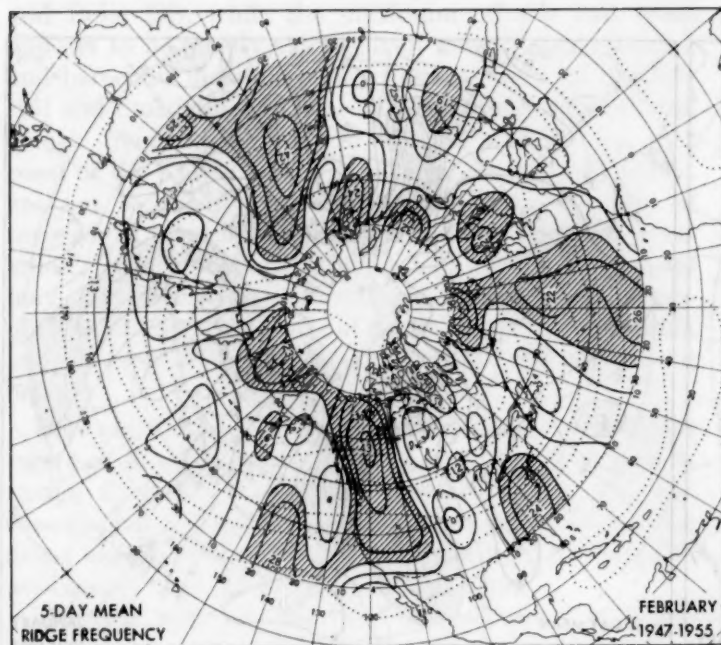
FIGURE 7.
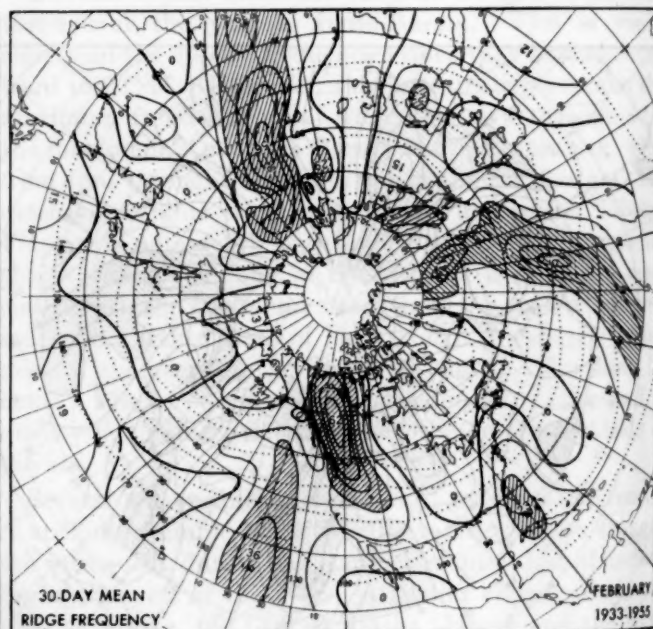
FIGURE 8.

and mid-Pacific. On the other hand, trough frequency increases markedly from April to May over the Pacific Northwest and in eastern Siberia.

The reversal from summer to winter patterns may also take place in an abrupt fashion at different times. Marked increases in trough frequency are evident from August to September over Japan, Alaska, the Gulf of Alaska, and the Mississippi Valley. Similar changes occur a month later (from September to October) in the central Mediterranean and Egypt. The opposite type of transition, from high to low trough frequency, is manifest over the northern Plateau region from August to September and

over Korea and Manchuria from September to October.

In some regions troughs are infrequent during practically all of the year. The most striking example is the area of the Canadian Divide, where frequencies reach as low as 0 or 1 percent on 23 out of the 24 charts for troughs. Other areas of rather persistent low trough frequency are the Texas gulf coast, the Greenland Plateau, and east-central portions of the Atlantic and Pacific.

In the central portion of the United States the frequency of 5-day mean troughs is somewhat greater than the frequency of 30-day mean troughs during the first 5 months of the year. This may reflect the well-known tendency
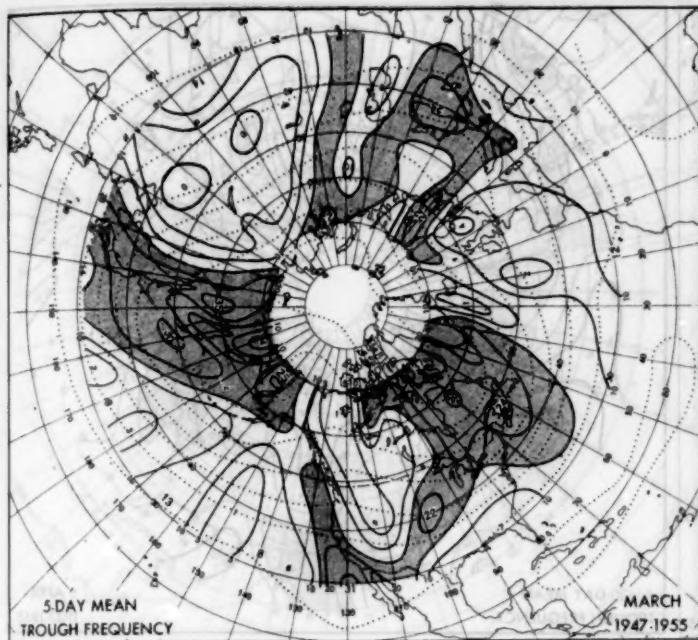
FIGURE 9.
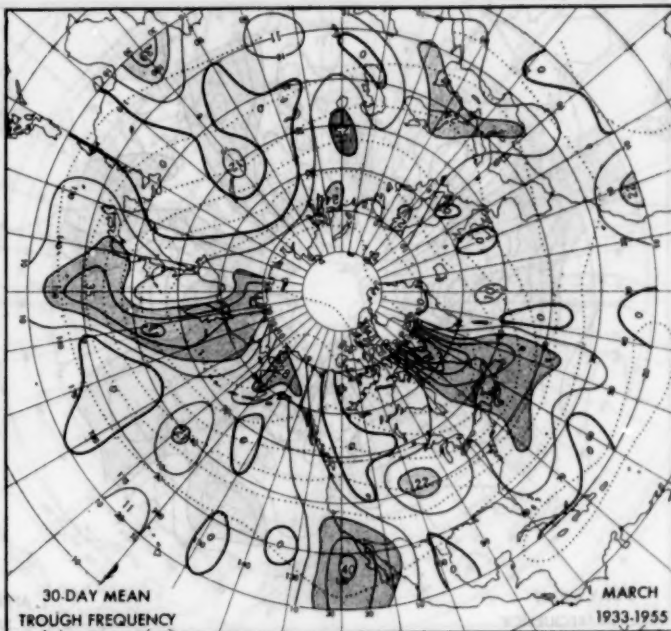
FIGURE 10.
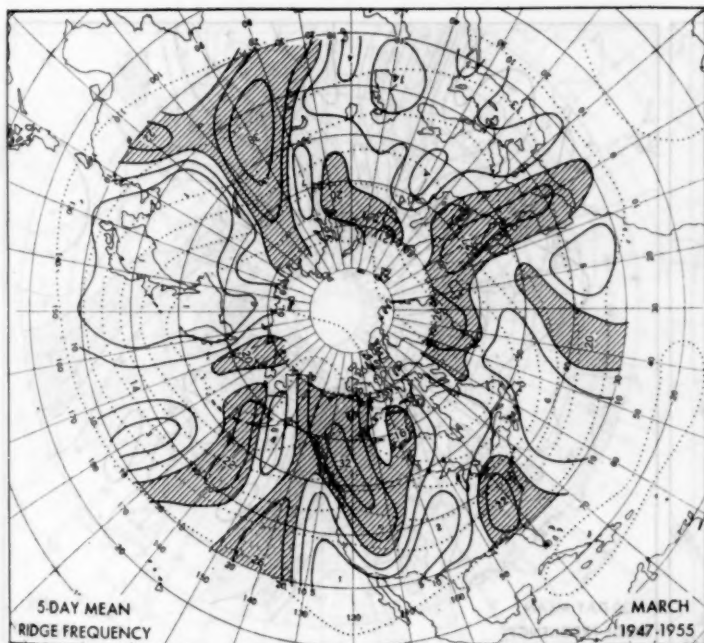
FIGURE 11.
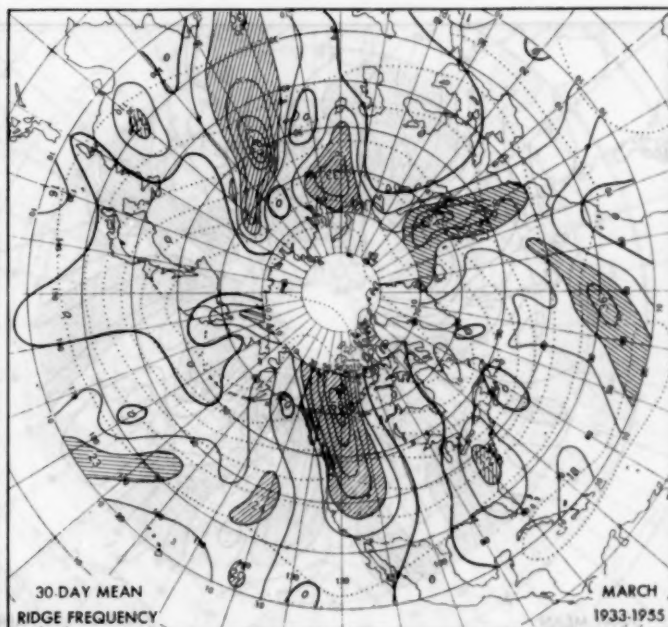
FIGURE 12.

for troughs on shorter period mean maps to develop in the lee of the Rocky Mountains and then to move rapidly eastward and deepen near the east coast [8, 12].

Another interesting feature is the tendency for a weak axis of maximum trough frequency to be located along or off the entire west coast of North America. This tendency is evident not only during the summer months, when a trough is present in the normal contours, but also during most other months of the year, when the normal contours indicate a ridge or straight flow. The orientation of the maximum frequency axis is generally parallel to the coastline and apparently reflects the fact that many

troughs in this area are favored by topographical features to assume a negative horizontal tilt; i. e., from northwest to southeast.

RIDGES

The frequency distributions of ridges are to a large extent inverse to those of troughs in corresponding months. Ridges are scarce most of the year in regions where troughs congregate, such as eastern Canada, the western Atlantic, Lower California, the eastern Mediterranean, and the west coast of Africa. A similar condition prevails during the colder months of the year along the east coast of Asia, in the central United States, and near the Hawaiian
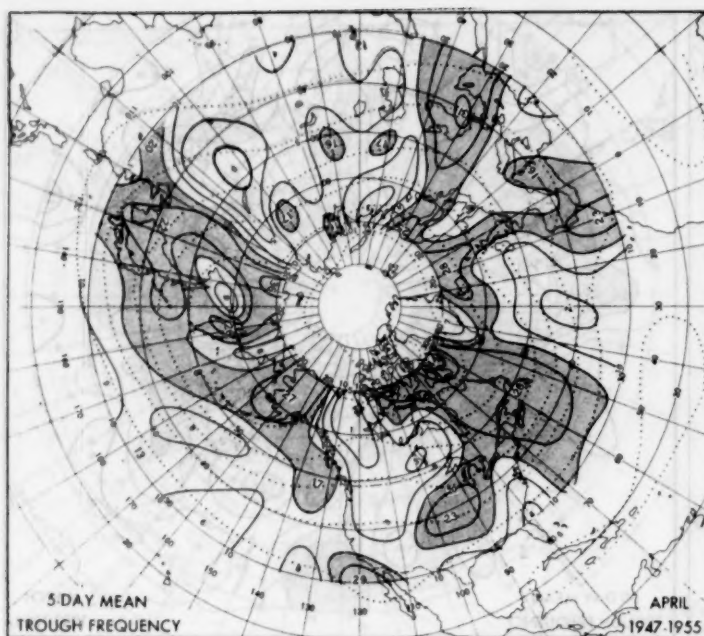
FIGURE 13.
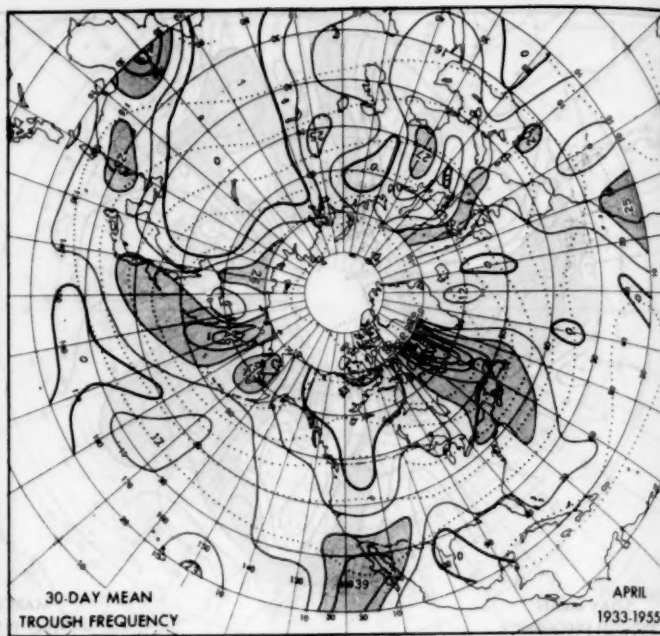
FIGURE 14.
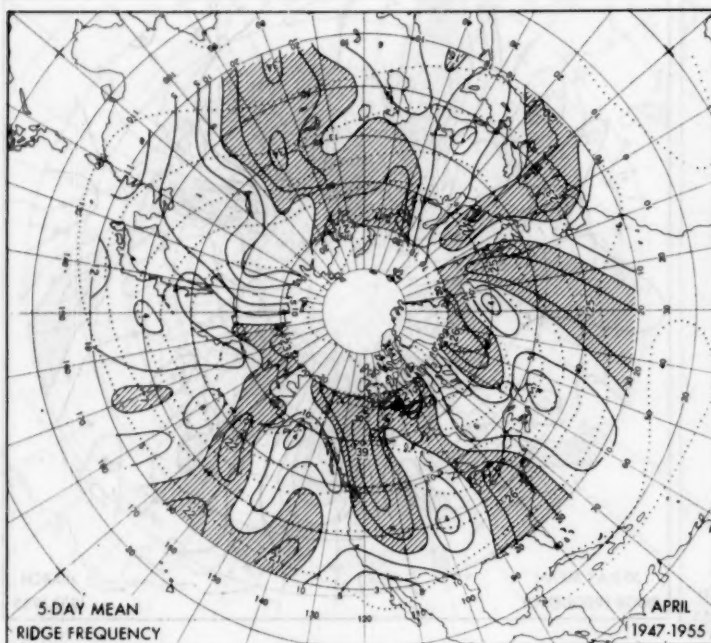
FIGURE 15.
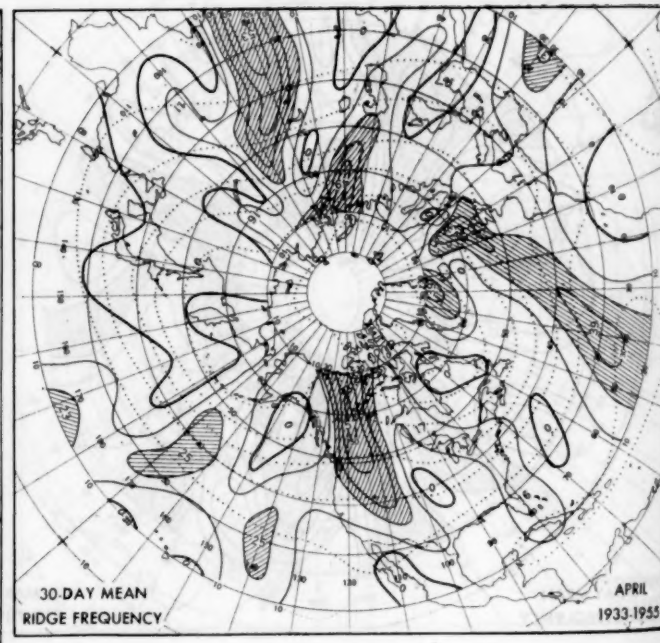
FIGURE 16.

Islands, and during the warmer months in the vicinity of the Bering Sea and the Black Sea.

On the other hand, ridges are abundant in sections with few troughs. The most conspicuous example is western Canada, where a strong concentration of ridges is found near the ridge in the normal contours over the Continental Divide during every month of the year. This preponderance of ridges west of the Rockies is generally attributed to divergence which results as westerly flow is forced to ascend the western slopes of the mountains (cf., Bolin [3] and Charney and Eliassen

[5]). The fact that the maximum frequency maintains over Canada throughout the year, while its southward extension weakens and shifts eastward in summer in conjunction with the seasonal decrease in westerlies over the western United States and southwestern Canada, lends support to this theory. Other areas with many ridges and few troughs during much of the year are the eastern portions of the oceans, in the vicinity of the semi-permanent Azores and eastern Pacific Highs, central Asia just west of Lake Baikal, and Greenland.

The seasonal variation of ridge frequency also tends
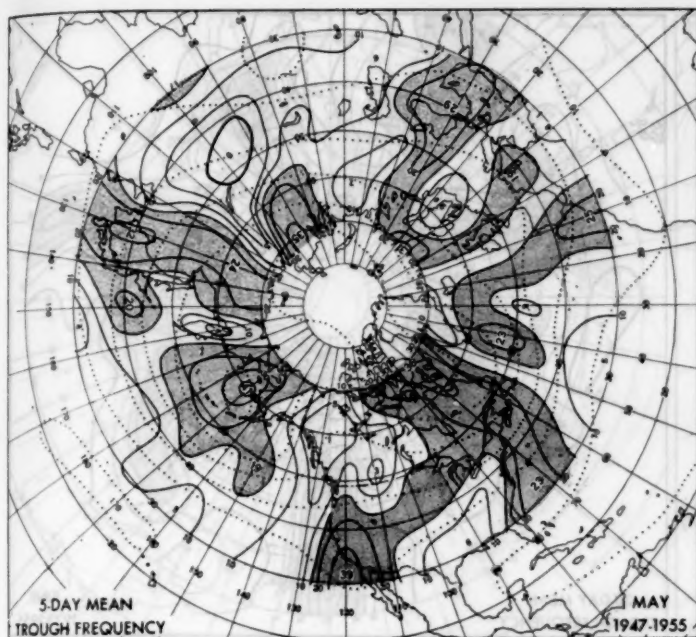
FIGURE 17.
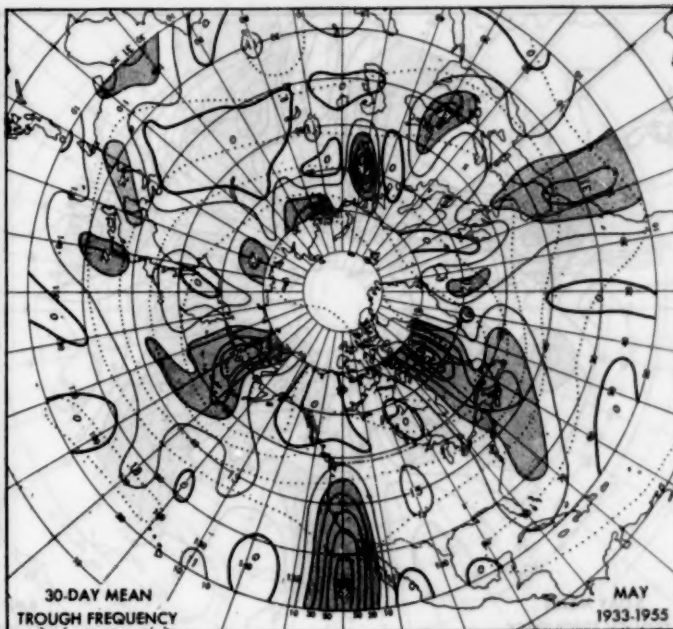
FIGURE 18.
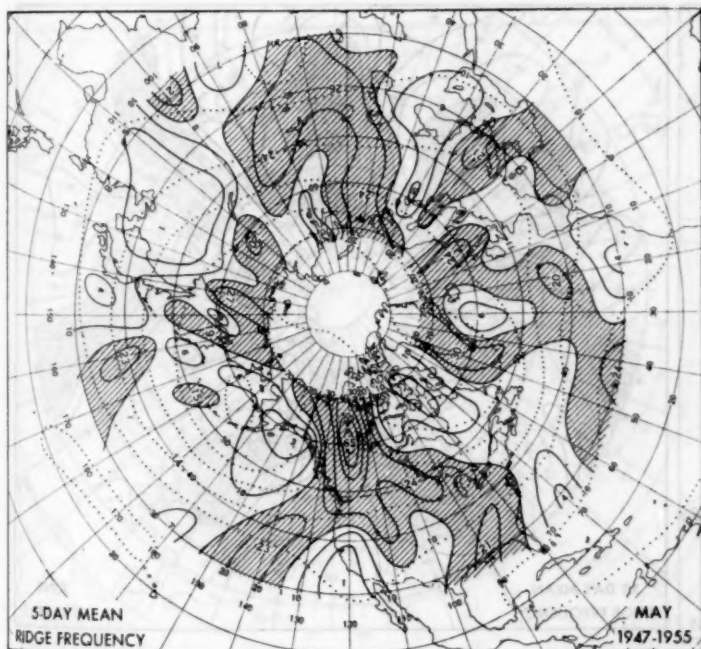
FIGURE 19.
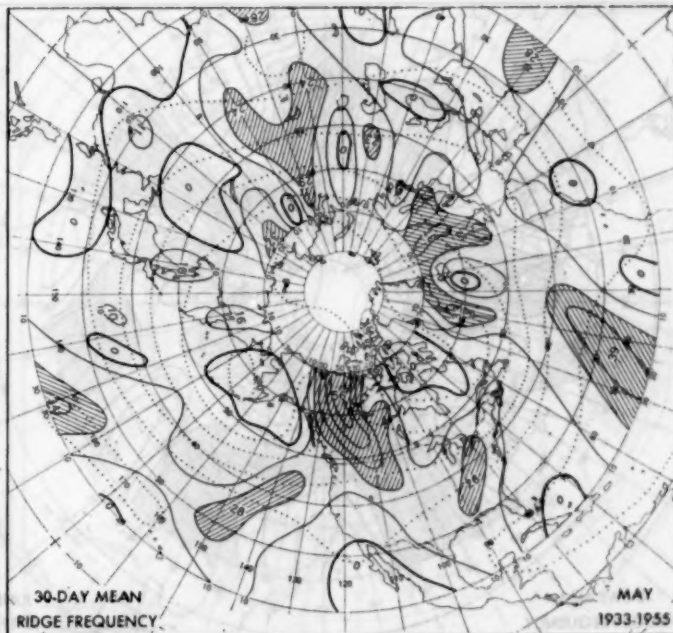
FIGURE 20.

to be the reverse of that of troughs. In areas where troughs are frequent during all but the summer months, ridges are frequent only during summer. This behavior can be noted in the central United States, in Japan and the Sea of Okhotsk, in Alaska and the Gulf of Alaska, and in the Mediterranean. An opposite type of seasonal variation, in which ridges are more frequent (and troughs less frequent) in winter than summer occurs in the Pacific Northwest region of the United States, over the British Isles, and in the Bering Sea, with much of the transition

occurring from May to June and from September to October.

The dominance of anticyclonic circulation over the central United States during summer has been attributed to surface heating over the continent by Reed [14] and to the downstream consequence of the thermally fixed west coast trough by Wexler [18]. The onset of the summer-type pattern is manifested by a sharp increase in ridge frequency in the Great Plains of the United States from June to July (figs. 23, 24, 27, 28), corresponding to a
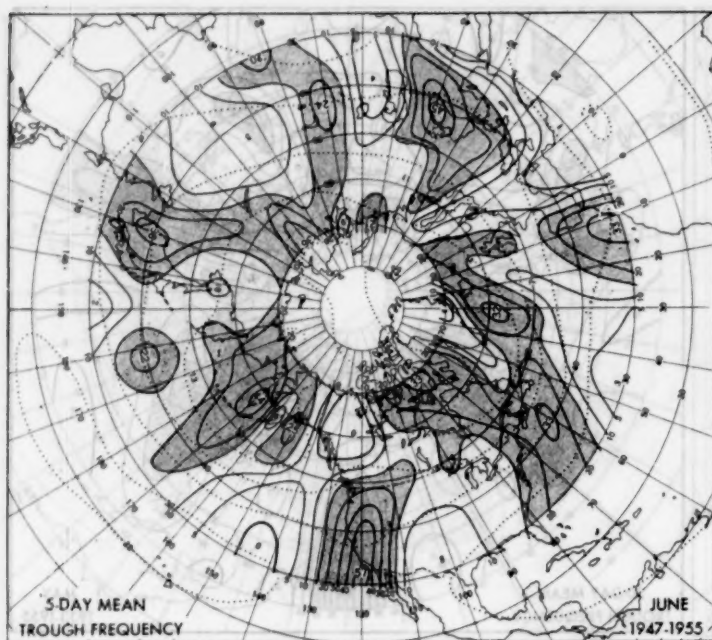
FIGURE 21.
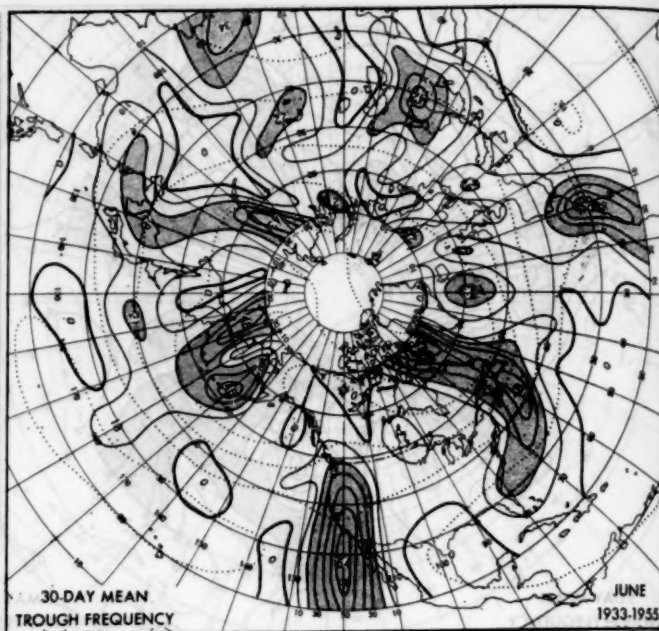
FIGURE 22.
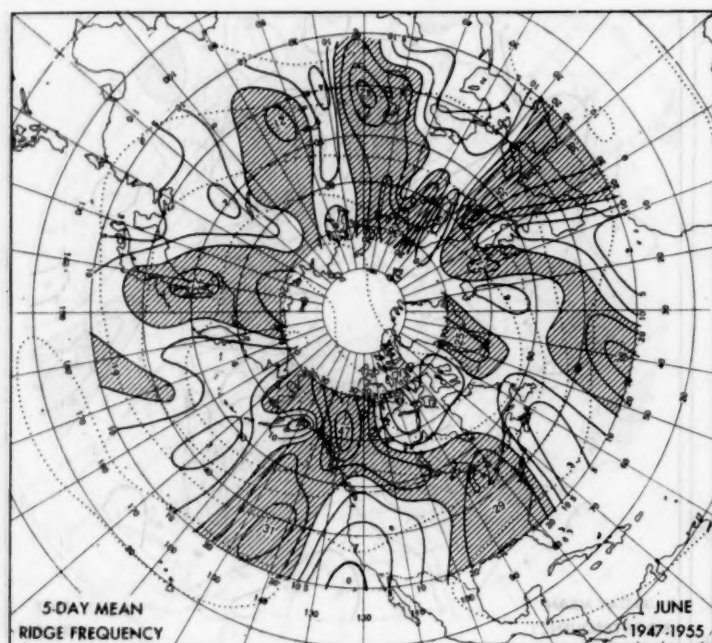
FIGURE 23.
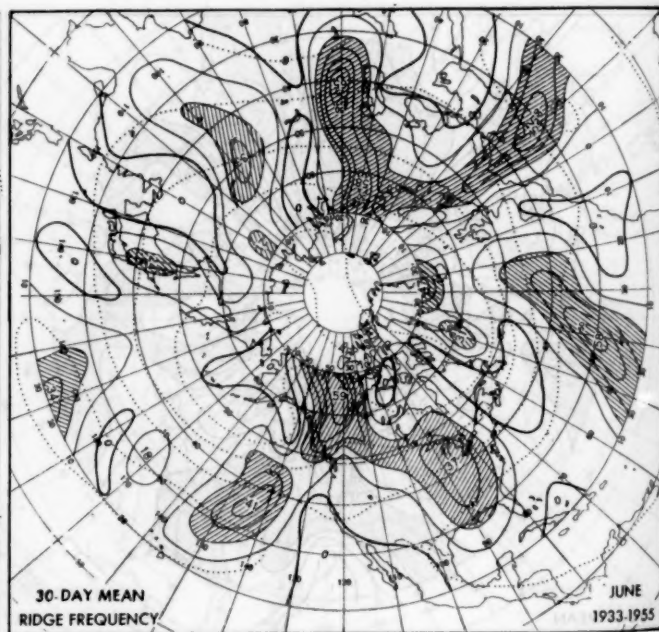
FIGURE 24.

well-known singularity in Arizona precipitation [4, 14]. This type of winter-summer reversal takes place a month earlier (from May to June) in Japan and Alaska, where surface heating is probably responsible.

In some areas both ridges and troughs are fairly frequent during certain months of the year; e. g., in parts of the Aleutians, the Icelandic region, and the east coast of North America. These are important centers of action in which the variability of 700-mb. height is relatively large. On the contrary, both ridges and troughs are infrequent around western Hudson Bay (in winter),

between Lake Baikal and the Sea of Japan (during the cold months), and in the western Gulf of Mexico (except fall). These are areas where relatively straight flow and small height variability normally prevail at the 700-mb. level. It would be especially difficult to anticipate the location of such regions from the normal 700-mb. contours alone.

ACKNOWLEDGMENTS
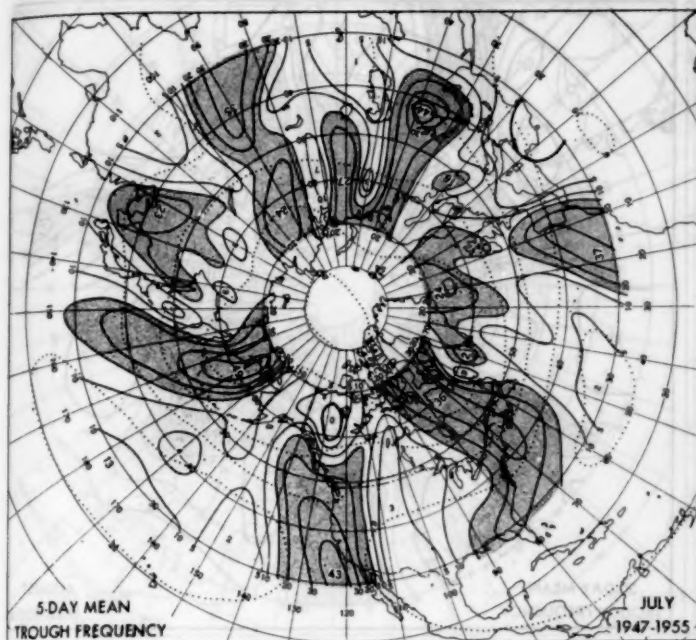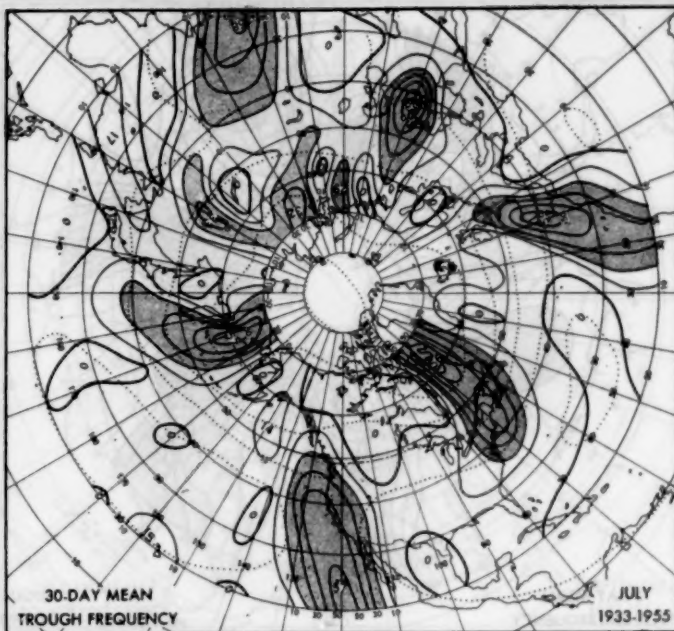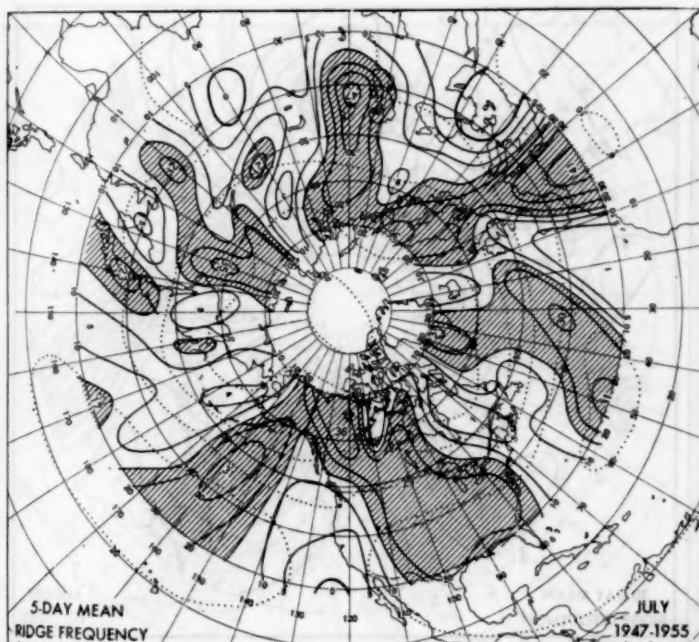
FIGURE 25.

FIGURE 26.

FIGURE 27.
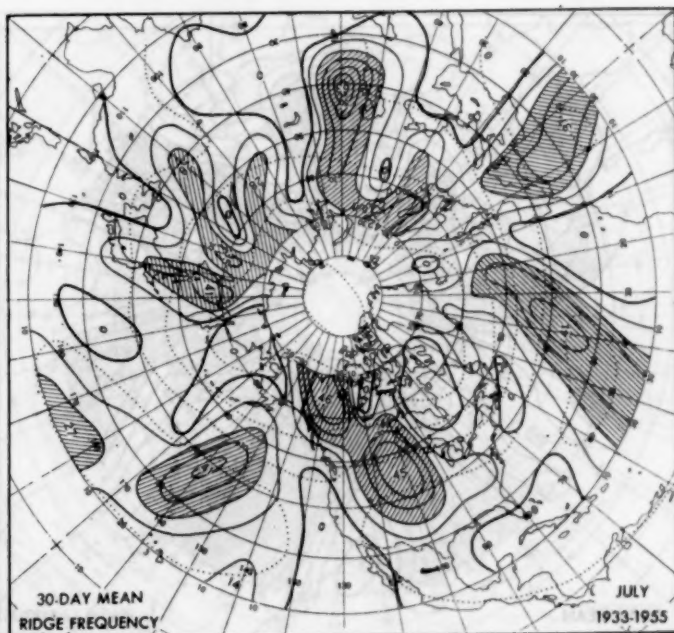
FIGURE 28.

for their valuable help in compiling and analyzing the data on trough-ridge frequency.

REFERENCES

1. J. M. Austin and Collaborators, "Aspects of Intensification and Motion of Wintertime 500 mb. Patterns," *Bulletin of the American Meteorological Society*, vol. 34, No. 9, Nov. 1953, pp. 383–392.

2. E. M. Ballenzweig, A Practical Equal-Area Grid, unpublished manuscript, Extended Forecast Section, U. S. Weather Bureau, 1958.

3. B. Bolin, "On the Influence of the Earth's Orography on the General Character of the Westerlies," *Tellus*, vol. 2, No. 3 Aug. 1950, pp. 184–195.

4. R. A. Bryson, and W. P. Lowry, "Synoptic Climatology of the Arizona Summer Precipitation Singularity," *Bulletin of the American Meteorological Society*, vol. 36, No. 7, Sept. 1955, pp. 329–339.

5. J. G. Charney and A. Eliassen, "A Numerical Method for Predicting the Perturbations of the Middle Latitude Westerlies," *Tellus*, vol. 1, No. 2, May 1949, pp. 38–54.

6. W. Dammann, "Die Verbreitung der Höhentröge in der 500-mb. Fläche und ihr Einfluss auf das Klima der gemässigten
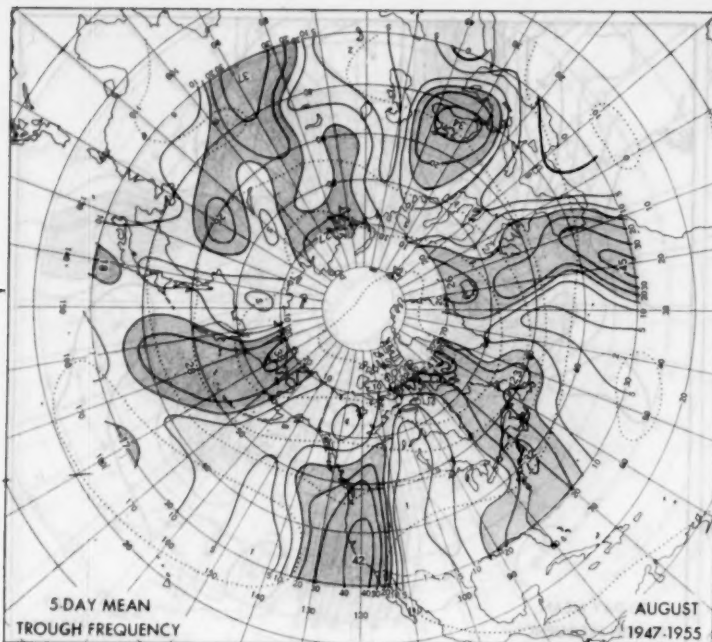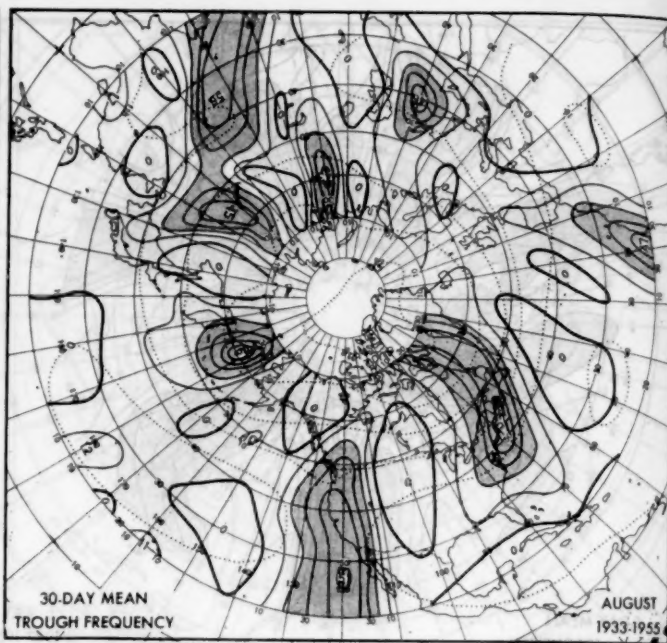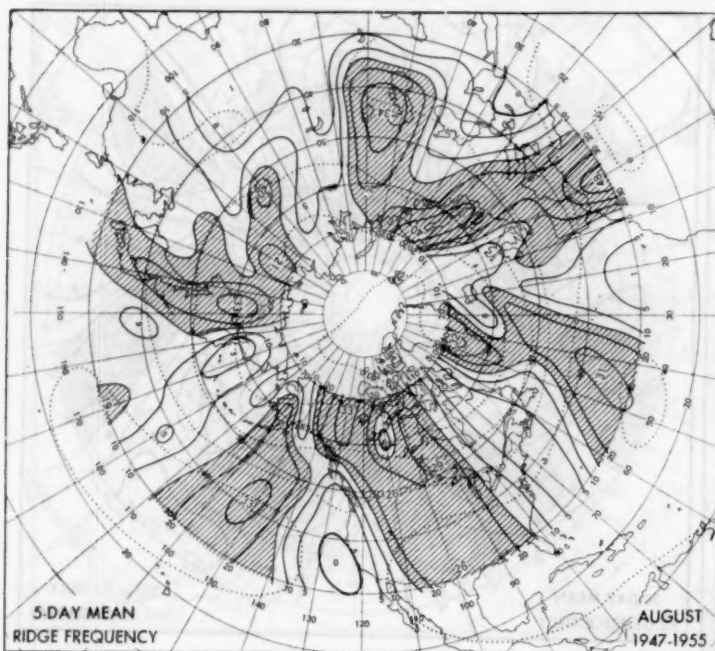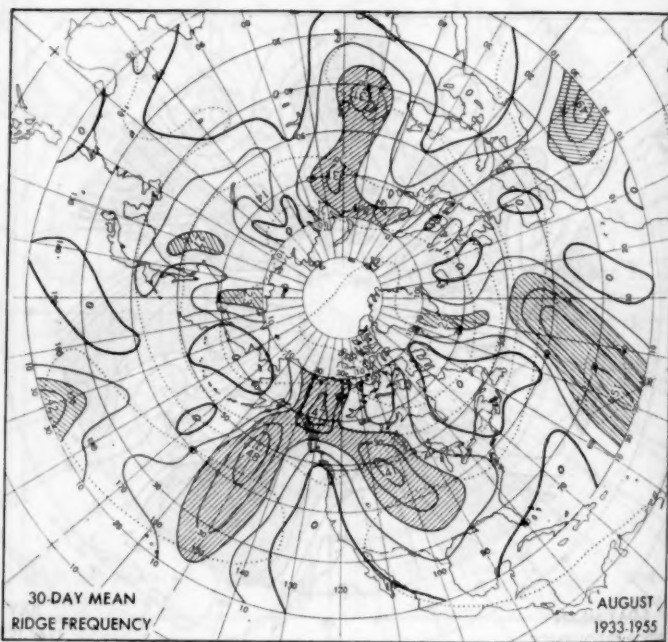
FIGURE 29.

FIGURE 30.

FIGURE 31.

FIGURE 32.

Breiten," *Berichte des Deutschen Wetterdienstes in der U. S. Zone*, No. 42, Knoch-Heft, 1952, Bad Kissingen, pp. 195–199.

7. O. Essenwanger, "Statistische Untersuchungen über die Zirkulation der Westdrift in 55° Breite," *Berichte des Deutschen Wetterdienstes*, No. 7, 1953, 22 pp.

8. W. H. Klein, "Some Empirical Characteristics of Long Waves on Monthly Mean Charts," *Monthly Weather Review*, vol. 80, No. 11, Nov. 1952, pp. 203–219.

9. W. H. Klein, "The Weather and Circulation of January 1955— A Month With a Mean Wave of Record Length," *Monthly Weather Review*, vol. 83, No. 1, Jan. 1955, pp. 14–22.

10. W. H. Klein, "Principal Tracks and Mean Frequencies of Cyclones and Anticyclones in the Northern Hemisphere," *Research Paper* No. 40, U. S. Weather Bureau, Washington, D. C., 1957, 60 pp.

11. J. E. Miller, "Studies of Large Scale Vertical Motions of the Atmosphere," *New York University Meteorological Papers*, vol. 1, No. 1, July 1948, 49 pp.

12. J. Namias, "Thirty-Day Forecasting: A Review of a Ten-Year Experiment," *Meteorological Monographs*, vol. 2, No. 6, American Meteorological Society, Boston, July 1953, 83 pp.

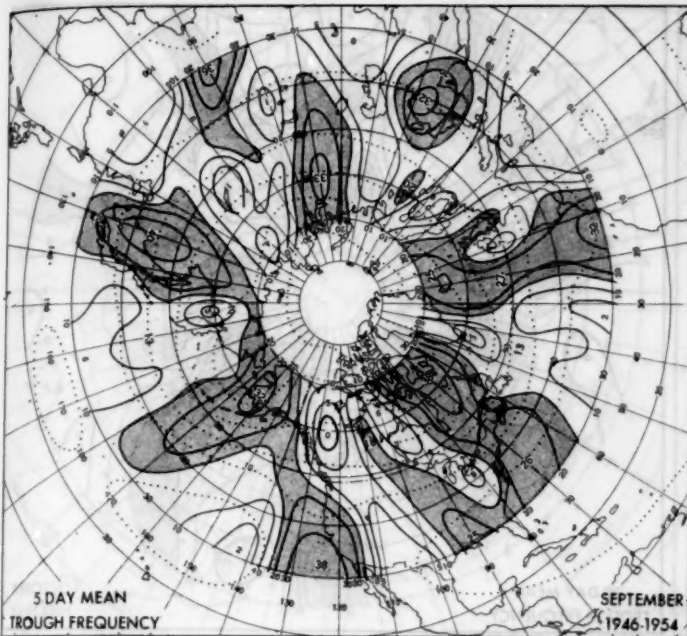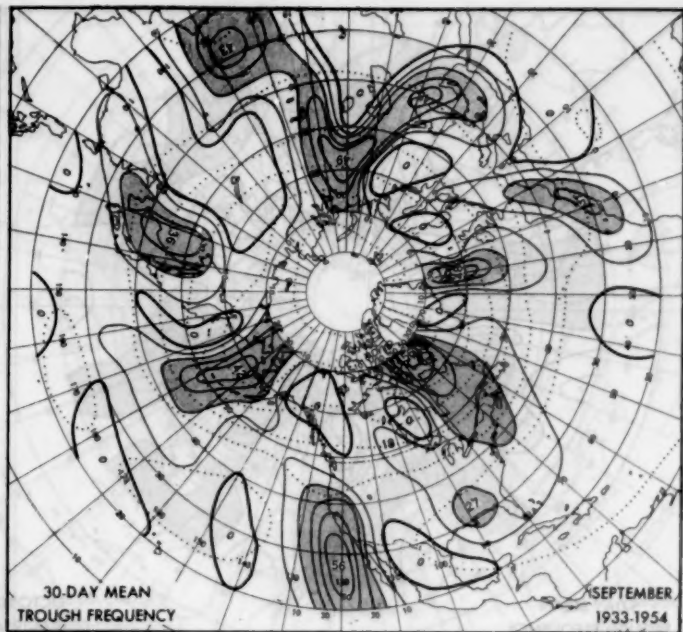13. J. Namias and P. F. Clapp, "Studies of the Motion and De-
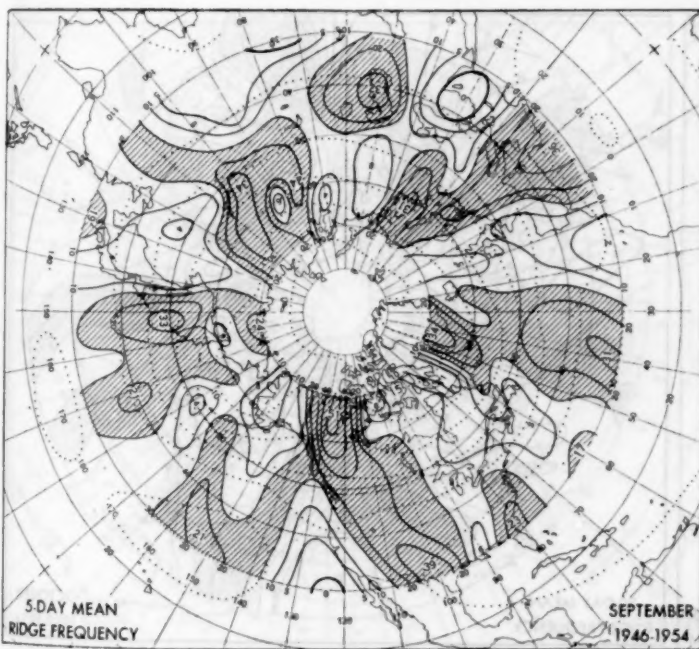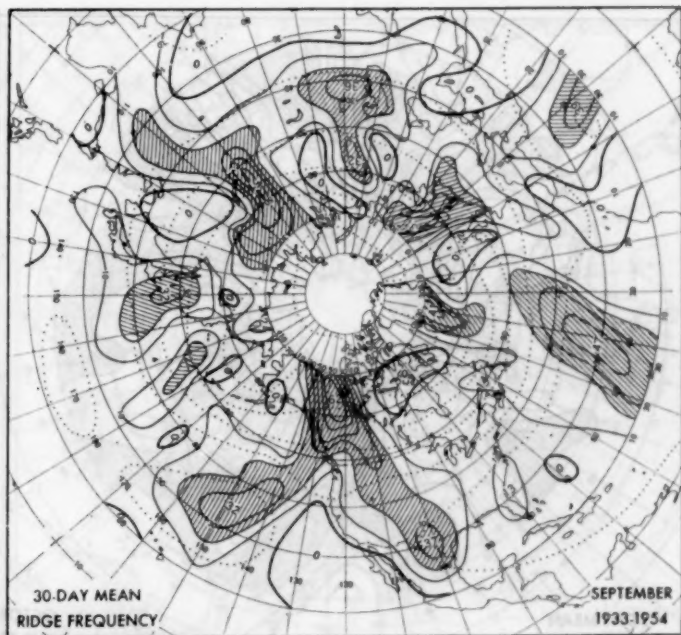
FIGURE 33.

FIGURE 34.

FIGURE 35.

FIGURE 36.

velopment of Long Waves in the Westerlies," *Journal of Meteorology*, vol. 1, Nos. 3 and 4, Dec. 1944, pp. 57–77.

14. T. R. Reed, "The North American High-Level Anticyclone," *Monthly Weather Review*, vol. 61, No. 11, Nov. 1933, pp. 321–325.

15. J. Smagorinsky, "The Dynamical Influence of Large-Scale Heat Sources and Sinks on the Quasi-Stationary Mean Motions of the Atmosphere," *Quarterly Journal of the Royal Meteorological Society*, vol. 79, No. 341, July 1953, pp. 342–366.

16. R. C. Sutcliffe, "Mean Upper Contour Patterns of the Northern Hemisphere—The Thermal-Synoptic View-point," *Quarterly Journal of the Royal Meteorological Society*, vol. 77, No. 333, July 1951, pp. 435–440.

17. U. S. Weather Bureau, "Normal Weather Charts for the Northern Hemisphere," *Technical Paper* No. 21, Washington, D. C., Oct. 1952, 74 pp.

18. H. Wexler, "Some Aspects of Dynamic Anticyclogenesis," *The University of Chicago, Institute of Meteorology, Miscellaneous Reports* No. 8, Jan. 1943, 28 pp.
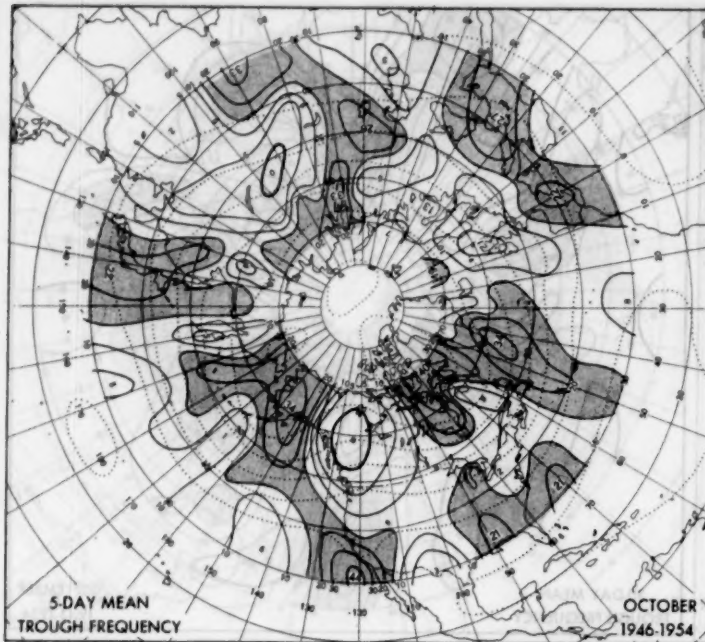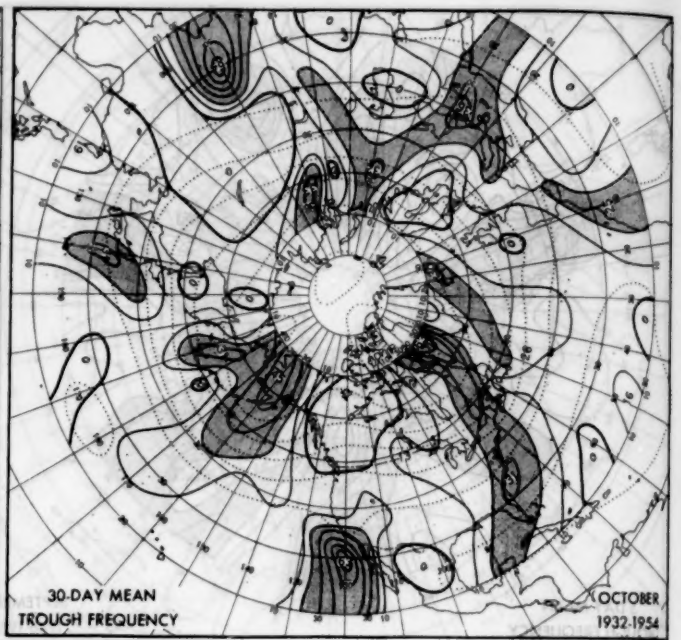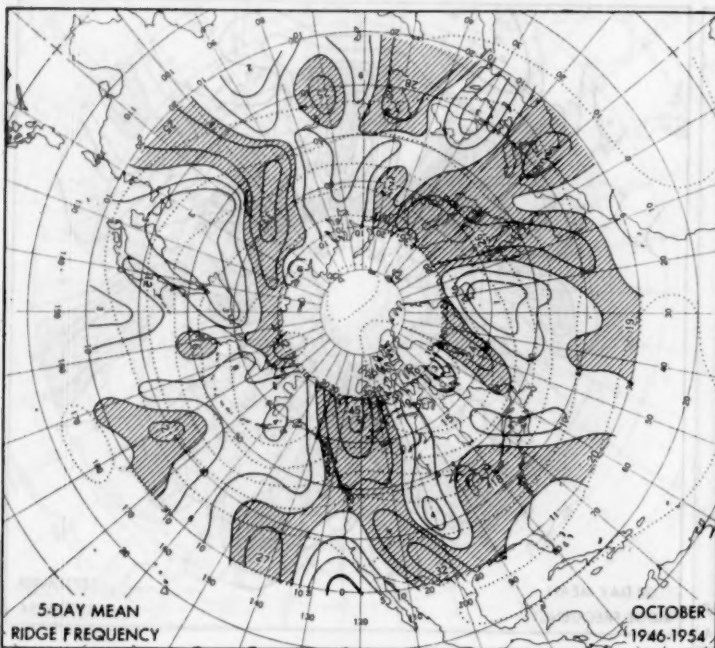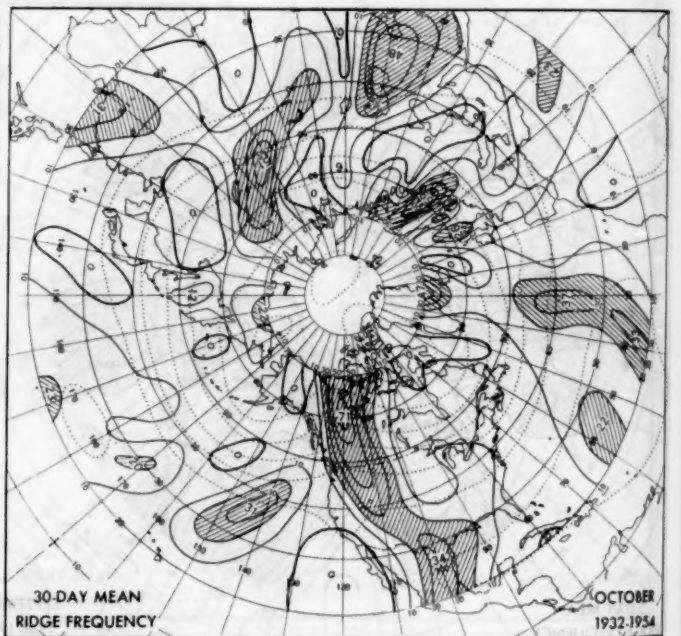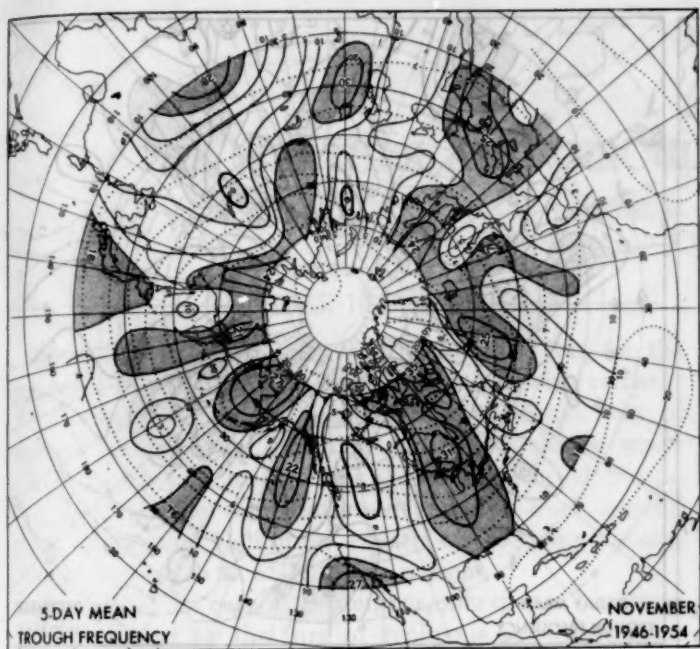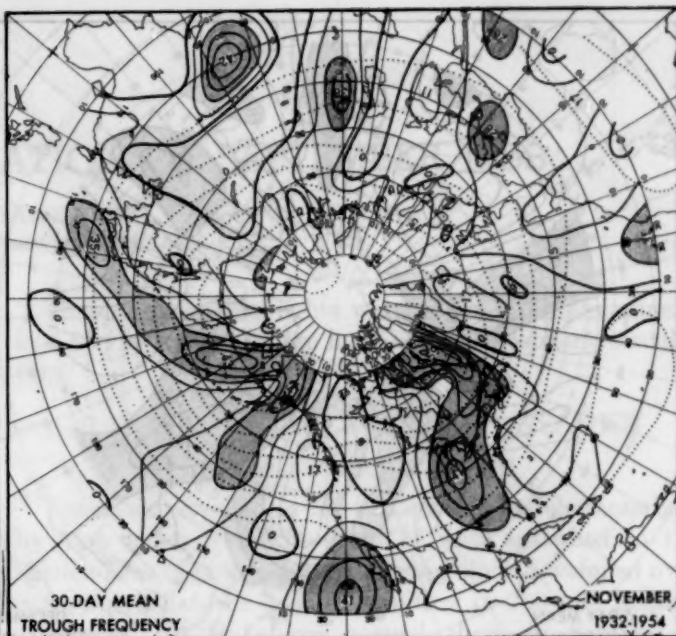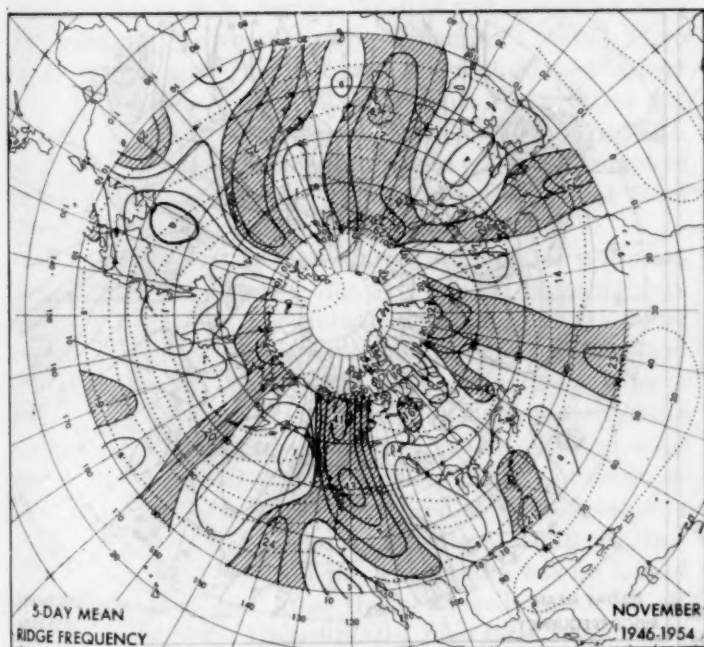
FIGURE 37.

FIGURE 38.

FIGURE 39.

FIGURE 40.

FIGURE 41.

FIGURE 42.

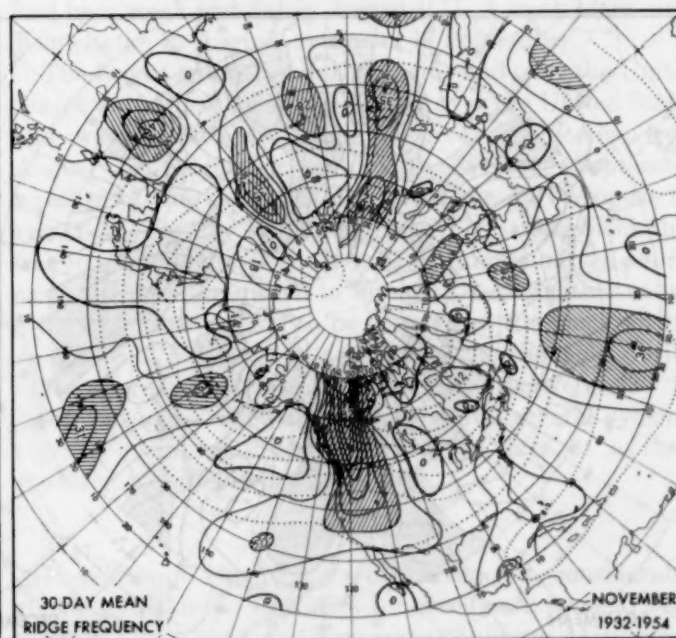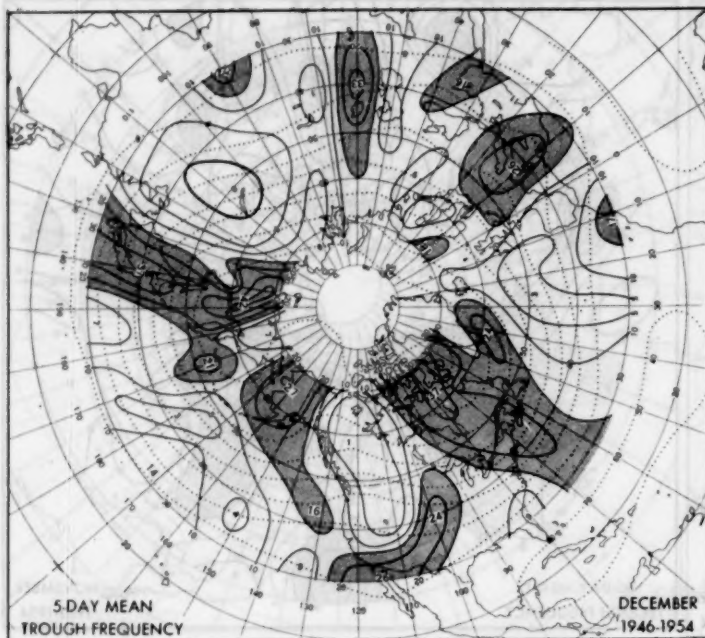FIGURE 43.

FIGURE 44.

FIGURE 45.
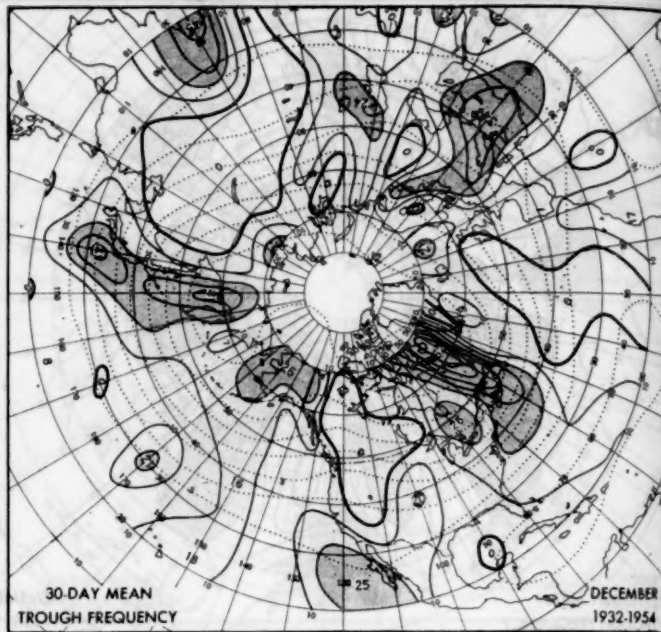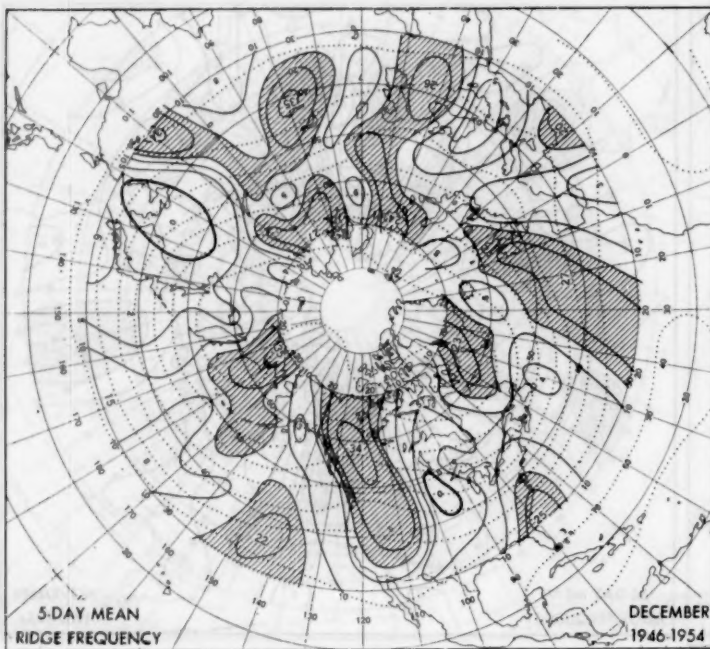
FIGURE 46.

FIGURE 47.

FIGURE 48.

THE WEATHER AND CIRCULATION OF SEPTEMBER 1958 [1]

EMANUEL M. BALLENZWEIG

Extended Forecast Section, U. S. Weather Bureau, Washington, D. C.

1. WEATHER HIGHLIGHTS

Local Climatological Data from Columbus, Ga., for the month of September 1958 included the following remark: "September brought nothing outstanding in the way of weather phenomena." Similar remarks could be made this September in many cities across the United States. The only sizable temperature departures from normal were along the California coast, where temperatures averaged as much as 8° F. above normal.

As is often the case in September, newspaper headlines were generated by the fury of typhoons and hurricanes. At least three severe typhoons occurred during the month: Grace, Helen, and Ida (fig. 1A). Typhoon Ida was attended by gusts of 175 m. p. h. before it crossed the Tokyo-Yokohama area on September 26 with winds in excess of 80 m. p. h. Serious flooding was associated with this typhoon, the worst to strike Japan in 24 years. More than 20 inches of rain fell on 4,300-foot Mount Amagi and the rushing waters of the swollen Kano River destroyed two villages on the Izu Peninsula, 70 miles south of Tokyo, sweeping people into the bay. The incomplete casualty toll includes 340 dead, 984 missing, and more than half a million people made homeless.

North America was also affected by tropical storm activity. Hurricane Helene (fig. 1B) was the biggest threat to the east coast of the United States since 1955. After feinting at the South Carolina coastal cities, Helene pursued a northward course along the Carolina coast, always keeping the center of its eye just offshore (approaching within 10 miles off Cape Lookout, N. C.). Record wind speeds were reported at many stations in the Carolinas, as gusts of 135 m. p. h. were experienced at Wilmington and 144 m. p. h. at Cape Lookout. Despite $11 million damages, largely as a result of the wind, there was no loss of life in the Carolinas. After Helene moved northward off the east coast of the United States, high tides, heavy seas, strong winds, and drenching rain caused damage in the Canadian Maritime Provinces.

Nature fashioned another headline in Texas where heavy to excessive rains fell in the western portion of the State and in the mountain areas of northern Mexico. This rainfall over the Rio Conchos River watershed produced the highest stage in 32 years on the Rio Grande River at Presidio, Tex. On September 28 the river crested at 21 ft.; flood stage is 10 ft. Heavy damage to farmlands resulted.

These weather highlights were not isolated phenomena and can be related to the large-scale atmospheric circulation.

2. THE CIRCULATION AND THE WEATHER

THE GENERAL CIRCULATION

The mean circulation for September was characterized by high index from the coast of Asia eastward to the British Isles (figs. 2 and 3). A strong block developed over Scandinavia late in August resulting in 700-mb. heights averaging 270 ft. above normal there in September. Downstream, an anomaly center of −370 ft. appeared at 700 mb. associated with a deep trough in the lee of the Urals. These two large anomaly centers effected a large change in the circulation over Europe and Asia where it had been weak and flat in August [17]. A weak block over Kamchatka in August continued in September.

The height anomalies in the Pacific and over the United States were all rather small. Those over the United States and western Atlantic exhibited great persistence from August to September as did the average September weather of the United States, after the July–August reversal described by Woffinden [17]. The strong block that was in extreme northern Canada in August moved southeastward and diminished in intensity. A negative anomaly center that seemed to be coupled to the block on the Asiatic side of the pole appeared over the pole during September and also weakened. Heights were 330 ft. below normal west of the British Isles as several cyclonic vortices remained anchored there for days at a time, attended by gales over a large area.

PRECIPITATION

Precipitation for the month averaged considerably above normal in an area stretching eastward from Arizona through New Mexico and Texas into Louisiana, Mississippi, and Alabama and thence northward into western Tennessee, Arkansas, and Missouri (Chart III). Figure 2 shows cyclonically curved anomalous flow from the south as the average condition during September in an area from Arizona eastward to Alabama. A similar circulation prevailed at sea level (Chart XI and inset). Such a flow favors advection of Gulf moisture into this region and encourages precipitation. Part of the extensive precipitation along the Gulf Coast and also in inland Texas can be traced to the remnants of hurricane Ella which advected moisture into that area (table 1). Further
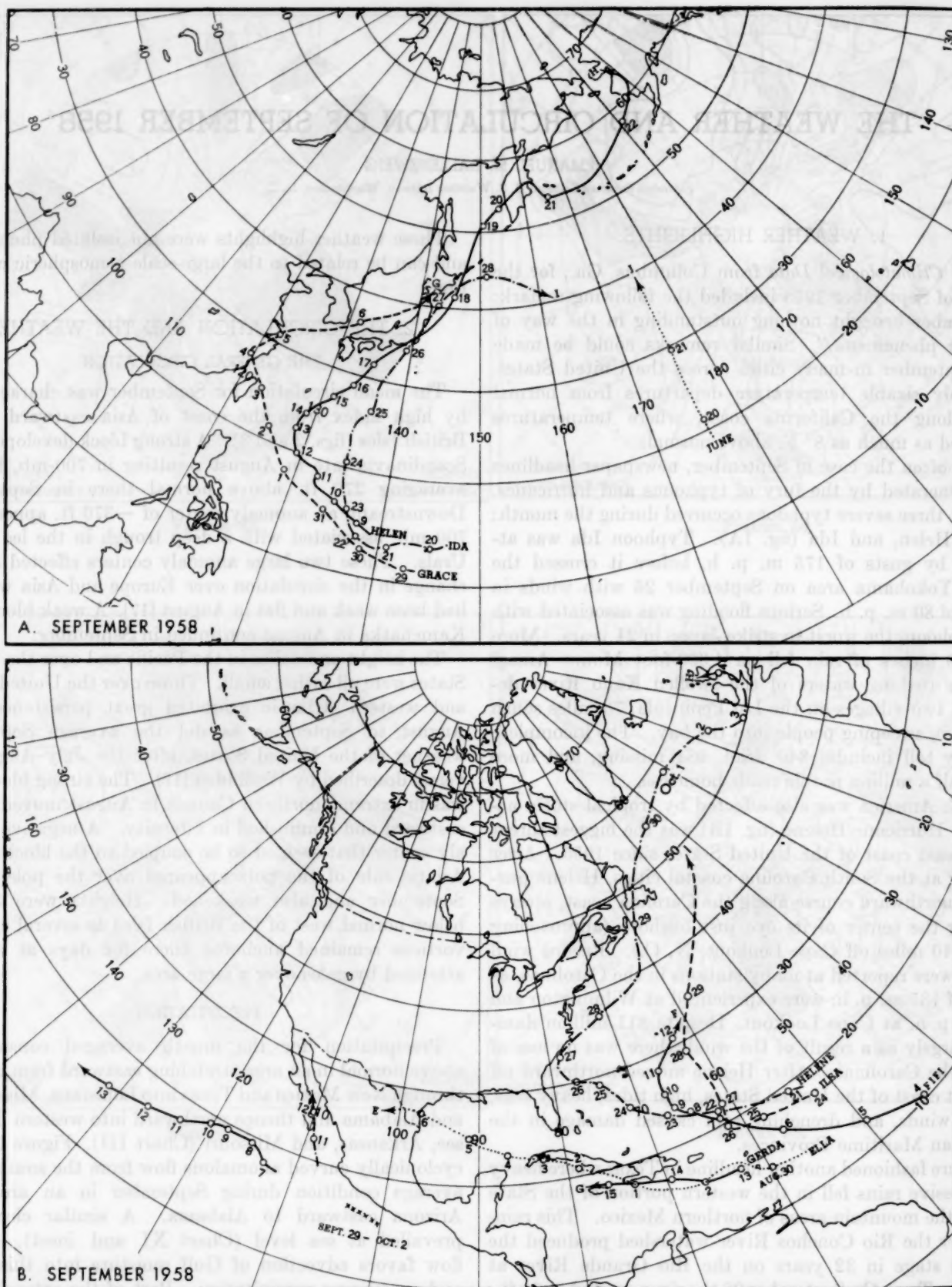
FIGURE 1.—Tropical storm tracks for September 1958, based on preliminary data. Open circles indicate 1200 GMT positions on dates given. (A) Western Pacific, (B) Atlantic and eastern Pacific.
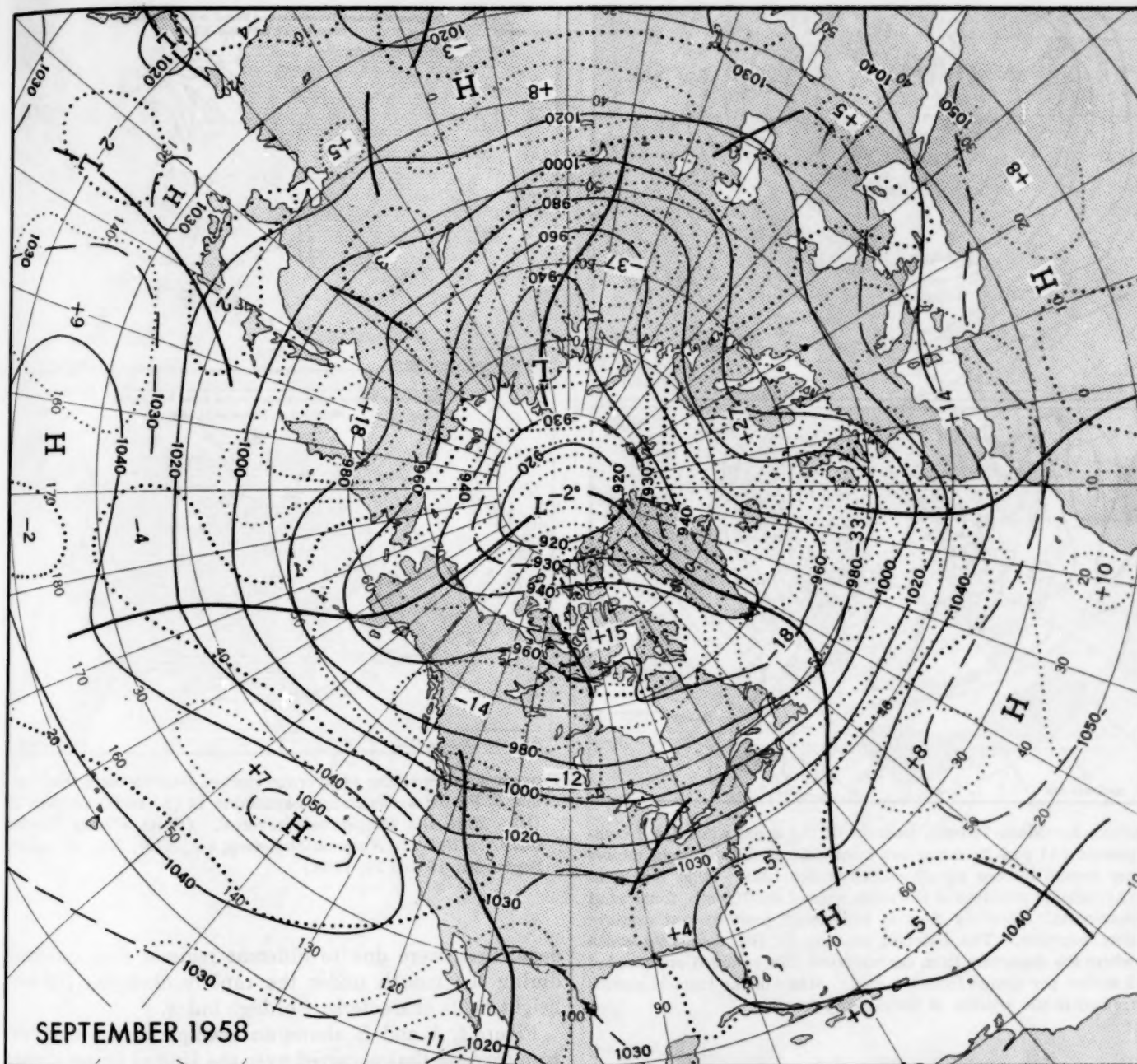
FIGURE 2.—Mean 700-mb. contours (solid) and height departures from normal (dotted), both in tens of feet, for September 1958.   Troughs are indicated by heavy vertical lines.   Note fast westerly flow from the coast of Asia eastward to the British Isles.

heavy precipitation occurred in Texas associated with a weak tropical depression in that area on the 19th and 20th. The heavy rainfall in western Texas caused flooding during the month.   Precipitation in the Missouri-Arkansas region was largely frontal in nature.

Other heavier than normal rainfall amounts occurred in Pennsylvania and southern New England, largely the result of one storm on the 19th to the 21st (Chart X) which is discussed fully in an adjoining article [13].   Rain was also copious along the California-Nevada-Oregon border, caused by two influxes of Pacific air, the first about the 7th to the 8th, and the second from the 22d to the 23d.

485868—58——3

TABLE 1.—Rainfall amounts associated with hurricane Ella 1958 and the percentage they represented of the total September rainfall at various stations in Texas

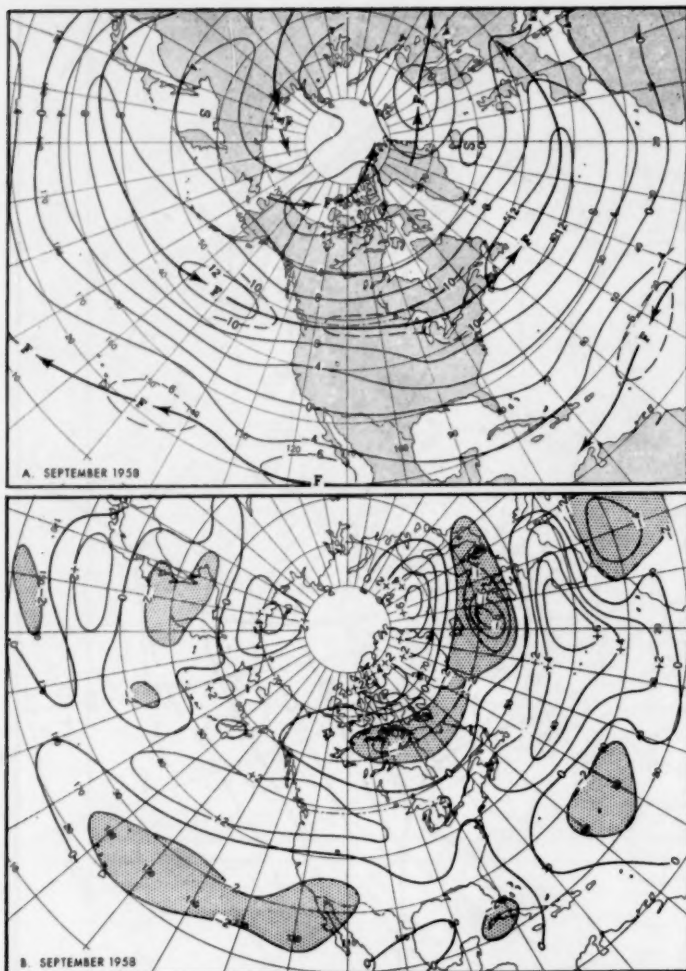| Stations	Amount (inches)	Percentage of monthly rainfall
Austin	2.66	39
Corpus Christi	3.67	44
Galveston (city office)	6.94	50
Galveston (airport)	13.98	56
Houston (airport)	7.04	46
Laredo	1.41	30
Port Arthur	3.78	26
San Antonio	1.85	22
Victoria	3.24	24
Waco	1.39	30

FIGURE 3.—Mean 700-mb. isotachs of the zonal wind speed component (A) and its departure from normal (B), both in meters per second for the month of September 1958. Solid arrows in (A) indicate positions of the mean axes of the 700-mb. zonal wind maximum. Westerly flow is considered positive and easterly flow negative. The hatched shading in (B) delineates areas where the departure from normal zonal flow equalled or exceeded 2 meters per second from the east. Many of the tropical storms formed in the vicinity of the easterly jet (A).

FIGURE 4.—Departure of average surface temperatures from normal (° F.) for weeks ending September 14 (A) and September 28 (B). Note the temperature reversal. (From *Weekly Weather and Crop Bulletin, National Summary*, vol. XLV, Nos. 37 and 39, September 15 and 29, 1958.)

The rainfall amounts were small, but were greater than the monthly normals which are less than an inch in this area. The remainder of the country was generally quite dry under anticyclonic conditions. The dryness in the Middle Atlantic States was interrupted by the passage of hurricane Helene which caused considerable precipitation along the Carolina coast. Cape Hatteras reported 4.46 inches (72 percent of its monthly total) and Wilmington, N. C., reported 8.24 inches (82 percent of its monthly total) during that 24-hour period.

TEMPERATURE

With the exception of the Pacific coast, temperatures for the month did not depart greatly from normal in most areas of the United States (Chart I-B) as height anomalies were also small. To some extent the small temperature
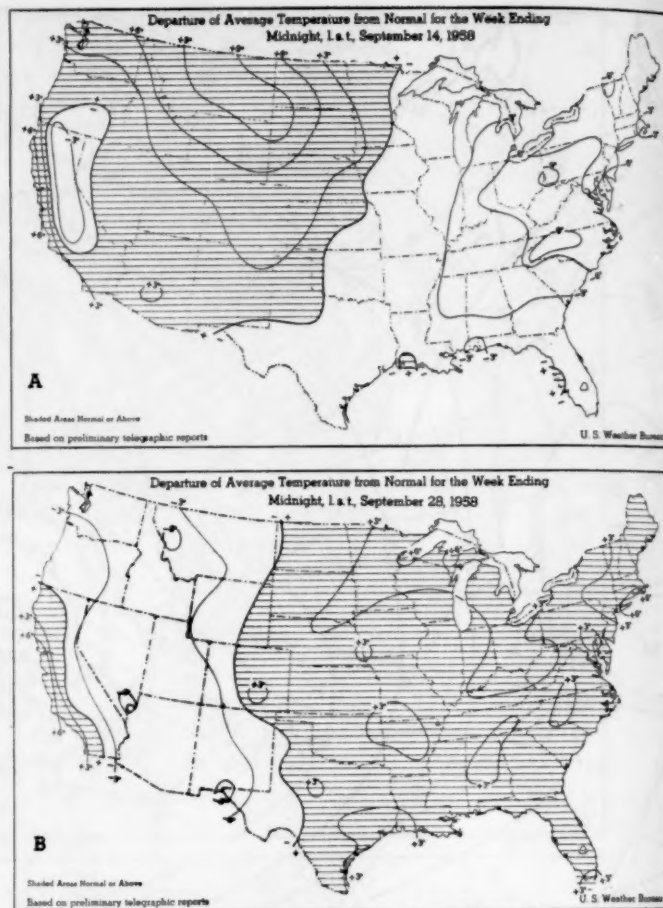
departures were due to different regimes that occurred during the month under the rapidly changing 700-mb. height fields characteristic of high index.

Figure 4, A and B, shows an example of the temperature reversal that occurred over the United States during the month. In the earlier period (fig. 4A), the temperatures were warm in the West and cold in the East as a large-amplitude planetary wave was situated over the United States with a ridge centered over the Plains States and a trough along the east coast (fig. 5C). With northerly flow, temperatures averaged as much as 12° below normal in Asheville, N. C., and as much as 9° below normal in Pittsburgh, Pa., as a large part of the East had negative temperature anomalies greater than 6°. In the West, the warmest temperatures were in Montana, Wyoming, and the Dakotas where anomalies were generally in excess of +6°, with Miles City and Great Falls, Mont., reporting the greatest departures (+11° and +10°, respectively). Temperatures along the Pacific coast continued warm, as they had been for the past months, with the greatest departures at San Francisco (+7°) and Eureka (+6°). A stagnant trough off the coast fed cool moist Pacific air
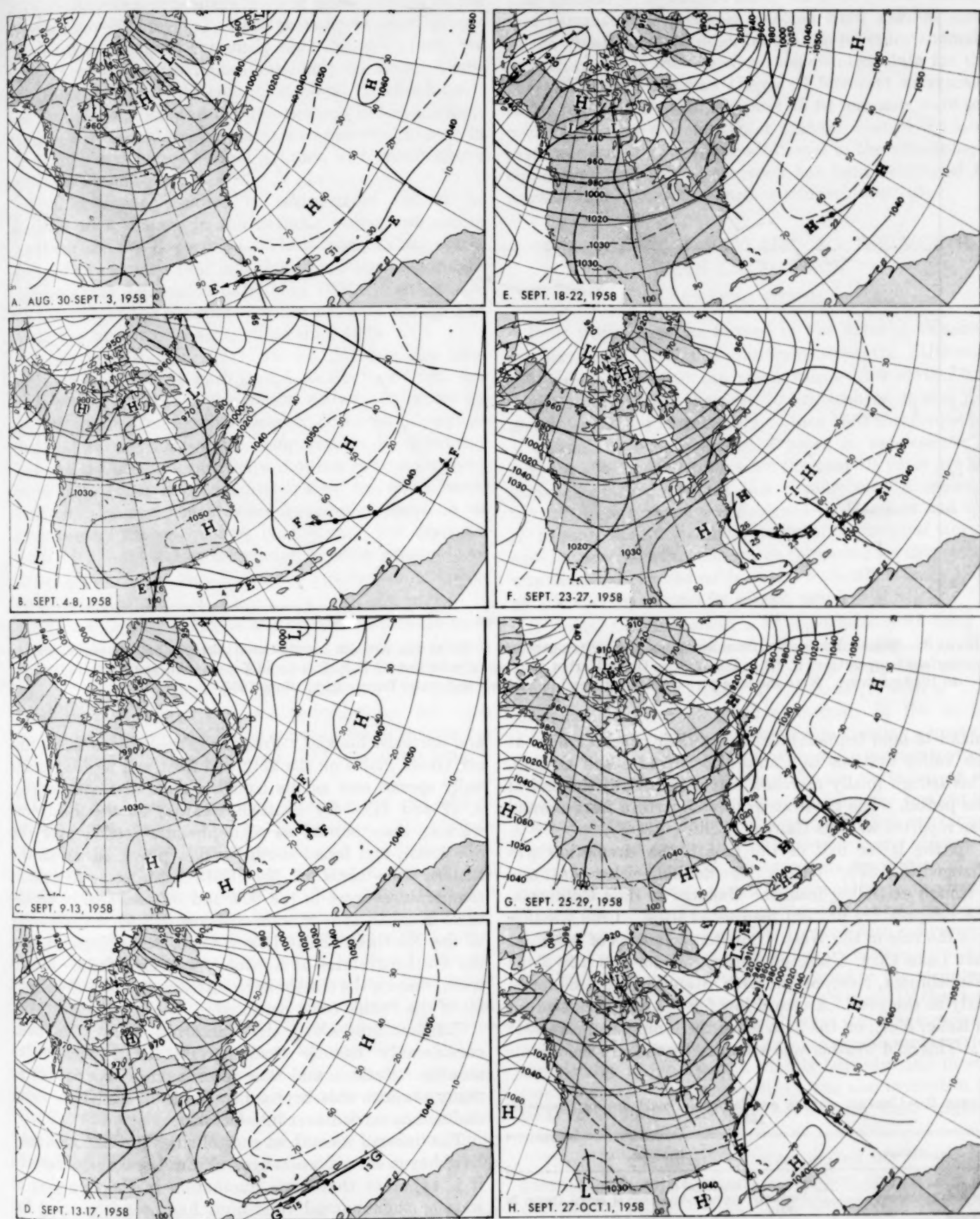
FIGURE 5.—A series of partially overlapping 5-day mean 700-mb. maps (contours in tens of feet) for selected periods in September 1958. The tracks of Ella, Fifi, Gerda, Helene, and Ilsa (labeled E, F, G, H, I) at sea level are shown by broad arrows. Solid circles indicate 1200 GMT positions on the dates given.
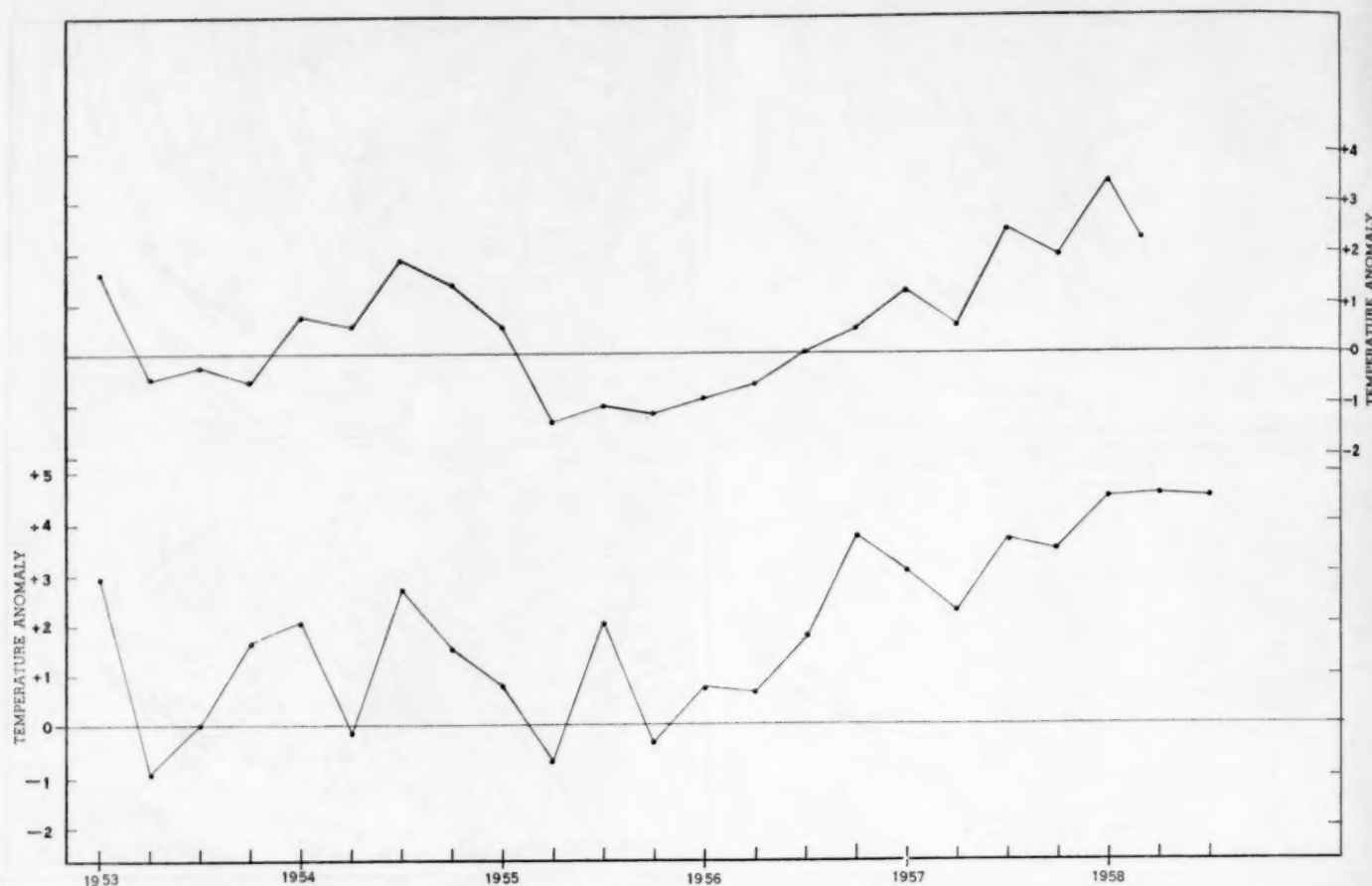
FIGURE 6.—Seasonal departure from normal of the air temperature (° F.) at Los Angeles International Airport (bottom curve) and sea surface temperatures (° F.) in Los Angeles Outer Harbor (top curve, provided by U. S. Coast and Geodetic Survey) from 1953 winter to 1958 summer. Note the long-period warming trend in both air and water temperatures since 1955.

inland to hold temperatures below their normal values at the valley stations in California, Nevada, and Oregon. This trough finally marched eastward toward the end of the period. The greatest weekly departure from normal was reported at Blue Canyon, Calif. (−7° F.).

In the latter half of the month the circulation was changed (fig. 5F). With a ridge flanking either coast and a trough extending from the Dakotas to Baja California, the temperature pattern readjusted itself. Cold weather was the rule in the West. Low temperatures of 31° F. at Salt Lake City, Utah, on September 25, and 12° F. at Winnemucca, Nev., on the 24th established records for so early in the year. A record low for the date was also set in Reno, Nev., on the 24th when the temperature was 21° F. This cold weather was attended by snow in the middle

TABLE 2.—*Unusual warmth on California coast during September 1958*

Station	Remarks
Los Angeles (city office)	3d warmest September in 81 years of record.
Los Angeles (airport)	Decidedly warmest September of record (begun in 1931).
Oakland	September average temperature 2.0° higher than record (begun in 1929).
San Diego	Second warmest September in 87 years of record.
San Francisco	Warmest of any month in 88 years of record.
Santa Maria	Warmest September in 20 years.

and northern Rockies. Freezing extended into the northern Great Plains on the 25th and frost and freezing gradually spread east as the trough advanced eastward (fig. 5, G and H). By contrast weather in the East was warmer than normal as high pressure settled over the Southeast, and broad southerly flow prevailed across the eastern two-thirds of the United States. Afternoon temperatures were in the 80's and 90's as weekly departures in excess of +5° were observed in such diverse areas as the Northern Great Lakes, Ohio, New England, and the southern States of Kentucky and Louisiana. Meanwhile, despite the change in circulation, the record warmth along the Pacific coast persisted.

Temperatures along the California coast have been considerably warmer than normal for 6 consecutive months. Records and near records were experienced at many stations this September (table 2) and this warm regime has carried over into October.

The unusual warmth at coastal cities in California may have begun several years ago. From Los Angeles records it is apparent that some fluctuation in the direction of warmer than normal conditions has been occurring for the last couple of years, with the greatest change along the coast. The airport station, about 3 miles inland, has been warmer than normal uninterruptedly since

May 1956, with temperature in 19 of these months in the "much above" category.[2] Such preponderance of events of a similar nature is extremely unlikely, if, in fact, the temperatures are distributed randomly in time. Compared to the airport, the city office, about 12 miles inland, has shown a similar warmth, but perhaps not as marked. Here below normal temperatures were observed 4 times in 29 months and above normal 5 times, with much above observed 14 times.

This apparent increase in temperature cannot be ascribed to a change in the normals used in computing the temperature departures. These normals were last changed in January 1953 and these persistent abnormalities were not discernible until May 1956. Furthermore the location of the thermometer has not been changed at either the airport or the city office since 1949.

It has been suggested [11, 12, 15, 16] that this phenomenon may be in part linked to above normal sea surface temperatures in the coastal waters. A report by the California Cooperative Oceanic Fisheries Investigations [3] stated that water temperatures in Monterey Bay and the ocean beyond have shown a general warming trend since 1955; shore conditions show the same trend. These oceanic temperatures are frequently related to air temperatures at neighboring land areas. For example, Gorton [6] found a close correlation between simultaneous air temperatures at San Diego and sea surface temperatures at La Jolla.

Figure 6, a time graph of the seasonal departure from normal of both the air temperature at Los Angeles Airport and the water temperature in Los Angeles Outer Harbor during the years 1953 to 1958, indicates the general parallelism of water and air temperatures for such averages. Note especially the warming trend in both sea and air temperature since about 1955 (about the time it was noted in Monterey Bay).

If the sea surface warming were general, its effects should be discernible at other coastal cities. San Diego's temperature record was examined and the same trend was present. The temperature fluctuated more or less around the normal up to May 1956. Since then the monthly mean temperature has been below normal only once, whereas it was much above normal for 15 months. A similar warming has been noted at San Francisco, where since May 1956 air temperatures have been below normal 3 times and much above 12 times. Oceanic warming has been noted at both San Diego and San Francisco coincidentally with the rise in air temperature.

There is additional evidence that air temperatures along the California coast have been warmer than suggested by the atmospheric circulation. An objective scheme for forecasting temperature at many cities including San Diego has been recently devised by Klein et al. [10].

This method is dependent solely on atmospheric circulation parameters objectively selected from 1947–57 data as the "best" ones to describe the temperature anomaly at each city. It was tested on independent data for the 1957–58 winter. At San Diego, 64 forecasts were made of the temperature anomaly, and all 64 forecasts were too cold. One may therefore infer that the bias of the forecasts was due to something additional to the atmospheric circulation, and this discrepancy has been attributed to warmer than normal sea surface temperatures [10].

4. TROPICAL STORMS RELATED TO THE MONTHLY MEAN CIRCULATION

ATLANTIC STORMS

Four tropical storms formed in the Atlantic this September; three developed hurricane strength. Although this was in excess of the mean values of 3 storms and 2 hurricanes during the past 70 Septembers, it was just about normal for recent years. Since 1953 this frequency of storms has been observed 6 years in succession. In fact the short-period means for the past 10 years are the same as observed values this September. A monthly storm intensity index was designed by Haggard and Cry [7] to show the relative importance of the tropical storminess for each month. The value computed for this month was exceeded in one-fourth of the Septembers since 1900, and was about normal for recent years.

Tropical storms showed a strong tendency to form in the vicinity of the Antilles this September (fig. 1A). The circulation this month resembled the composite picture found favorable for genesis in this area [1] with a ". . . large circular area of positive anomaly in the central Atlantic with a negative anomaly area cresting across the north. . . . Associated with this anomaly pattern is strong easterly flow at low latitudes. To the northeast of the Antilles the mean wind is 8 m. p. s. from the east; to the northwest 5 m. p. s. from the east. Such a convergent picture may be associated with the deepening of easterly waves in that vicinity." Compare the description of the composite picture with the circulation observed this month (figs. 2, 3A, 3B). The storms (fig. 1B) formed in the vicinity of the mean easterly jet (fig. 3A) with convergence indicated to the north of the Antilles. The tropical storms of the Pacific also apparently developed in the vicinity of the easterly jet. This supports Dunn's thesis [4] that tropical storms *do not* form in the doldrums and is in agreement with Klein's observation [9] of cyclogenesis occurring in the vicinity of jets both in middle latitudes and in subtropical areas. Cyclonic vorticity was also evident in the area of formation, as may be inferred from negative anomaly in figure 2.

Three of this month's storms moved northward in a broad trough and southerly anomalous flow off the east coast of the United States. The relation of these tropical storm tracks to shorter-period mean circulation will be discussed in the next section.

---

[2] In a statistical breakdown of temperatures at a given station, used in the Extended Forecast Section, one-fourth of the cases are in each of three categories (above, normal, and below) and one-eighth of the cases in each of the extreme groups (much above, much below).
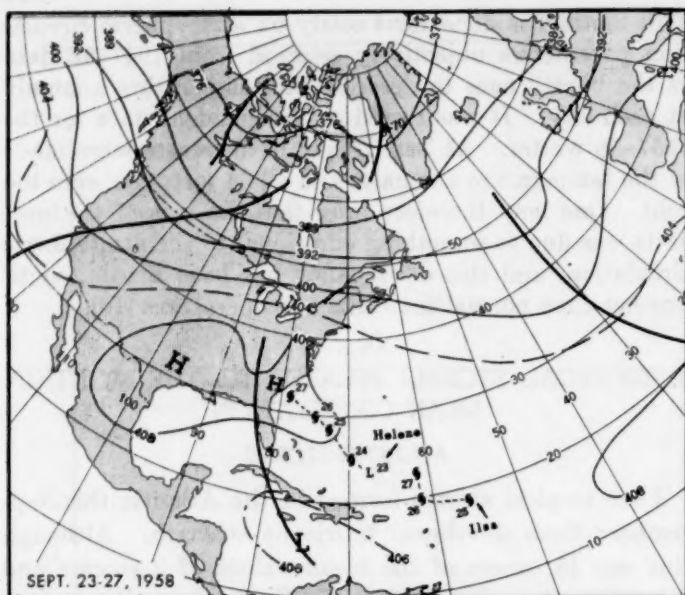
FIGURE 7.—Mean 200-mb. height contours for September 23-27, with tracks of hurricanes Helene and Ilsa superimposed. Helene developed to hurricane strength under northerly flow aloft.

EASTERN PACIFIC

Of interest were the three tropical storms which formed in the eastern Pacific near Mexico (fig. 1B) in an area where heights were considerably below normal (fig. 2). Note the negative anomaly center of 110 ft., the greatest of record for September in this area. All three of the storms were steered quite well by both the mean flow and the anomaly flow, which were in phase over the eastern Pacific. The storm with the long westward track was the only one to attain hurricane strength.

WESTERN PACIFIC

When the month began Typhoon Grace had already formed and was moving through the East China Sea just to the north of Formosa (fig. 1A). It thence recurved, passing into the Yellow Sea to the south of Korea. During September, only three typhoons formed, which was less than the normal for the month [5]. The northward steering of Helen and Ida were well indicated by the southerly flow evident on the monthly mean chart (fig. 2). They both skirted the east shore of Honshu, a common track for typhoons in September [8]. June formed in a rare longitude for typhoons and took an even rarer path, but one which was in accordance with the performance of many storms, moving northward in a mean trough.

5. TROPICAL STORMS RELATED TO THE 5-DAY MEAN CIRCULATIONS

The relationships between tropical storm motion and the circulation [2] are somewhat coarser the longer the time-period involved. When we study shorter-period mean circulations, the dominant features governing the path of the storms are often more evident; but in times of rapid change this is not always the case. Some of the characteristic behavior of hurricanes in relation to the concurrent large-scale circulation patterns can be seen in this section, where each 5-day mean 700-mb. map is discussed in chronological order with respect to the track(s) of the tropical storm(s) of that period.

Ella developed on August 30 in a strong easterly wave. Traveling west-northwestward imbedded in easterly flow (fig. 5A), Ella developed into a hurricane on August 31 west of Puerto Rico. After crossing the southern peninsula of Haiti with winds of 110 m. p. h. on September 1 and causing extensive damage there, the hurricane continued in a track along the southern coast of Cuba. The circulation became disorganized in crossing the Sierra Maestra Range, and the storm never did regain its potency as it once more encountered water in the Gulf of Mexico on the 3d. With no westerly trough to its north, Ella continued its west-northwestward path across the Gulf of Mexico (fig. 5B) entering the southern Texas coast on the 6th. This is an unusual port-of-entry for September storms originating in the Antilles. An additional note concerning Ella: In its first 2 days, the storm moved at a pace more rapid than considered normal, but its speed was justified by the strength of the flow (fig. 5A).

At the time Ella was moving across the Gulf of Mexico, another easterly wave was developing a circulation to the east of the Antilles (fig. 5, A and B). The western lobe of the Bermuda High (fig. 5A) had progressed eastward (fig. 5B), and meanwhile another high center developed in the southeastern United States. Fifi moved on a northwest track until the 9th, heading toward the weak trough between the two Highs, attended by winds reaching 85 m. p. h. on the 6th. Winds weakened thereafter as the circulation aloft was not favorable for continued deepening. The anticyclone in the Atlantic progressed farther eastward and intensified as the wave pattern from the Pacific to the Atlantic amplified (fig. 5C). Fifi recurved as the flow in its environment became more southerly. On the 11th its movement accelerated to the northeast as it moved into the westerlies near Bermuda.

By mid-September, the circulation from the Pacific to the Atlantic had regained its high index characteristics (fig. 5D). On the 13th, Gerda, a weak cyclonic circulation, was estimated to be located about 130 miles west of Martinique. Never developing into much more than a fast-moving, moderately strong, easterly wave, Gerda's track was associated with strong easterly flow at 700 mb. (fig. 5D).

Helene formed in an easterly wave and developed into a storm on the 23d. It took a normal west-northwestward track south of the subtropical High (fig. 5E) and shifted more northwestward as the flow in that area changed (fig. 5F). The storm reached hurricane strength on the afternoon of the 24th when it was under the northerly flow of the anticyclone on the 200-mb. mean chart for the period September 23-27 (fig. 7). This is the divergent condition aloft that Riehl considers important for the deepening of tropical storms [14]. Helene's northwestward track until the 26th may have been motivated by height rises at 500 mb. in the Northeast on the 23d and

24th associated with energy dispersion out of a deepening trough in the Central Pacific (cf. fig. 5, E and F).[3] The rapidly changing broad-scale circulation underwent another fluctuation as heights fell strongly on the 26th at 70° and 80° W. as a trough approached the east coast. Against this background hurricane Helene started its recurve (fig. 5G), which sharpened on the 27th as the trough pushed through the Northeast. Helene sped northward contributing cyclonic vorticity to the Low south of Greenland (fig. 5, G and H).

Ilsa formed shortly after Helene in the same general area and moved eastward initially, its path paralleling that of its predecessor. Ilsa reached hurricane strength on the 25th; its deepening cannot be related to the mean 200-mb. chart (fig. 7), but the daily charts showed it to be in a favorable location with respect to a high-level anticyclone. On the 26th Ilsa curved sharply to the north in response to the falling away of heights in the north (previously discussed in the case of Helene) and continued to deepen, its wind speeds reaching 140 m. p. h. Associated with falling heights was the acceleration of a trough in eastern Canada eastward into the Davis Straits to amalgamate with a negatively tilted trough in the eastern Atlantic (fig. 5, F and G). This allowed the subtropical anticyclone to progress eastward and heights built in the western Atlantic behind the trough (fig. 5, G and H). Increased meridional flow in the Atlantic shifted the course of Ilsa to the north and then to the northeast as it entered the fast westerlies to the north. Ilsa lost its identity as an individual circulation on the morning of the 30th as the circulation of Helene engulfed it.

REFERENCES

1. E. M. Ballenzweig, "Formation of Tropical Storms Related to Anomalies of the Long-Period Mean Circulation," *National Hurricane Research Project Report* No. 21, U. S. Weather Bureau, September 1958, 16 pp.
2. E. M. Ballenzweig, "Relation of Long-Period Circulation Anomalies to Tropical Storm Formation and Motion," *Journal of Meteorology*, (to be published).

[3] Height changes at 500 mb. not reproduced.

3. California Cooperative Oceanic Fisheries Investigations, "1957—The Year of Warm Water and Southern Fish Off the California Coast," *Commercial Fisheries Review*, vol. 20, No. 9, Sept. 1958, pp. 15–24.
4. G. E. Dunn, "Areas of Hurricane Development," *Monthly Weather Review*, vol. 84, No. 2, Feb. 1956, pp. 47–51.
5. G. E. Dunn, "Tropical Cyclones," *Compendium of Meteorology*, American Meteorological Society, Boston, 1951, pp. 887–901.
6. A. F. Gorton, "Pacific Ocean Indications of California Seasonal Precipitation," *Proceedings of the Fifth Pacific Science Congress*, vol. 3, 1933, pp. 1767–1773.
7. W. H. Haggard and G. W. Cry, "A Climatological Index for North Atlantic Tropical Storm Activity," Paper presented at Hurricane Technical Conference, Miami Beach, Fla., November 20, 1958.
8. H. F. Hawkins, Typhoon Tracks in the Western Pacific Area, unpublished manuscript, U. S. Weather Bureau, July 1945.
9. W. H. Klein, "The Frequency of Cyclones and Anticyclones in Relation to the Mean Circulation," *Journal of Meteorology*, vol. 15, No. 1, Feb. 1958, pp. 98–102.
10. W. H. Klein, B. M. Lewis, and I. Enger, Objective Prediction of Five-Day Mean Temperatures During Winter, Manuscript in preparation, U. S. Weather Bureau, 1958.
11. J. Namias, "The Meteorological Picture, 1957–58," Paper presented at the Symposium on the Years of Change—1957–58, held at Rancho Santa Fe, N. Mex., June 2–4, 1958.
12. J. F. O'Connor, "The Weather and Circulation of June 1958—Record Cold in Northeast and Warmth in Northwest," *Monthly Weather Review*, vol. 86, No. 6, June 1958, pp. 229–236.
13. D. A. Richter and R. A. Dahl, "Relationship of Heavy Precipitation to the Jet Maximum in the Eastern United States, September 19–21, 1958," *Monthly Weather Review*, vol. 86, No. 9, Sept. 1958, pp. 368–376.
14. H. Riehl, "Formation of Hurricanes," *Final Report of the Caribbean Hurricane Seminar Held at Ciudad Trujillo, D. N., Dominican Republic, February 16–25, 1956*, Ciudad Trujillo, 1956, pp. 69–79.
15. P. Stark, "The Weather and Circulation of April 1958," *Monthly Weather Review*, vol. 86, No. 4, Apr. 1958, pp. 132–140.
16. H. B. Stewart, Jr., B. D. Zetler, and C. B. Taylor, "Recent Increase in Coastal Water Temperatures and Sea Level, California to Alaska," U. S. Coast and Geodetic Survey, *Technical Bulletin* No. 3, May 1958, 11 pp.
17. C. M. Woffinden, "The Weather and Circulation of August 1958—A Month With an Unusual Temperature Reversal," *Monthly Weather Review*, vol. 86, No. 8, Aug. 1958, pp. 312–318.

RELATIONSHIP OF HEAVY PRECIPITATION TO THE JET MAXIMUM IN THE EASTERN UNITED STATES, SEPTEMBER 19-21, 1958

DONALD A. RICHTER AND ROY A. DAHL

National Weather Analysis Center, U. S. Weather Bureau, Washington, D. C.

1. INTRODUCTION

During September 19–21, 1958, precipitation, which had been occurring in rather large amounts over the western Gulf States, began spreading northeastward through the Ohio River Valley without benefit of any marked surface cyclogenesis. This paper analyzes the relationship between the rainfall pattern and the progression of wind maxima along the jet.

In addition, the paper investigates a semi-objective method for 24-hour quantitative precipitation forecasting using vertical motion charts of the Joint Numerical Weather Prediction (JNWP) Unit. This method of quantitative precipitation forecasting was developed on an experimental basis by Gilman et al. [1] and has been adopted by the National Weather Analysis Center (NAWAC) with some modifications aimed at reducing the time consumed in lengthy computation.

2. SYNOPTIC SITUATION

At the surface at 1200 GMT, September 19, 1958 (fig. 1A), a fairly large ridge extended from eastern Canada south-southwestward to the Central States and a weak stationary front stretched across the northern Gulf of Mexico. Another very weak and diffuse stationary front extending north-south through the Plains States was subsequently frontolized because of lack of thermal support (note superimposed thickness lines). Meanwhile, a strong maritime polar front had entered the Pacific Northwest.

At 500 mb. (fig. 1B), a ridge lay over the Ohio Valley in a position similar to that of the surface High and a trough extended from the Dakotas southward through New Mexico. Farther west a pronounced short-wave trough accompanying the surface system was located just off the west coast.

Twelve hours later (fig. 2B), the western trough had progressed inland to the Rocky Mountains. The height rises induced in the ridge ahead of this trough had caused the trough previously located over the Plains States to fill and move eastward more rapidly in the northern portion, thus to shear off from the southern portion of the trough. A weak Low appeared to be forming just east of Amarillo, Tex., and the downstream ridge moved eastward over the Appalachian Mountains.

At the surface (fig. 2A) a poorly defined area of cyclogenesis appeared in eastern Texas in conjunction with the cutoff 500-mb. Low forming near Amarillo.[1] A general katabaric area of 4 mb. per 12 hours covered the entire Mississippi Valley as the ridge of high pressure moved toward the Atlantic coast; larger pressure falls occurred in the Northern Plains States ahead of the approaching maritime polar system.

At 1200 GMT, September 20 (fig. 3A), the diffuse Low in the Gulf States which had moved rather slowly during the preceding 12 hours was near the Louisiana-Texas border, and the High lay over the east coast. Meanwhile, the maritime polar system in western United States had been steadily advancing eastward and was situated in the eastern Dakotas.

Concurrently, the westernmost trough at 500 mb. (fig. 3B) had progressed east of the Continental Divide and a more definite Low in association with the surface system in the Lower Mississippi Valley region had appeared in southwestern Missouri.

By 0000 GMT, September 21 (fig. 4A), the Gulf States surface Low had moved quite rapidly and become better defined over Kentucky, even though very little deepening had occurred possibly due to the absence of thermal advection. The ridge to the east was now off the Atlantic coast and the advancing maritime polar front was steadily narrowing the distance between itself and the Low in Kentucky.

The associated trough and Low at 500 mb. (fig. 4B) had been forced to accelerate northeastward to a position just south of Lake Michigan as a result of the more vigorous and relatively fast-moving trough now over the Northern and Central Plains States. Twelve hours later, at 1200 GMT, September 21 (fig. 5B), all that remained of the first short-wave trough was a minor indentation over Lake Erie in the general circulation of the more pronounced trough over the Minnesota-Iowa area.

The conditions that existed at the 500-mb. level were reflected at the surface (fig. 5A). The Low near Pittsburgh, Pa., had deepened several millibars, and was moving northward toward the region of falling pressures preceding the maritime polar system approaching from the west. Subsequent maps at both the surface and 500 mb.

---

[1] If the remnant of tropical storm Gerda [2], which had weakened from a closed circulation to an easterly wave near Jamaica 4 days earlier, had moved at approximately the speed indicated by continuity, its location near eastern Texas at this time conceivably could have been the triggering device for cyclogenesis. However, lack of surface ship reports in the Gulf of Mexico and the diffuse character of the easterly wave made tracking the storm from chart to chart extremely difficult.
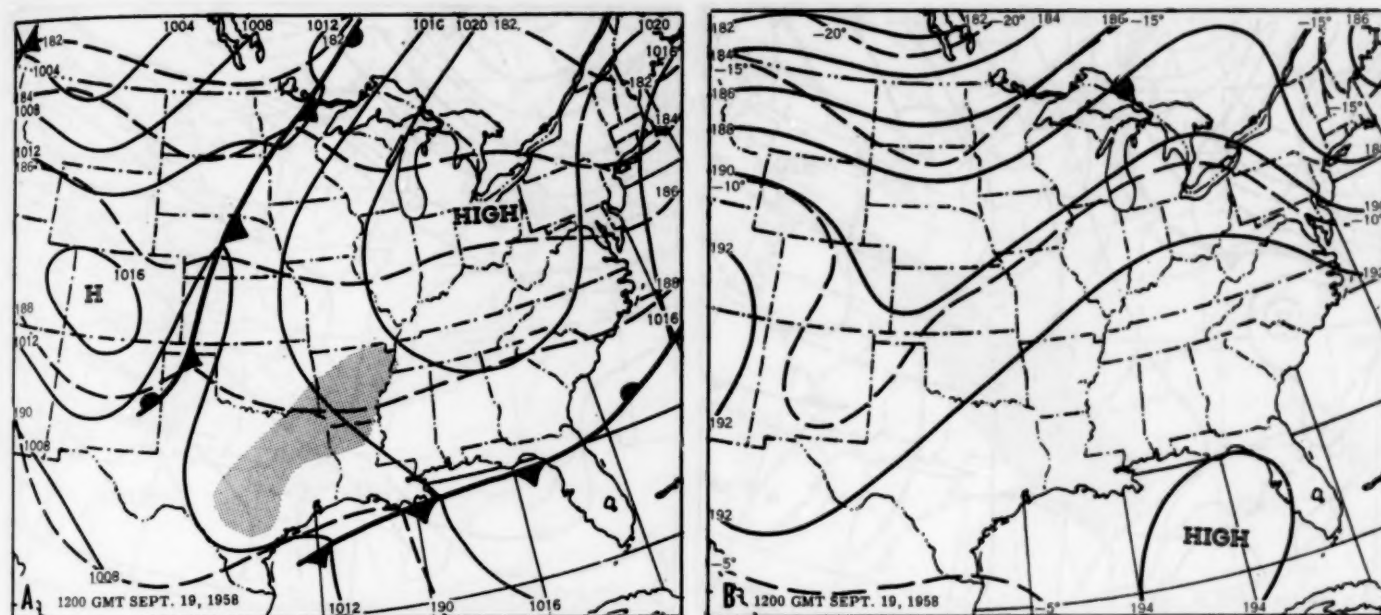
FIGURE 1.—1200 GMT, September 19, 1958. (A) Surface synoptic chart with superimposed 1,000–500-mb. thickness lines (dashed) in hundreds of geopotential feet. Shaded areas correspond to current precipitation. (B) 500-mb. contours (solid lines in intervals of 200 geopotential feet) and isotherms (dashed lines in ° C.).
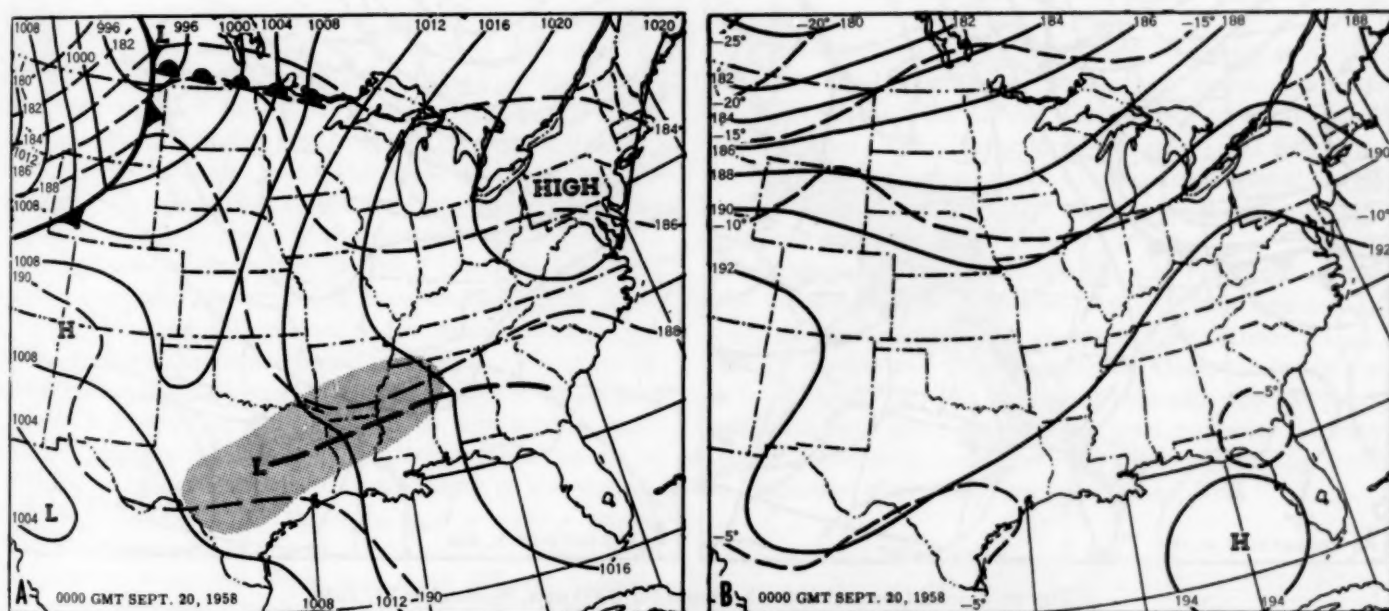

FIGURE 2.—Surface and 500-mb. charts for 0000 GMT, September 20, 1958.

(not shown) revealed that this small cyclone was eventually absorbed into the more dominant, larger-scale circulation. It is noteworthy how much stronger was the thermal advection associated with the maritime polar front in the Northern Plains States than the thermal advection of the weaker low pressure system.

3. RELATIONSHIP OF PRECIPITATION TO ADVECTION OF RELATIVE VORTICITY

In this section, we briefly summarize some relationships between vorticity advection and precipitation areas,

based on a study by Riehl et al. [3]. These relationships, which will serve in section 4 as a basis for discussing effects of the jet stream on precipitation, are:

1. Advection of cyclonic vorticity, that is, flow across the gradient of vorticity from regions of greater to lesser cyclonic relative vorticity, results in divergence aloft which leads to upward vertical motion, a necessary condition for pressure falls and/or precipitation.

2. The vorticity distribution in a wave in the mid-troposphere zonal westerlies—cyclonic relative vorticity in the trough and anticyclonic relative vorticity on the
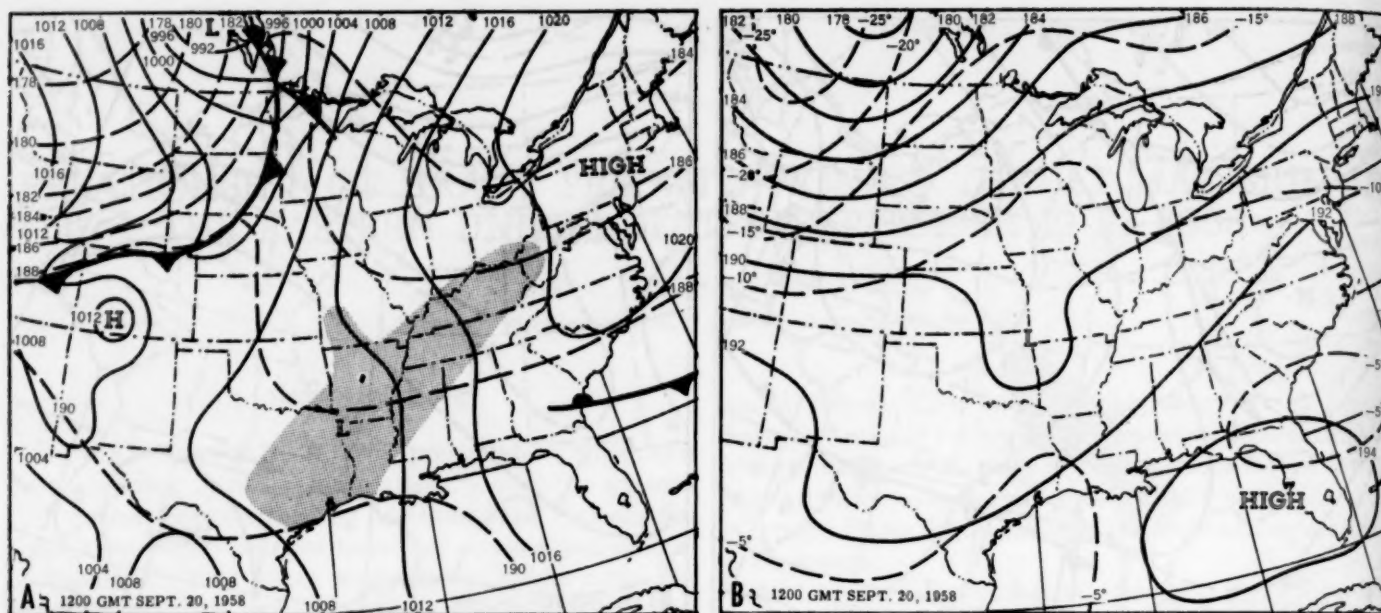
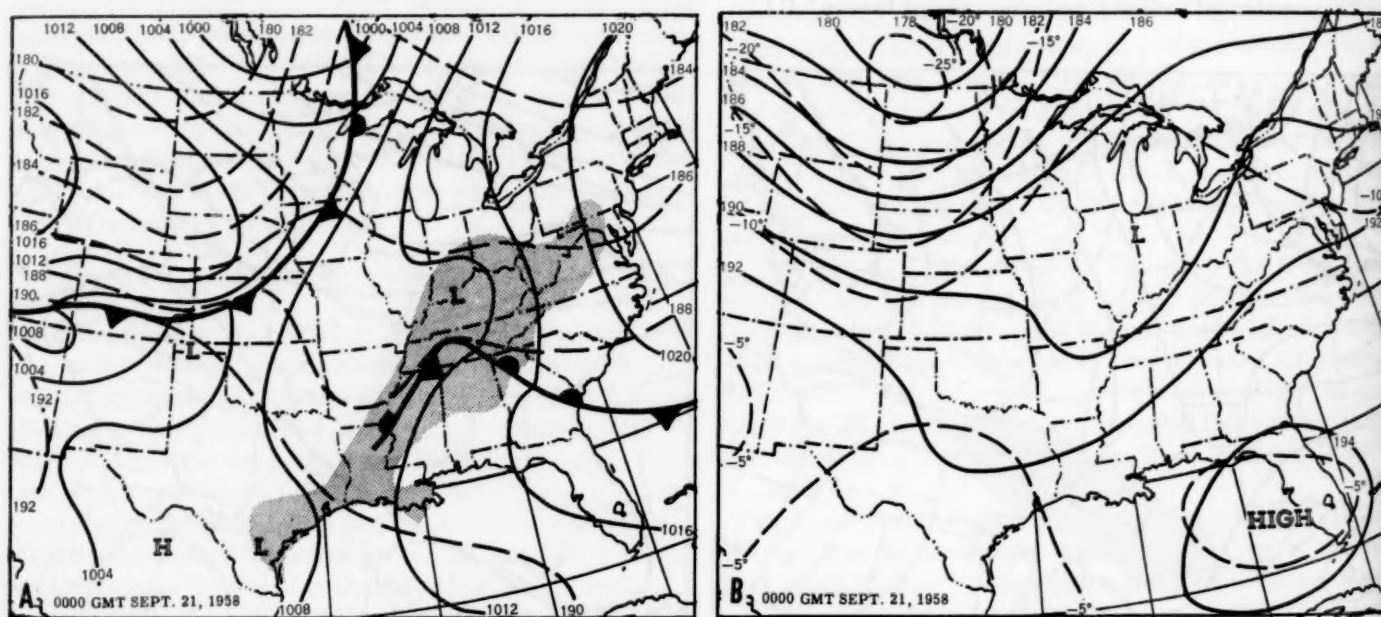FIGURE 3.—Surface and 500-mb. charts for 1200 GMT, September 20, 1958.

FIGURE 4.—Surface and 500-mb. charts for 0000 GMT, September 21, 1958.

ridge—makes the area between the trough and the ridge favorable for precipitation.

3. The vorticity distribution around a wind maximum in the jet stream similarly indicates areas of cyclonic relative vorticity advection and therefore potential precipitation.

Riehl [4] has developed a model for the distribution of vorticity around a wind maximum in the jet stream. Assuming no curvature, relative vorticity is a function only of the wind shear (cf. [5]). From figure 6 it is evident that the cyclonic wind shear is greatest to the north and the anticyclonic wind shear greatest to the south of the wind maximum, and both decrease upstream and down-

stream. Therefore, the flow is from greater to lesser cyclonic relative vorticity in quadrant 1 and from lesser to greater anticyclonic relative vorticity in quadrant 3. These quadrants thus have the requisite advection of cyclonic relative vorticity for upward vertical motion leading to precipitation. In quadrants 2 and 4 the advection is reversed and conditions are considered unfavorable for precipitation.

4. EFFECTS OF JET ON PRECIPITATION

In the lower troposphere conditions were extremely favorable for precipitation during the entire period under
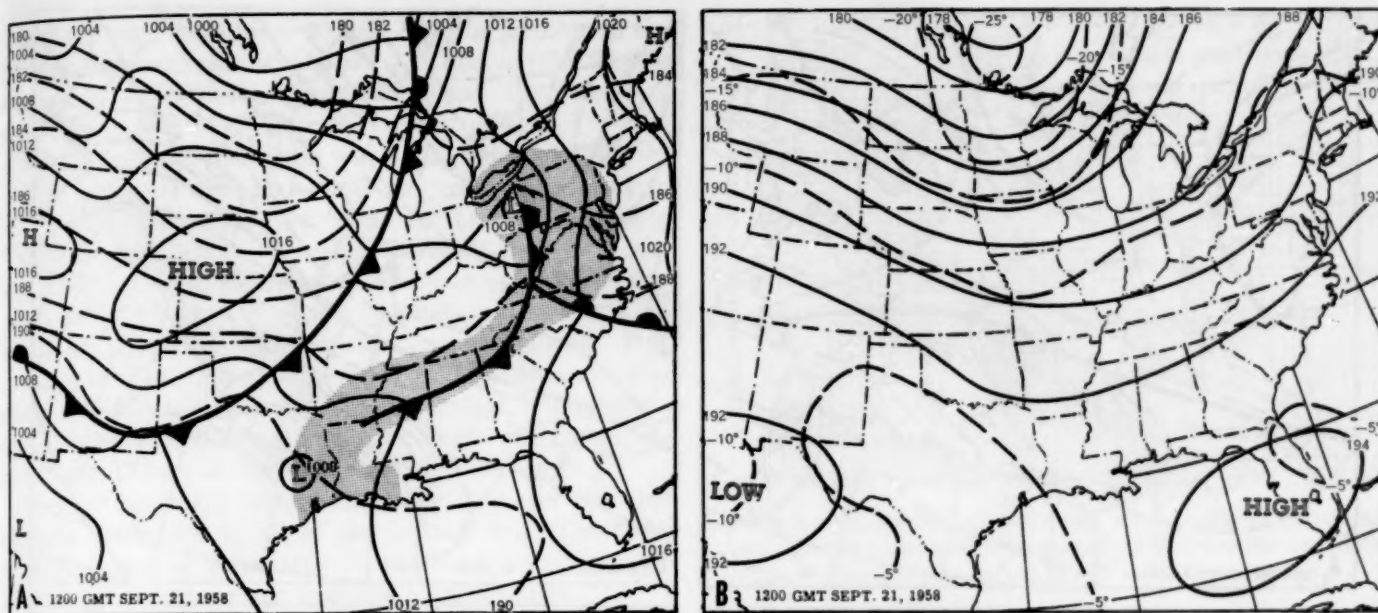
FIGURE 5.—Surface and 500-mb. charts for 1200 GMT, September 21, 1958.

study [6]. The moisture content of the atmosphere over the western Gulf States was near saturation (see fig. 9B) and the stability index chart (not shown) indicated the mT airmass was fairly unstable [7]. The low-level southerly flow from the Gulf of Mexico during the period had absorbed much moisture and was directed normal to the temperature gradient (note thickness lines on surface chart, fig. 1A), ensuring continuous warm air advection and low-level convergence in the western Gulf States.

At 1200 GMT, September 19 (fig. 7A), a jet with two distinct wind maxima extended from southern New Mexico through northern Tennessee to the Atlantic Coast near the North Carolina-South Carolina border. The position of the current rainfall over Arkansas, northern Louisiana, and northeastern Texas in relation to the definite wind maximum on the jet axis near Nashville, Tenn. could be described as being in quadrant 3 according to the scheme of figure 6; in figure 7A this quadrant is over a region where the surface isobars had no curvature. The active precipitation in central Texas was more difficult to associate with favorable high-level conditions. While the isotach analysis on the jet chart indicated another wind maximum, which incidentally remained generally near the New Mexico-Texas border throughout the entire 3-day period, it was considered to be in an unfavorable position (quadrant 4) for explaining that rainfall area.

The corresponding surface map (fig. 1A) shows weak cyclonic curvature of the isobars in southeastern Texas. As the air from the Gulf of Mexico moved over land, the increased friction caused the wind to blow across the isobars at a greater angle, thereby creating low-level convergence and upward vertical motion and thus abetting showers [8]. These tropical-like showers, which could have been enhanced by some undetected impulse of low-level vorticity advection from the remains of Gerda, were

apparently not affected by conditions in the upper troposphere.

Twelve hours later, at 0000 GMT, September 20 (fig. 7B), the wind maximum, which was previously near Nashville, Tenn., had moved northward and wind speeds had increased. The intensity of the associated precipitation had increased as is shown by the superimposed 2-inch isohyet representing the latest 12-hour total amounts ending at the synoptic time.

Once again there was the problem of rationalizing the rains in eastern Texas because the jet chart again indicated decreasing anticyclonic shear downstream; i. e., unlikely conditions for precipitation. Observations of the sea level chart (fig. 2A), on the other hand, showed practically the same picture as the previous map with perhaps a slight increase in low-level convergence resulting from the formation of a weak Low near Waco, Tex.
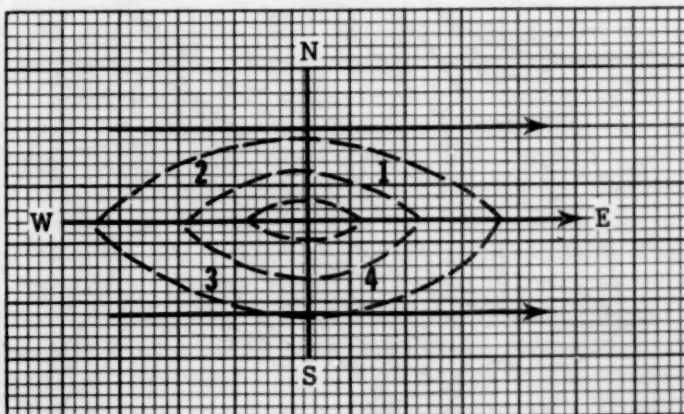

FIGURE 6.—Model for distribution of vorticity around a wind maximum in the jet stream. Streamlines (solid lines), isotachs (dashed lines).
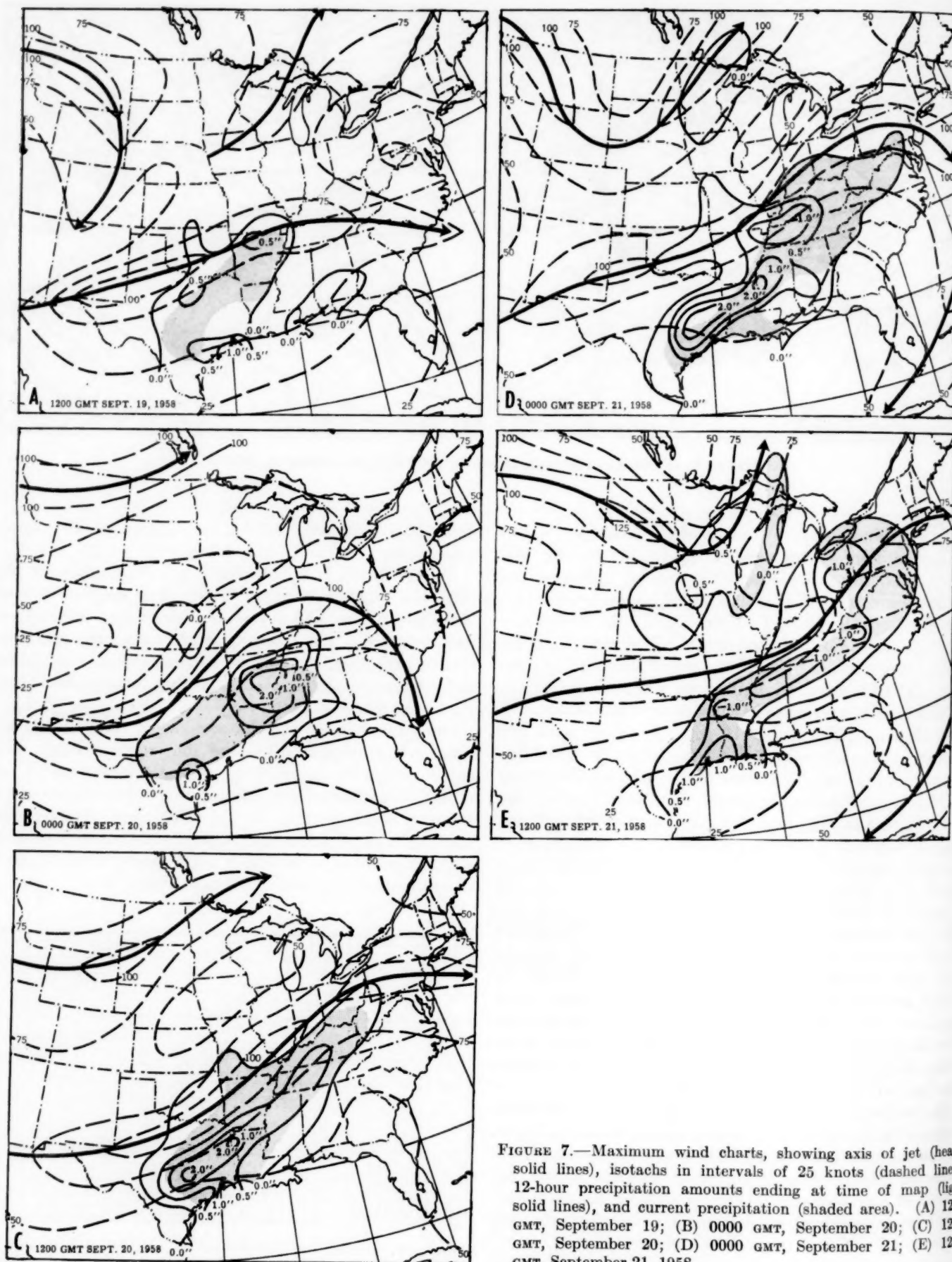
FIGURE 7.—Maximum wind charts, showing axis of jet (heavy solid lines), isotachs in intervals of 25 knots (dashed lines), 12-hour precipitation amounts ending at time of map (light solid lines), and current precipitation (shaded area). (A) 1200 GMT, September 19; (B) 0000 GMT, September 20; (C) 1200 GMT, September 20; (D) 0000 GMT, September 21; (E) 1200 GMT, September 21, 1958.

At 1200 GMT, September 20 (fig. 7C), the position of the jet and the maximum winds along it had moved farther northward to central Pennsylvania and the rain had spread into southern Ohio and western West Virginia. A second region of maximum winds was found over southeastern Missouri with its associated current precipitation and heavy 12-hour amounts over the Lower Mississippi Valley located in the favorable quadrant 3. (It is not the intention of the authors to discount completely any relationship whatsoever of the precipitation to the wind maximum in certain areas of the previous charts. But rather, there were no doubt several wind maxima running along the jet, and the lapse in time between observations and the distance between reporting rawin stations made detection of these oscillations nearly impossible [9].)

The corresponding surface chart (fig. 3A) now revealed cyclonic curvature in all of the isobars from the Low, which had moved northeastward to near Shreveport, La., to the high pressure ridge over the Atlantic coast.

At 0000 GMT, September 21 (fig. 7D), the previous two separate wind maxima consolidated into a single maximum located over eastern Pennsylvania-New Jersey. Again the precipitation belt was in quadrant 3, extending eastward to western Virginia, western Maryland, and southern Pennsylvania. The 1-inch isohyet over western Kentucky and western Tennessee, representing the area of heaviest 12-hour rainfall amounts, was also in that favorable position for nearly the entire half-day period. Of course it should be noted that the surface Low (fig. 4A), then located over western Kentucky with still a weak but definite closed circulation, moved directly over this rainfall area; the increased low-level convergence certainly increased the total precipitation. The rains in northern Mississippi and Louisiana, doubtless under the influence of the jet for a good part of the period, were interspersed with regions of thunderstorm activity, thus accounting for that precipitation maximum. Concurrently, a weak tropical depression had entered the southern Texas coast causing considerable rainfall and in turn, the third maximum 12-hour rainfall area in southeastern Texas.

During the next 12 hours, the precipitation spread northeastward to western New York and New Jersey (fig. 5A) in association with the now more pronounced Low over southwestern Pennsylvania. The corresponding jet map (fig. 7E), showed current rainfall amounts of any consequence to be north of the axis of highest winds for the first time. It must be remembered, however, that the surface system was by that time occluded, and the jet, which previously had been found exclusively north of the Low, was dropping southward. The jet eventually crossed the occluded front but still remained north of the warm and cold fronts, a usual occurrence according to Vederman's [10] idealized model relating the life cycle of extratropical cyclones to the jet. A second wind maximum over southern Kentucky accounted for the precipitation in Tennessee, northern Alabama, northern Mississippi, and southeastern Arkansas. Since the rainfall in Louisiana and eastern Texas was not associated with the jet, we
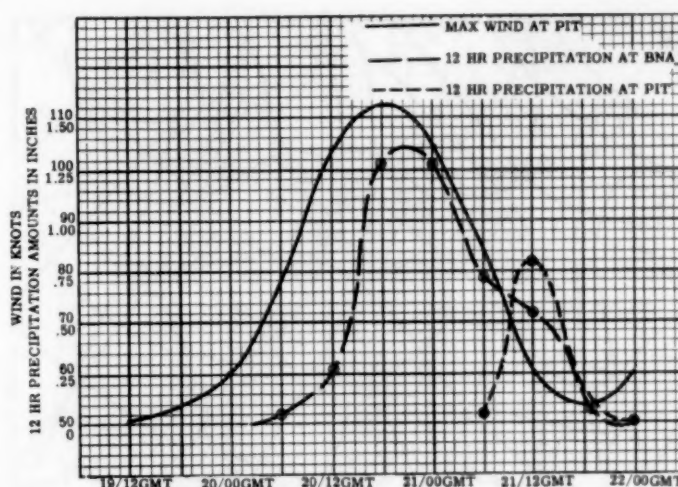

FIGURE 8.—Comparison of maximum wind profile at Pittsburgh with 12-hour accumulated precipitation at Nashville and Pittsburgh. (Precipitation plotted at end of 12-hour periods.)

refer to the surface chart (fig. 5A). The precipitation was caused by the abundant moisture and low-level convergence being propagated northeastward by the weak tropical Low located in eastern Texas.

At 0000 GMT, September 22 (chart not shown), as the sea level Low previously near Pittsburgh, Pa., was absorbed into the general circulation of the polar system to its west, the associated jets amalgamated over the northeastern United States. The southernmost jet then dissipated in the Central Mississippi Valley region and the precipitation over the Gulf States eventually tapered off to some scattered showers along the gulf coast itself.

Figure 8 illustrates the relationship with time of the jet maximum at Pittsburgh, Pa., to the 12-hour precipitation at Nashville, Tenn. The relationship is consistent with Riehl's quadrant 3 position as being a likely location for the heaviest amounts of precipitation to occur. Since Nashville is approximately 400 miles southwest of Pittsburgh, Nashville's 12-hour precipitation amounts reached a peak at nearly the same time as the wind in the jet core over Pittsburgh attained its highest speed; that is, the rainfall maximum lagged the jet maximum with time. This relationship can better be seen by noting the lag of about 18 hours between the wind maximum and the precipitation maximum observed at Pittsburgh.

There was also a noticeable difference in the peak amounts of observed 12-hour rainfall at Nashville and Pittsburgh even though the available precipitable water over both of these cities was the same at their respective times. Comparison of figures 7D and 7E over the northeastern United States reveals a marked reduction in the speed of the wind maximum and also in the velocity gradient south of the jet in the 12-hour period. Thus the half-inch difference in peak precipitation totals could be attributed to the decrease in the gradient of wind shear and therefore of vorticity advection.
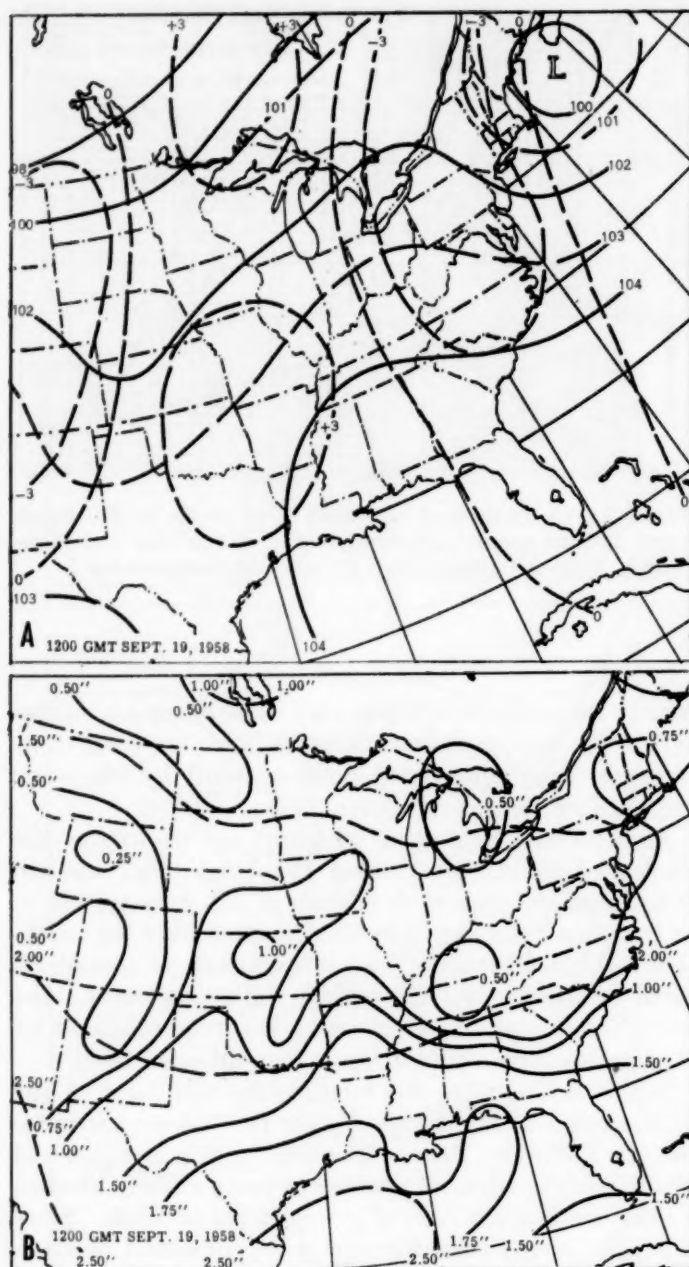
FIGURE 9.—1200 GMT, September 19, 1958. (A) 700-mb. chart, with contours (solid lines) in hundreds of geopotential feet, and vertical motion isolines (dashed) in millimeters per second. (B) Precipitable water chart. Available moisture isolines (solid) in inches. Saturation isolines (dashed) in inches.

5. TEST OF A METHOD OF FORECASTING 24-HOUR QUANTITATIVE PRECIPITATION

A procedure for forecasting quantitative precipitation, based mainly on surface considerations and requiring 3 hours to complete, was developed by the Hydrometeorological Section and tested by some of its members [1]. NAWAC has adopted a part of this procedure, namely, the relationship which exists among the expected area of precipitation, the inflow area, the available moisture, and the efficiency factor. The procedure below, while not pre-

sented as an improvement on the original method, incorporates some time-saving modifications that were necessary for the procedure to be operationally successful at NAWAC. These include the use of the initial and prognostic 700-mb. charts, the current and prognostic JNWP vertical motion charts, and the 1,000–500-mb. precipitable water chart. Consequently, the procedure as presented here involves the following parameters: (1) the area of expected 24-hour precipitation, A_p; (2) the area of 24-hour inflow at the 700-mb. level, A_i; (3) the 1,000–500-mb. mean available moisture, $\overline{W}$, over both the precipitation and inflow areas; and (4) the efficiency factor.

With minor refinements, the +3 mm./sec. vertical motion isoline was related to the area of expected precipitation. For example, on the initial vertical motion chart (fig. 9A) the area enclosed by the +3 mm./sec. isoline, minus that portion where a dry tongue of air extended southward over Oklahoma (fig. 9B), corresponded to the initial precipitation area (fig. 1A). The 24-hour precipitation area, A_p, then became the area swept out by the refined area enclosed by the +3 mm./sec. isoline on the initial vertical motion chart plus that area enclosed by the +3 mm./sec. isoline on the prognostic vertical motion chart. The 24-hour inflow area, A_i (fig. 10A), was determined by going upstream on the 700-mb. chart a calculated distance based on the expected 24-hour mean wind at the rear of A_p. For example, a 20-knot mean wind at the rear of A_p would correspond to an inflow area having a penetration of 480 nautical miles or 8 degrees of latitude into the airmass to the rear of A_p.

The dimensions of A_p and A_i are unimportant because all that is needed is a proportional relationship. In this situation a sheet of graph paper was placed over A_i and A_p and the squares covering each of these areas counted. The totals were 38 for A_p and 27 for A_i. Then, by placing the area represented by both A_p and A_i over the initial precipitable water chart an average value of the available moisture, $\overline{W}$, was computed to be 1.55 inches. Assuming that all of the available moisture will fall out, we apply the formula $\overline{W}(A_p+A_i)/A_p$ to obtain the average expected precipitation, which in this case was 2.65 inches per 24 hours. But, since we know from experience that not all of the available moisture does fall out, a highly subjective efficiency factor must be introduced. In this case an efficiency factor of 55 to 60 percent was suggested which reduced the 2.65-inch average over A_p to a more realistic 1.5 inches.

The efficiency factor is of critical importance to the success of this particular quantitative precipitation forecast method. Limited testing has indicated that the value of the efficiency factor should be near 50 percent most of the time, but may approach 100 percent for very small areas of expected precipitation which are located in and downstream from regions containing large amounts of available moisture. The efficiency factor drops off for large areas of expected precipitation, areas of low available moisture, and for airmasses with moisture concentration at high levels. The stability of the airmass must also

influence the efficiency factor, but this effect is unknown at this time.

The maximum precipitation area, P_m (fig. 10A) is defined as that portion of A_p enclosed by the isohyet of the average value. Recent studies at NAWAC concerning summertime-type precipitation areas suggest that the depth-distance curves should approximate the "normal" curve and that the mean isohyet should enclose the central one-fifth to one-sixth of the total precipitation area. Wintertime-type precipitation areas would logically have a more uniform precipitation distribution and, consequently, a larger centrally located P_m relative to the total precipitation area. Since the precipitation area under discussion was definitely a summertime-type, the 1.5-inch isohyet might be expected to enclose the central one-fifth to one-sixth portion of A_p. However, a refinement became apparent since the +3 mm./sec. vertical motion line enclosed part of the southwestern portion of A_p for the entire 24-hour period, and, for this reason, P_m was shifted toward the southwest from the geometric center.

The correlation of both A_p and P_m with precipitation which actually occurred (fig. 10B) was reasonably good, although both were displaced slightly to the east of the verification area. The error apparently developed because the +3 mm./sec. vertical motion isoline progressed more rapidly than did the higher available moisture values. Further refinements could make this forecast method more accurate, but time-consuming modifications would detract from its usefulness at NAWAC.

6. CONCLUSIONS

The authors do not intend to minimize the value of generally recognized tools for forecasting cloudiness, precipitation, and the movement and subsequent deepening of extratropical wave cyclones. We do feel, however, that there is much merit in using maximum wind forecasts along the jet as an additional means of arriving at regions of expected rainfall. Since there is a definite time lag between wind maxima and precipitation maxima at a given location, the problem becomes one of determining the approximate elapsed interval between the two maxima or of correlating the distance between the wind maximum at one station and the precipitation maximum at another.

The semi-objective quantitative precipitation forecast method presented in this article is based on limited testing, and quite certainly improvements of the subjective techniques advanced here will result from further usage. The immediate benefit from this method will be improved forecasting of the magnitude and the location of the 24-hour maximum precipitation area. At NAWAC established procedures for precipitation forecasting, especially in rain or no-rain situations with respect to time, will continue to be based primarily on the prognostic patterns of the respective surface and 500-mb. charts.
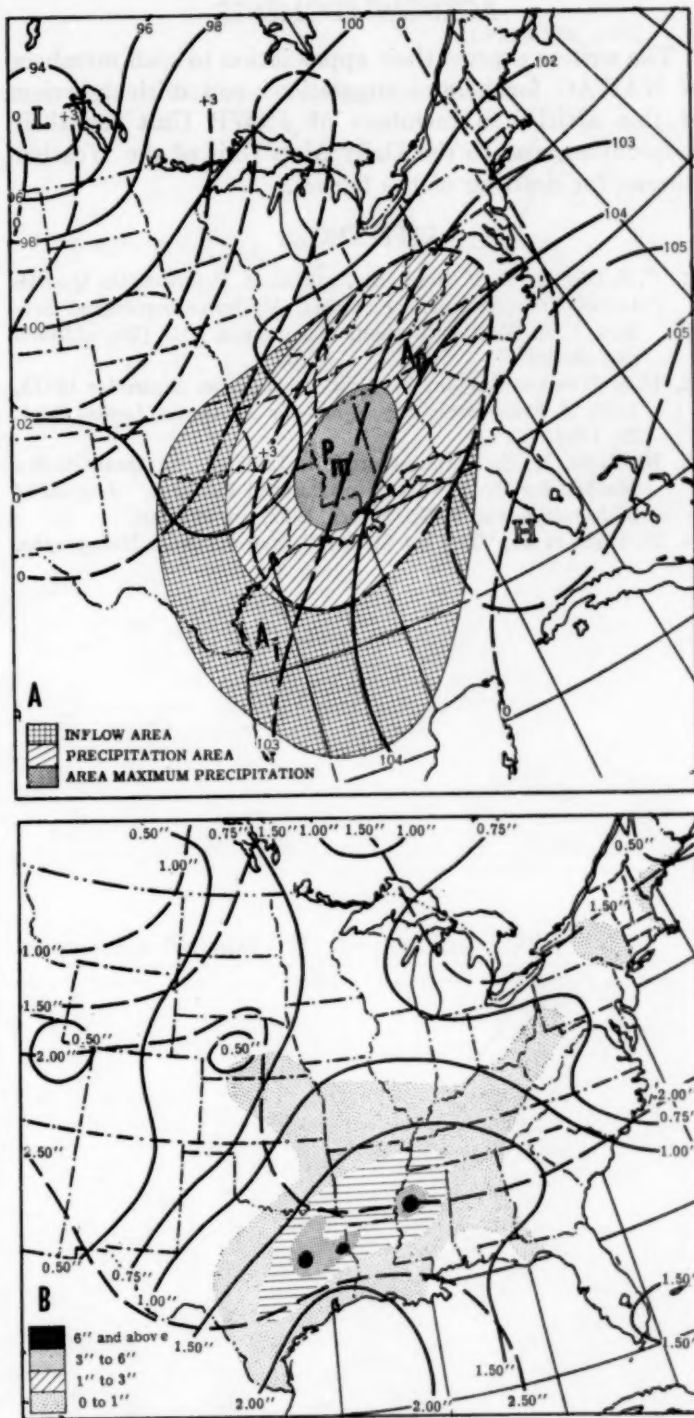

FIGURE 10.—1200 GMT, September 20, 1958. (A) 700-mb. chart with contours (solid lines) in hundreds of geopotential feet. Vertical motion isolines (dashed) in millimeters per second. A_p represents area of expected 24-hour precipitation ending at 1200 GMT, September 20. A_i represents area of expected 24-hour inflow ending at 1200 GMT, September 20. P_m shows area of expected maximum 24-hour rainfall ending at 1200 GMT September 20, 1958. (B) Precipitable water chart. Available moisture isolines (solid). Saturation isolines (dashed). Isohyetal lines represent 24-hour precipitation amounts ending at 1200 GMT, September 20, 1958.

ACKNOWLEDGMENTS

REFERENCES

1. C. S. Gilman, H. V. Goodyear, and K. R. Peterson, On Quantitative Precipitation Forecasting, Hydrometeorological Section, U. S. Weather Bureau, Washington, 1958 (Unpublished manuscript).

2. U. S. Weather Bureau, *Tropical Storm Gerda, September 13–15, 1958, A Preliminary Report and the Advisories Issued*, Sept. 30, 1958.

3. H. Riehl, K. S. Norquest, and A. L. Sugg, "A Quantitative Method for the Prediction of Rainfall Patterns," *Journal of Meteorology*, vol. 9, No. 5, Oct. 1952, pp. 291–298.

4. H. Riehl et al., "The Jet Stream," *Meteorological Monographs*, vol. 2, No. 7, American Meteorological Society, August 1954, 100 pp.

5. H. Panofsky, *Introduction to Dynamic Meteorology*, The Pennsylvania State University, University Park, Pa., 1956, 243 pp.

6. S. Teweles, Jr., "A Test of the Relation Between Precipitation and Synoptic Patterns at 200 and 300 Millibars," *Journal of Meteorology*, vol. 10, No. 6, Dec. 1953, pp. 450–456.

7. V. J. Oliver and R. F. Shaw, "Heavy Warm-Sector Rains from Illinois to the Middle Atlantic Coast, May 26–28, 1956," *Monthly Weather Review*, vol. 84, No. 5, May 1956, pp. 198–204.

8. S. Petterssen, *Weather Analysis and Forecasting*, vol. II, McGraw-Hill Book Co., Inc., New York, 1956.

9. J. Badner and M. A. Johnson, "Relationship of Tropopause and Jet Streams to Rainfall in Southeastern United States, February 4–9, 1957," *Monthly Weather Review*, vol. 85, No. 2, Feb. 1957, pp. 62–68.

10. J. Vederman, "The Life Cycles of Jet Streams and Extratropical Cyclones," *Bulletin of the American Meteorological Society*, vol. 35, No. 6, June 1954, pp. 239–244.

Chart I.   A. Average Temperature (°F.) at Surface, September 1958.
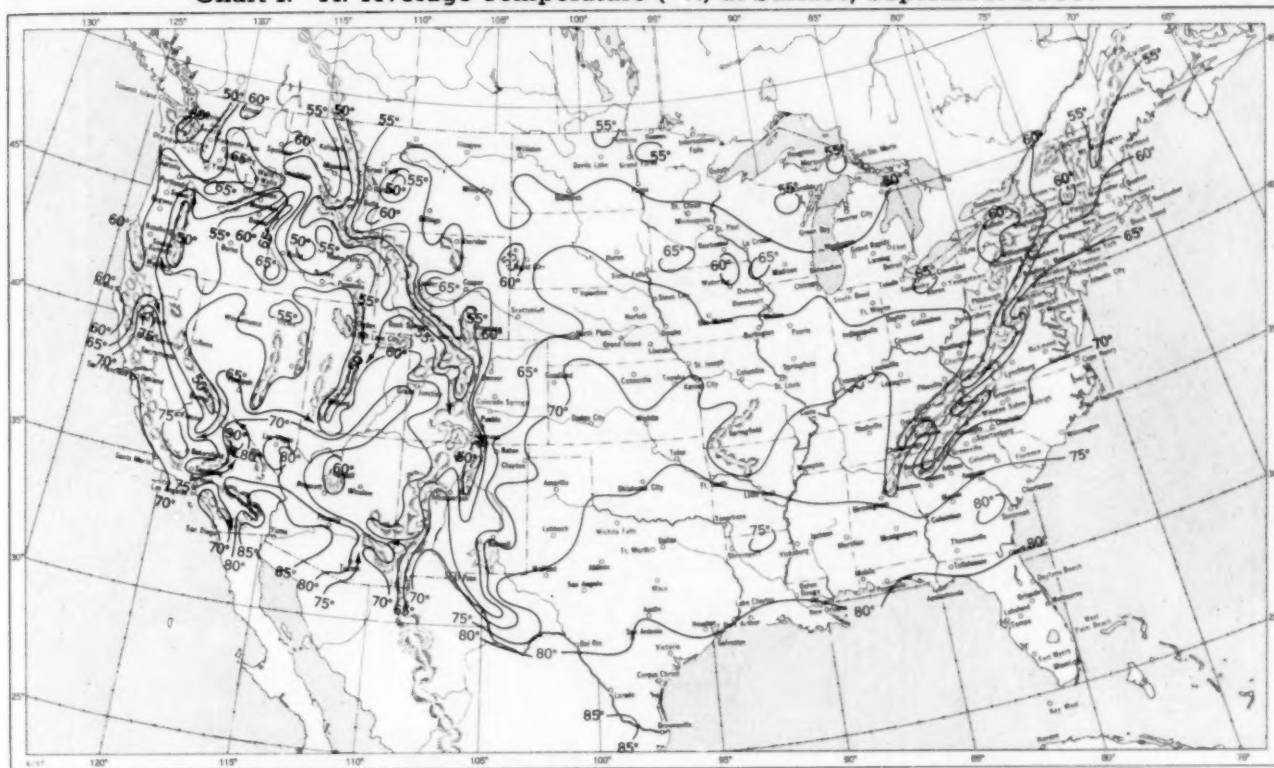
B. Departure of Average Temperature from Normal (°F.), September 1958.
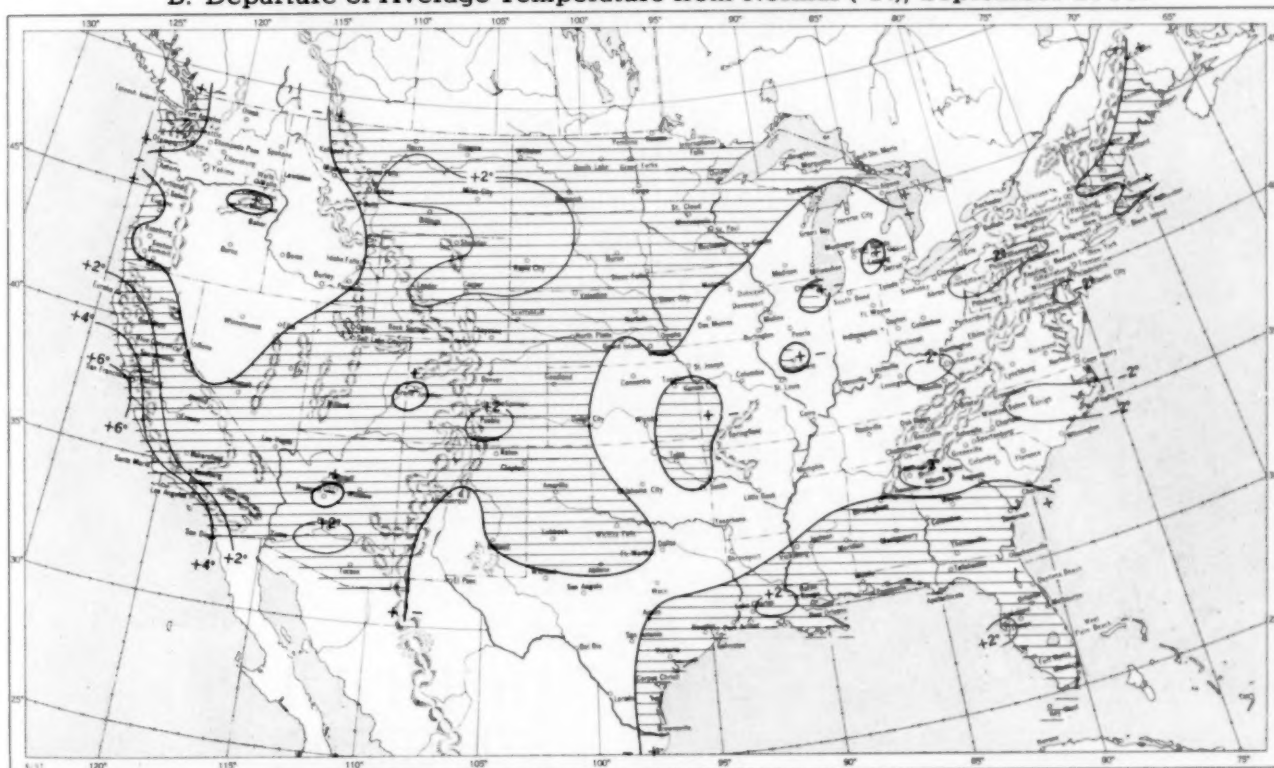

A. Based on reports from over 900 Weather Bureau and cooperative stations. The monthly average is half the sum of the monthly average maximum and monthly average minimum, which are the average of the daily maxima and daily minima, respectively.
B. Departures from normal are based on the 30-yr. normals (1921-50) for Weather Bureau stations and on means of 25 years or more (mostly 1931-55) for cooperative stations.
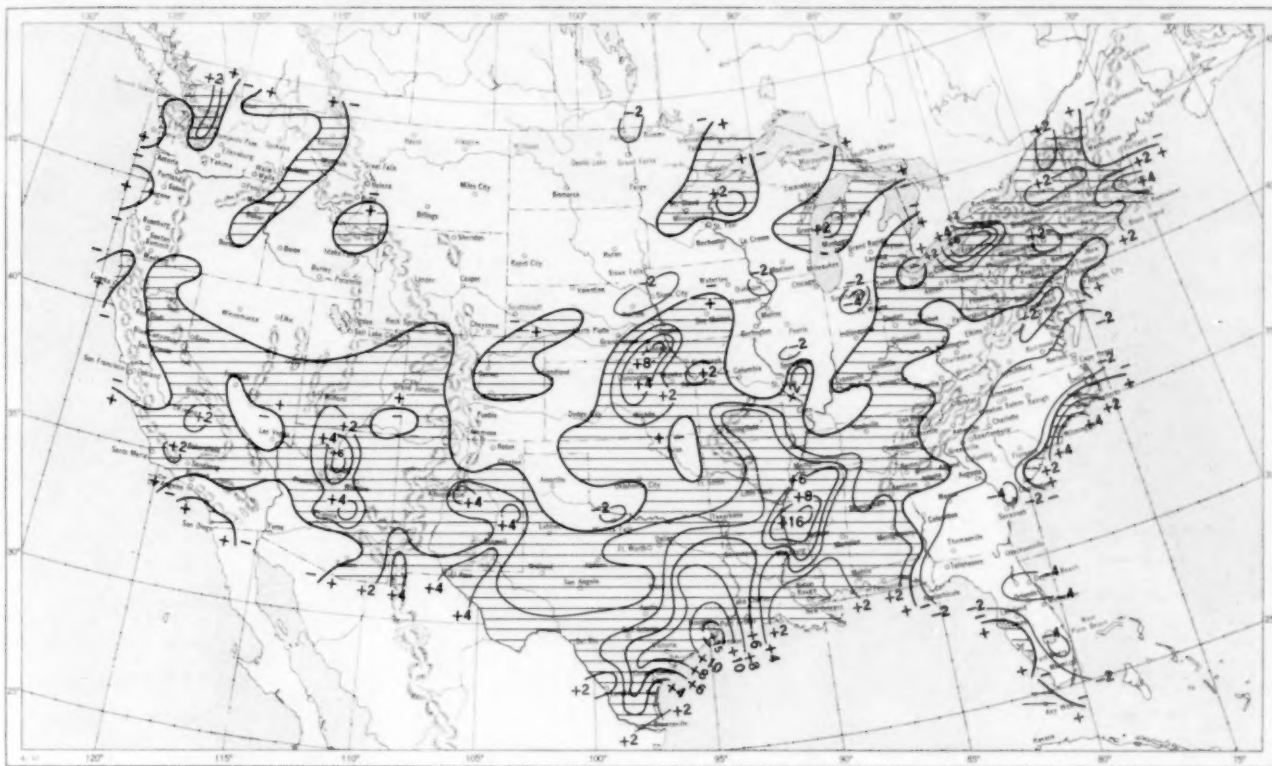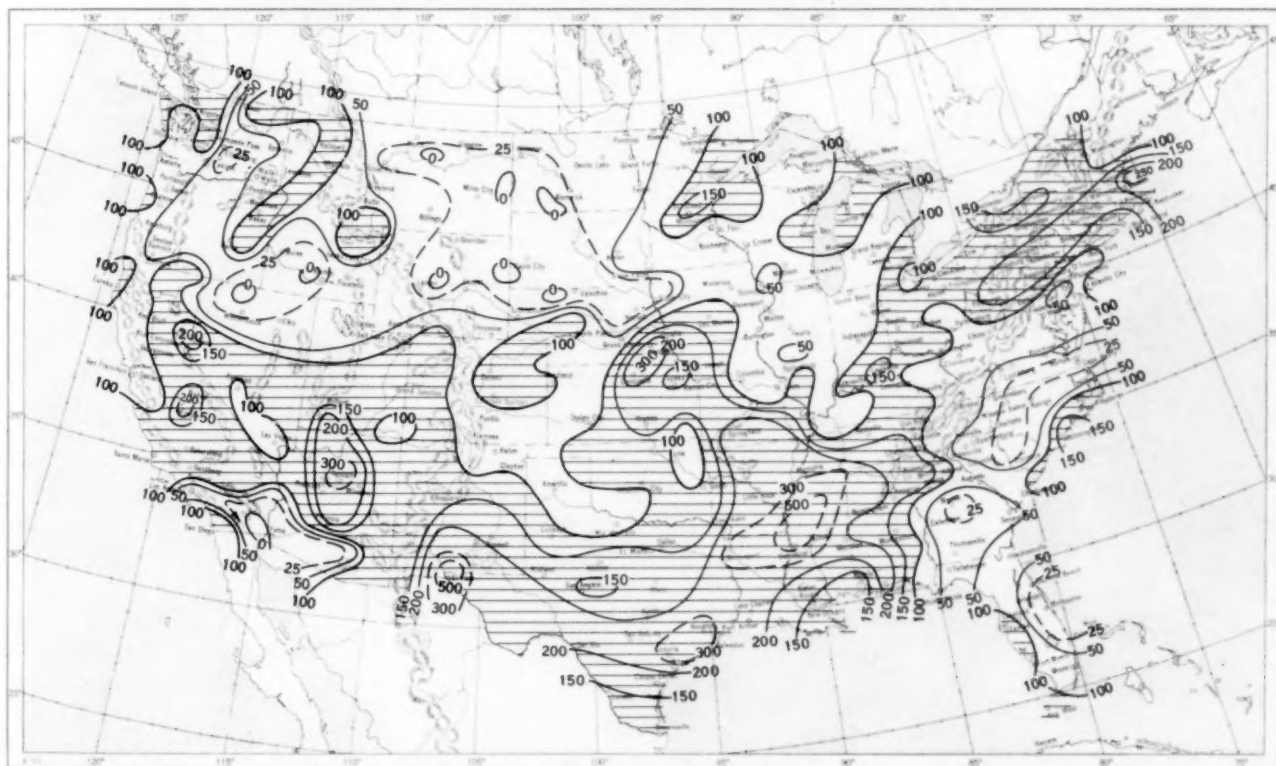
Chart II. Total Precipitation (Inches), September 1958.
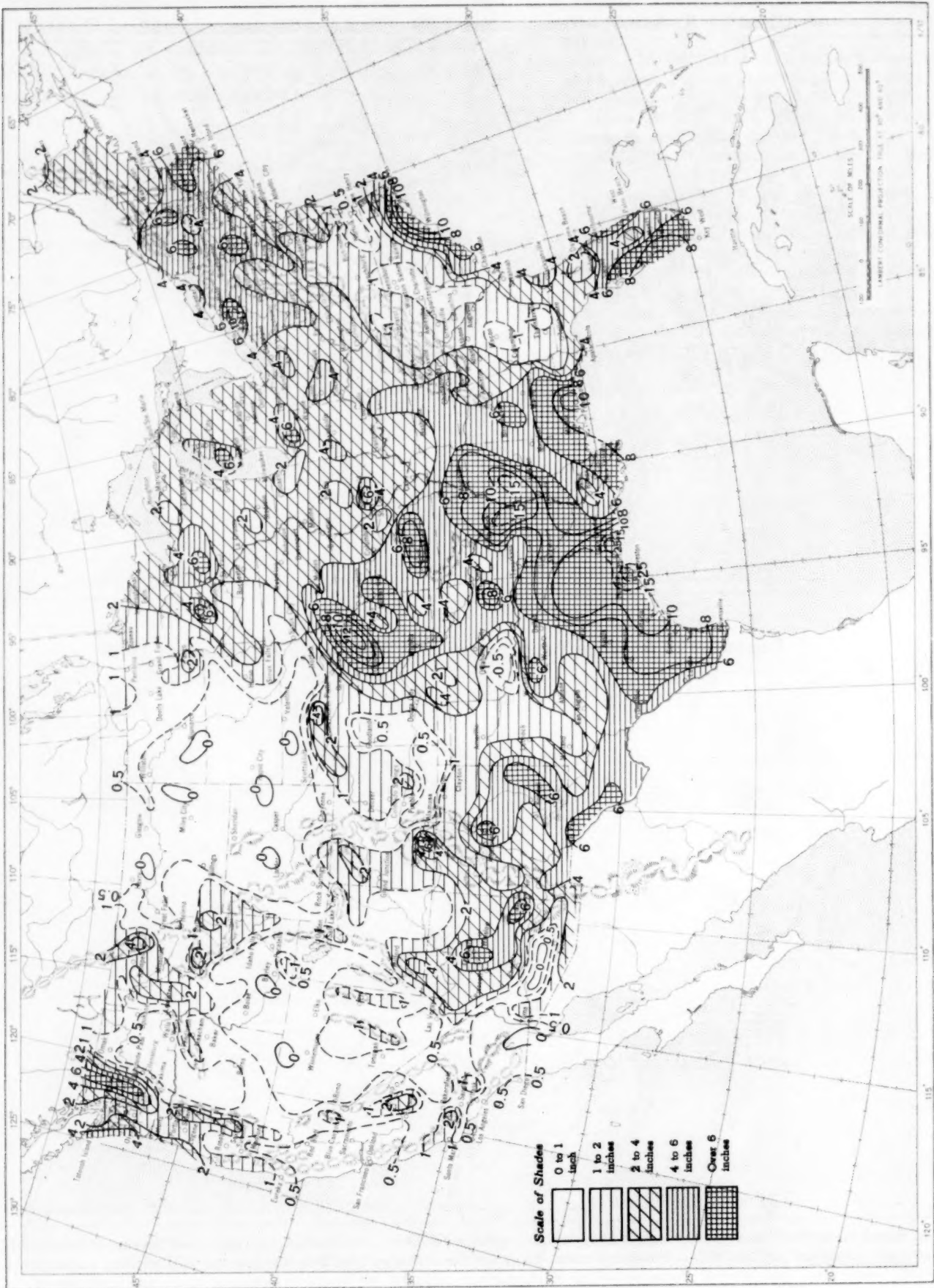
Based on daily precipitation records at about 800 Weather Bureau and cooperative stations.

Chart III.   A. Departure of Precipitation from Normal (Inches), September 1958.
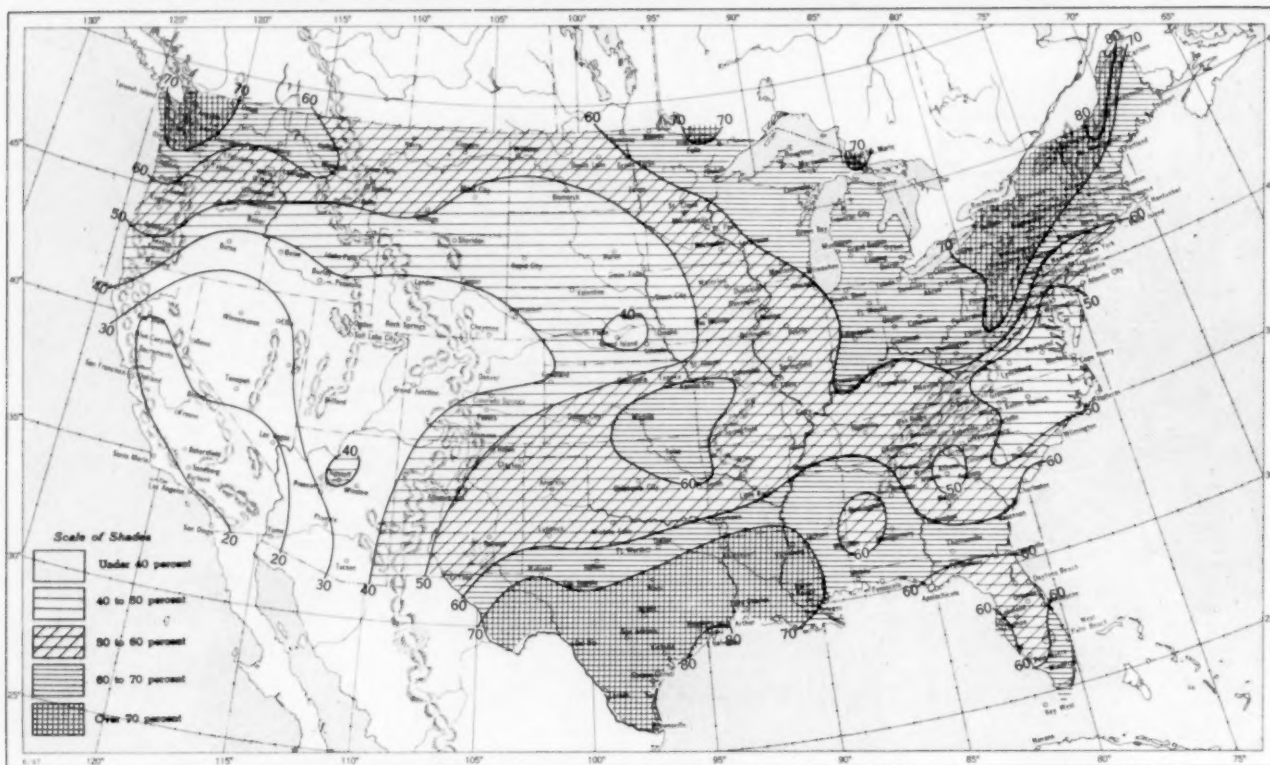

## B. Percentage of Normal Precipitation, September 1958.

Normal monthly precipitation amounts are computed from the records for 1921-50 for Weather Bureau stations and from records of 25 years or more (mostly 1931-55) for cooperative stations.

Chart VI.   A. Percentage of Sky Cover Between Sunrise and Sunset, September 1958.


B. Percentage of Normal Sky Cover Between Sunrise and Sunset, September 1958.
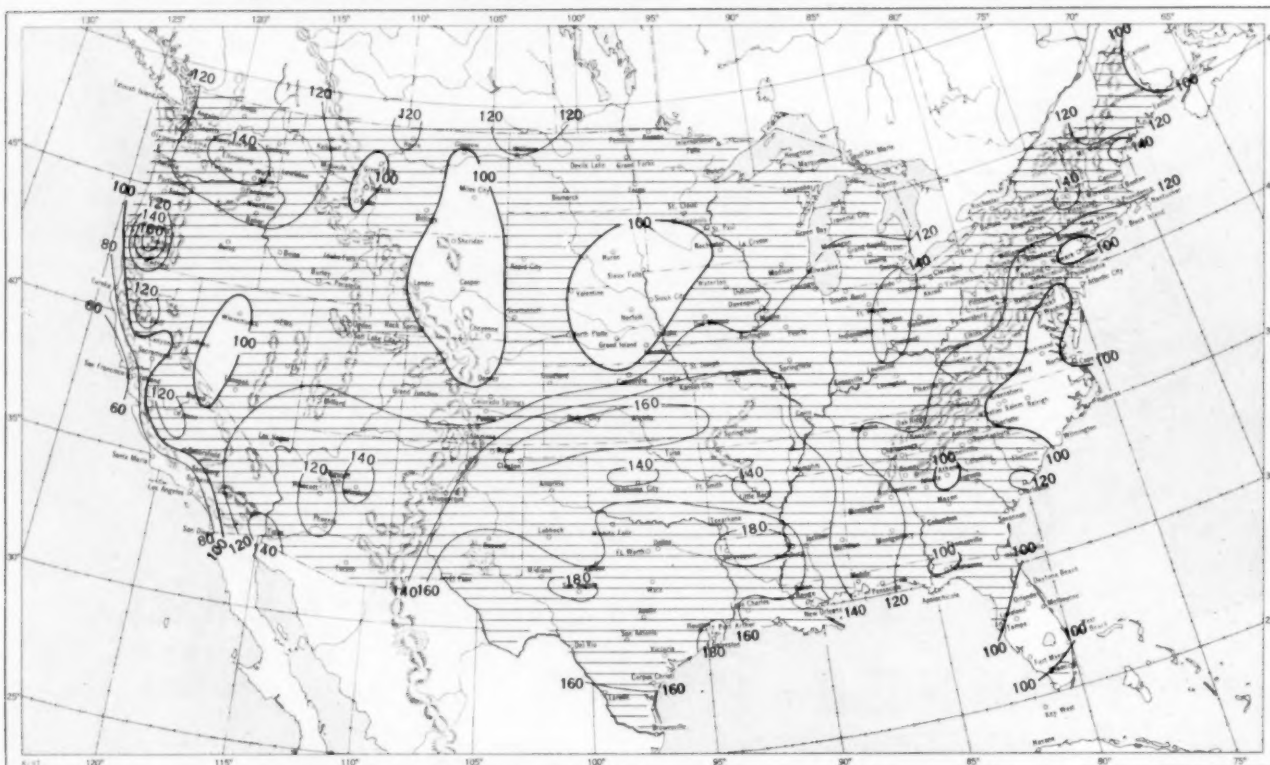

A. In addition to cloudiness, sky cover includes obscuration of the sky by fog, smoke, snow, etc.   Chart based on visual observations made hourly at Weather Bureau stations and averaged over the month.   B. Computations of normal amount of sky cover are made for stations having at least 10 years of record.

Chart VII.   A. Percentage of Possible Sunshine, September 1958.
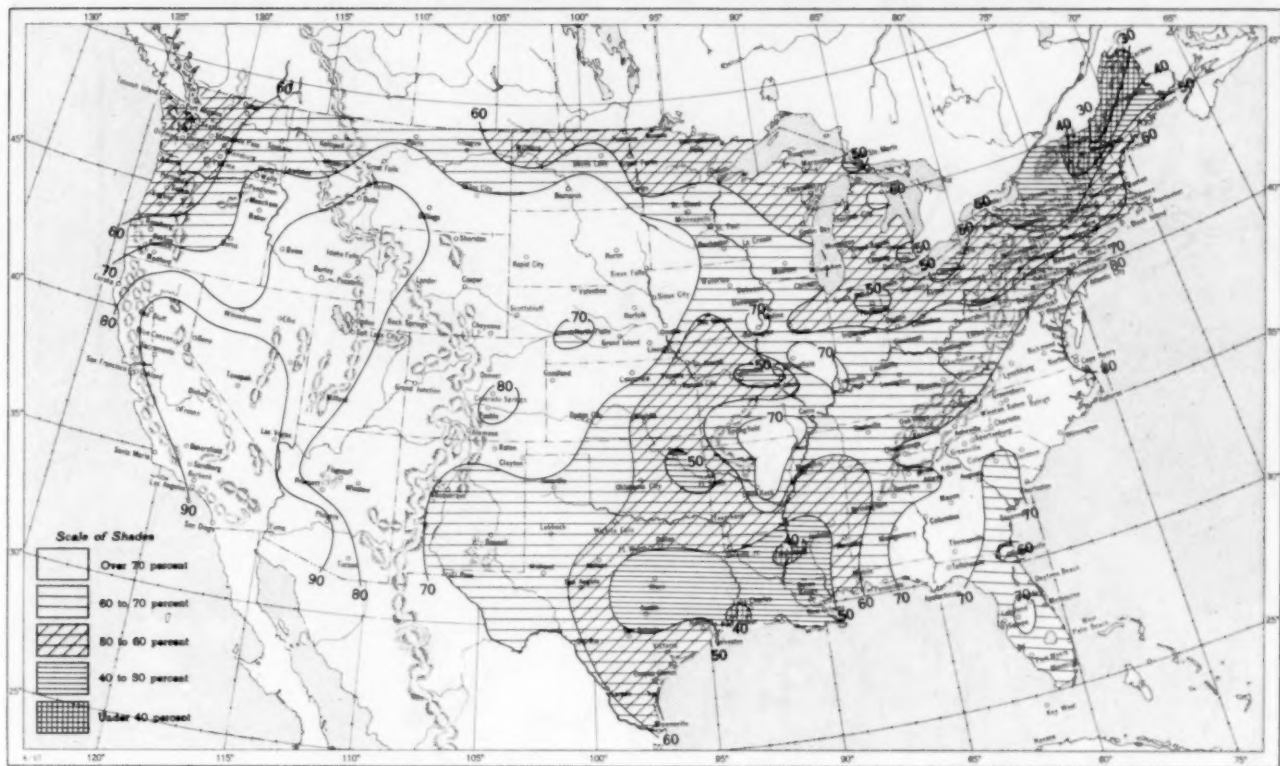
B. Percentage of Normal Sunshine, September 1958.
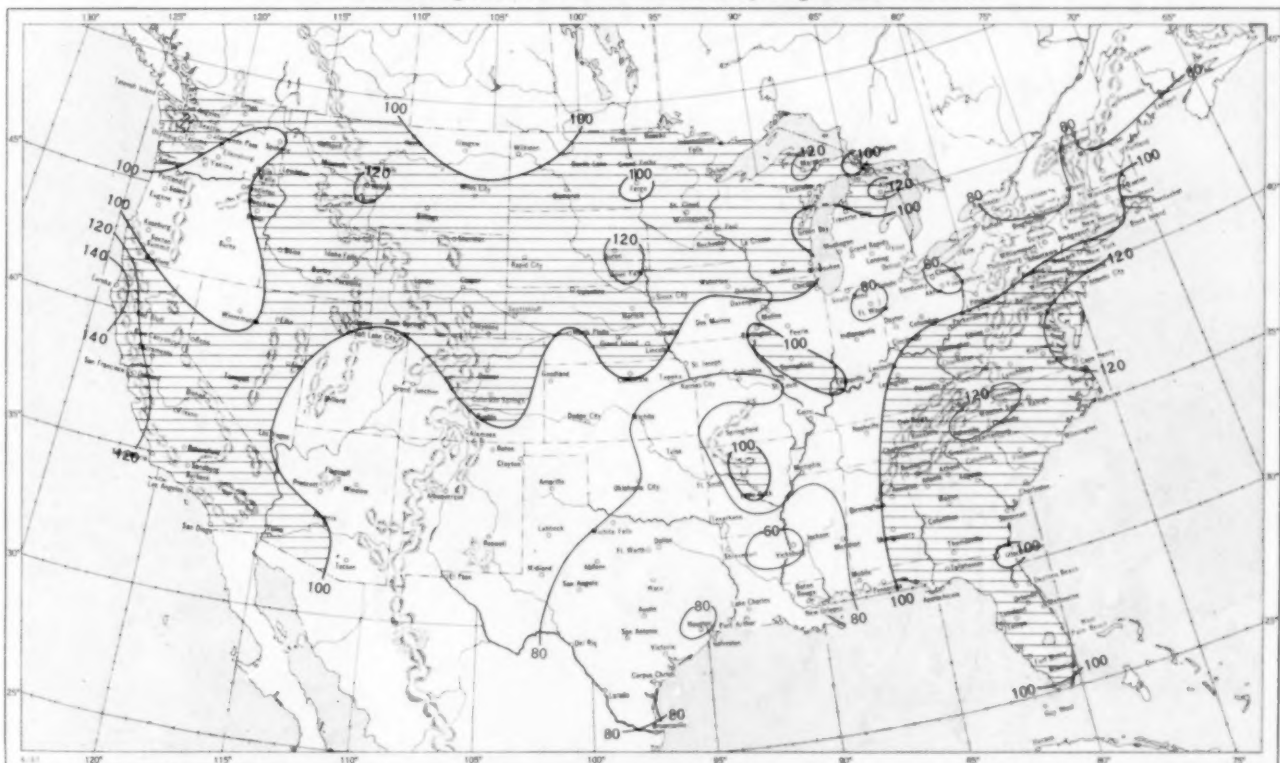
A. Computed from total number of hours of observed sunshine in relation to total number of possible hours of
sunshine during month.   B. Normals are computed for stations having at least 10 years of record.

Chart VIII. Average Daily Values of Solar Radiation, Direct + Diffuse, September 1958. Inset: Percentage of Mean
Daily Solar Radiation, September 1958. (Mean based on period 1951-55.)
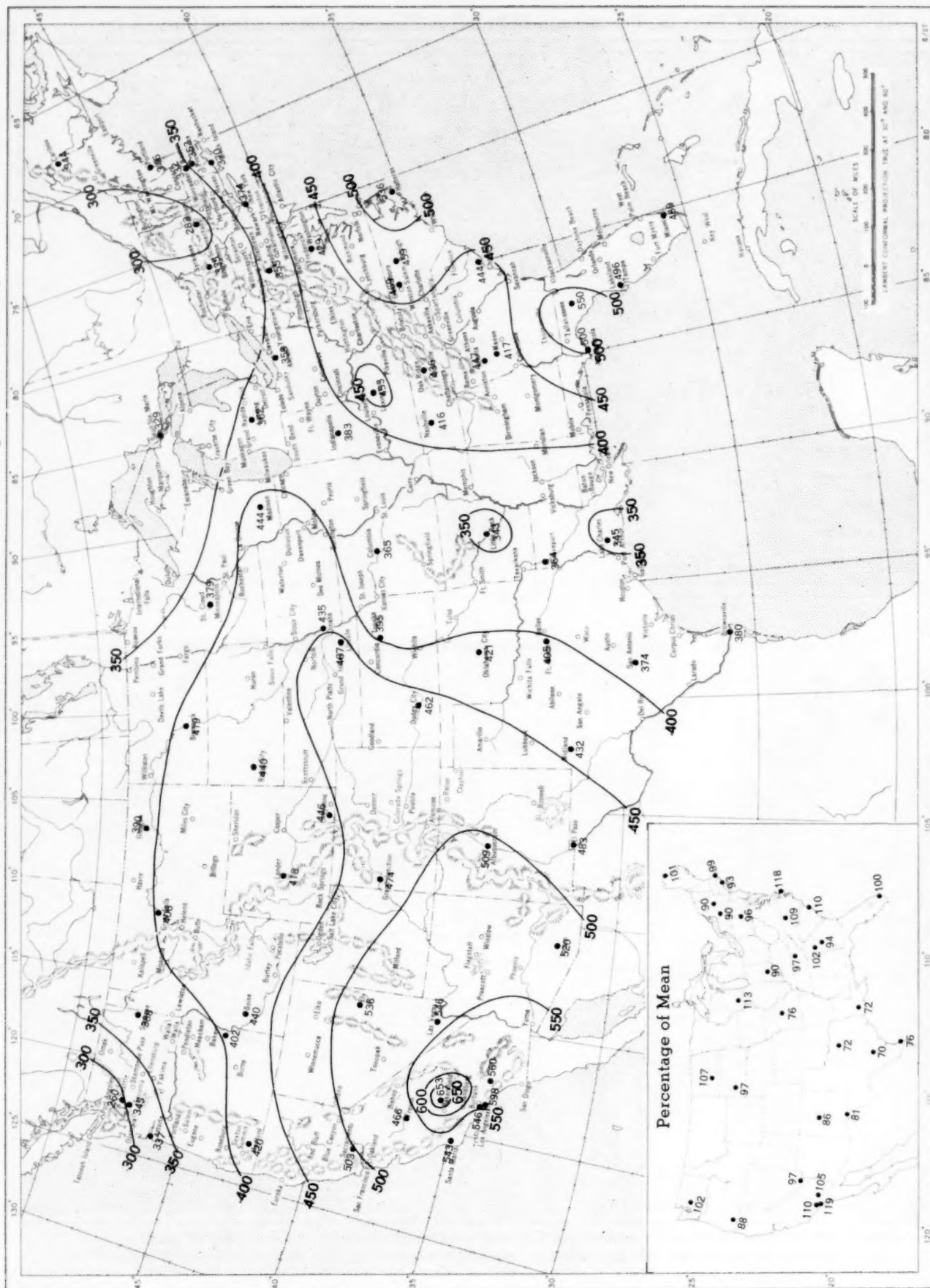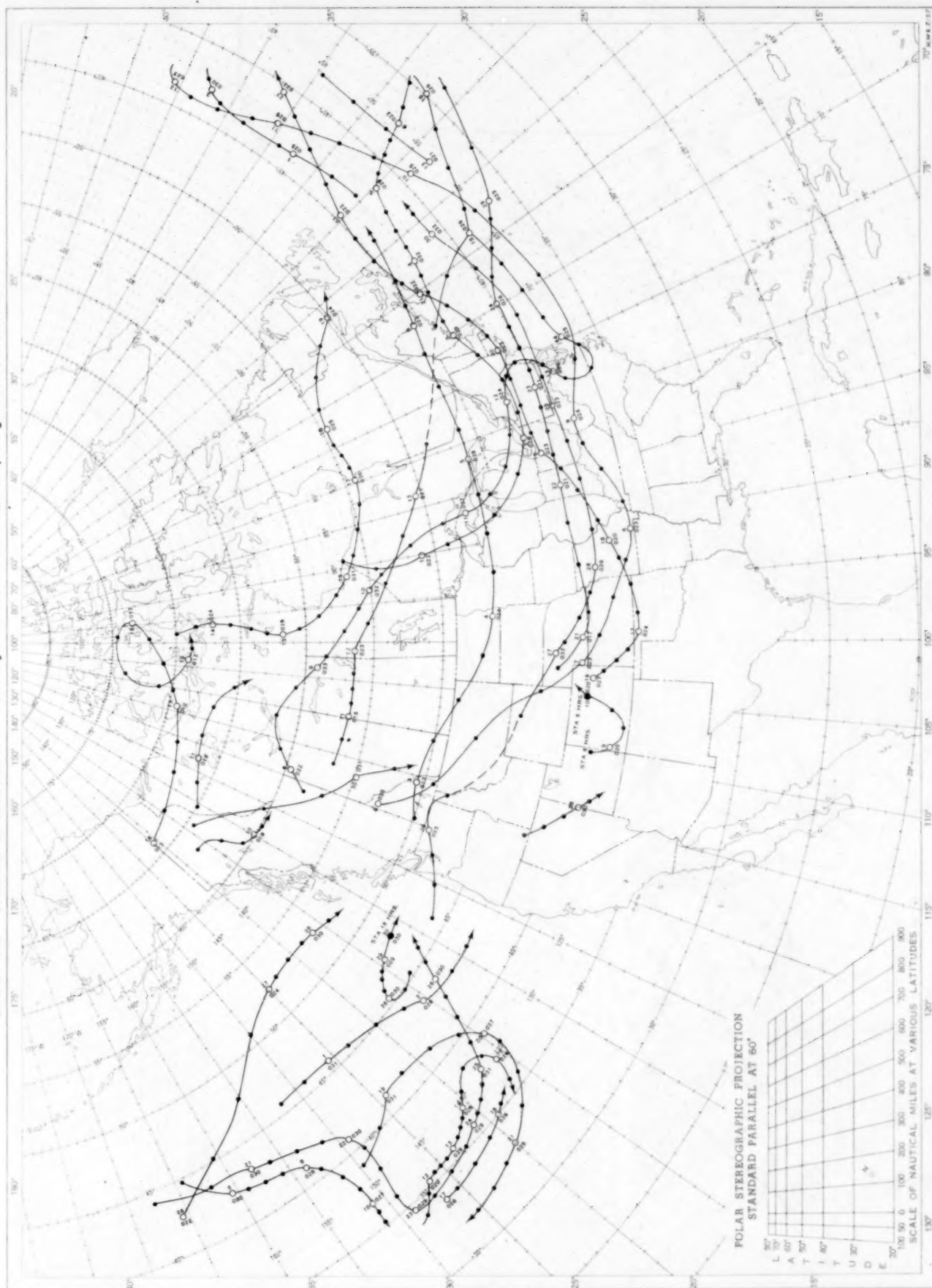

Chart shows mean daily solar radiation, direct + diffuse, received on a horizontal surface in langleys (1 langley = 1 gm. cal. cm.$^{-2}$). Basic data for isolines
are shown on chart. Further estimates are obtained from supplementary data for which limits of accuracy are wider than for those data shown.
The inset shows the percentage of the mean based on the period 1951-55.

Chart IX.   Tracks of Centers of Anticyclones at Sea Level, September 1958.

POLAR STEREOGRAPHIC PROJECTION
STANDARD PARALLEL AT 60°

SCALE OF NAUTICAL MILES AT VARIOUS LATITUDES

Circle indicates position of center at 7:00 a. m. E. S. T.   Figure above circle indicates date, figure below, pressure to nearest millibar.
Dots indicate intervening 6-hourly positions.   Squares indicate position of stationary center for period shown.   Dashed line in track
indicates reformation at new position.   Only those centers which could be identified for 24 hours or more are included.

Chart X. Tracks of Centers of Cyclones at Sea Level, September 1958.

POLAR STEREOGRAPHIC PROJECTION
STANDARD PARALLEL AT 60°

SCALE OF NAUTICAL MILES AT VARIOUS LATITUDES

Circle indicates position of center at 7:00 a. m. E. S. T.   See Chart IX for explanation of symbols.
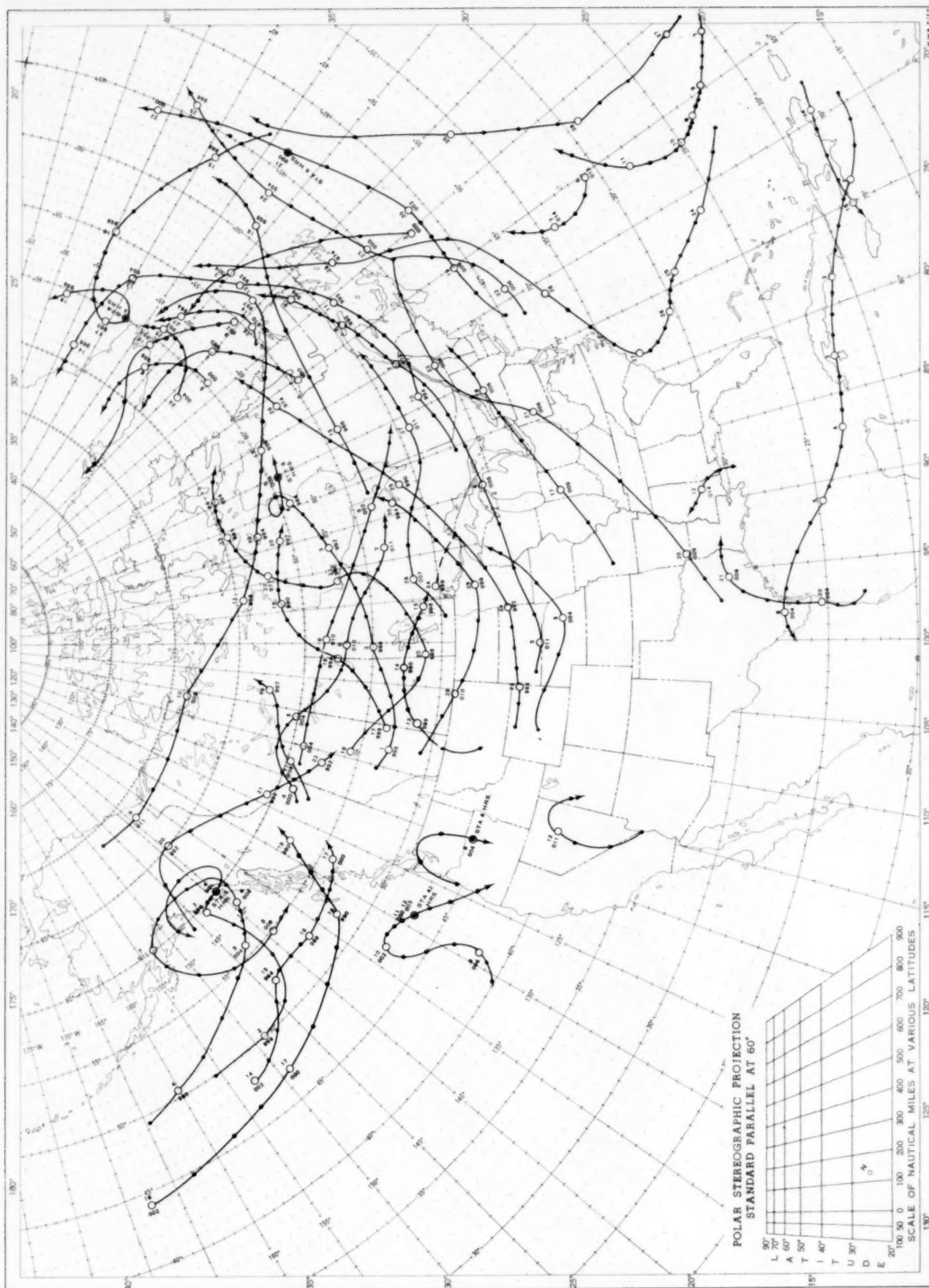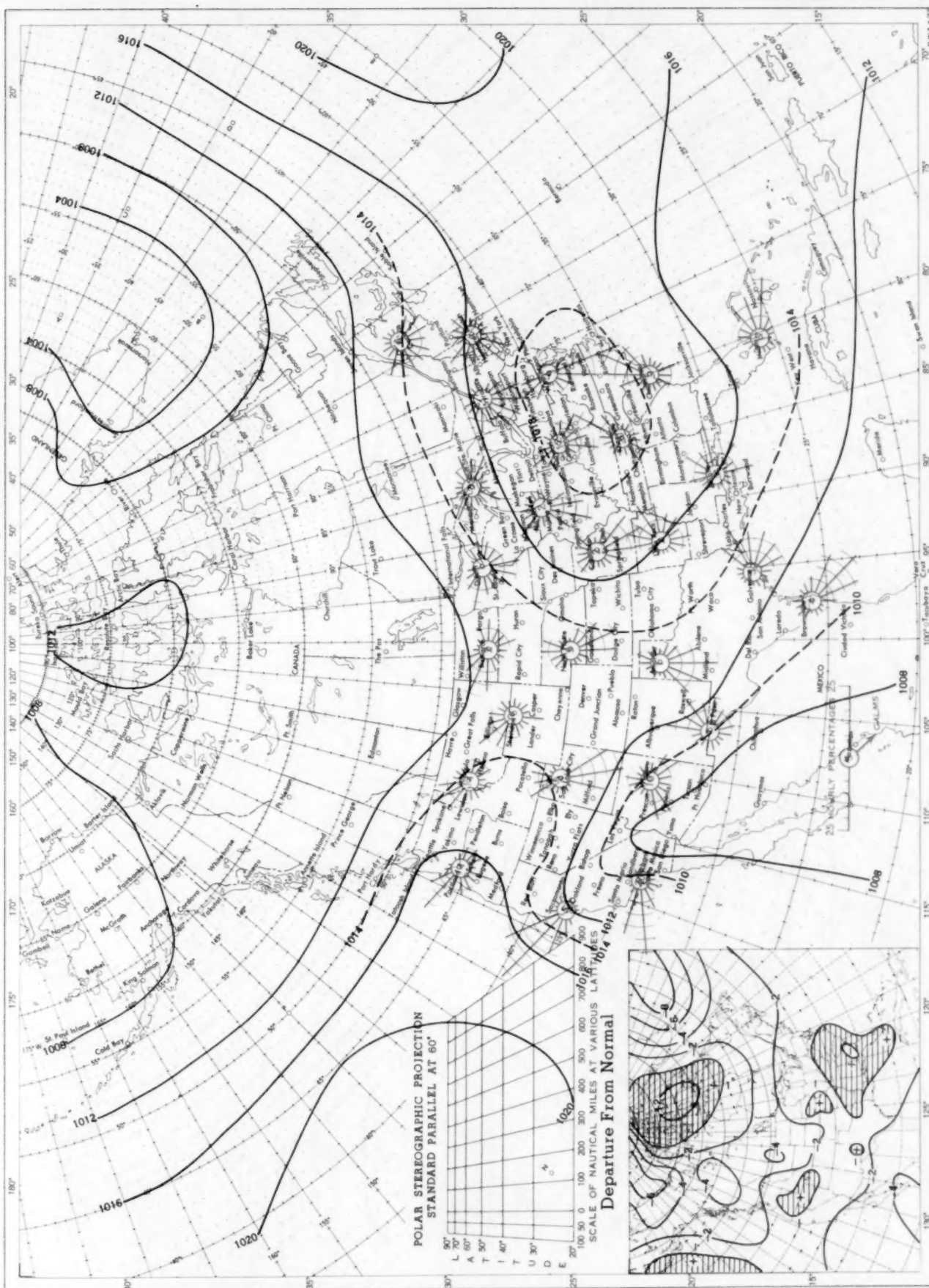
Chart XI. Average Sea Level Pressure (mb.) and Surface Windroses, September 1958. Inset: Departure of Average Pressure (mb.) from Normal, September 1958.

POLAR STEREOGRAPHIC PROJECTION
STANDARD PARALLEL AT 60°

SCALE OF NAUTICAL MILES AT VARIOUS LATITUDES

Departure From Normal

Average sea level pressures are obtained from the averages of the 7:00 a. m. and 7:00 p. m. E. S. T. readings. Windroses show percentage of time wind blew from 16 compass points or was calm during the month. Pressure normals are computed for stations having at least 10 years of record and for 10° intersections in a diamond grid based on readings from the Historical Weather Maps (1899–1939) for the 20 years of most complete data coverage prior to 1940.

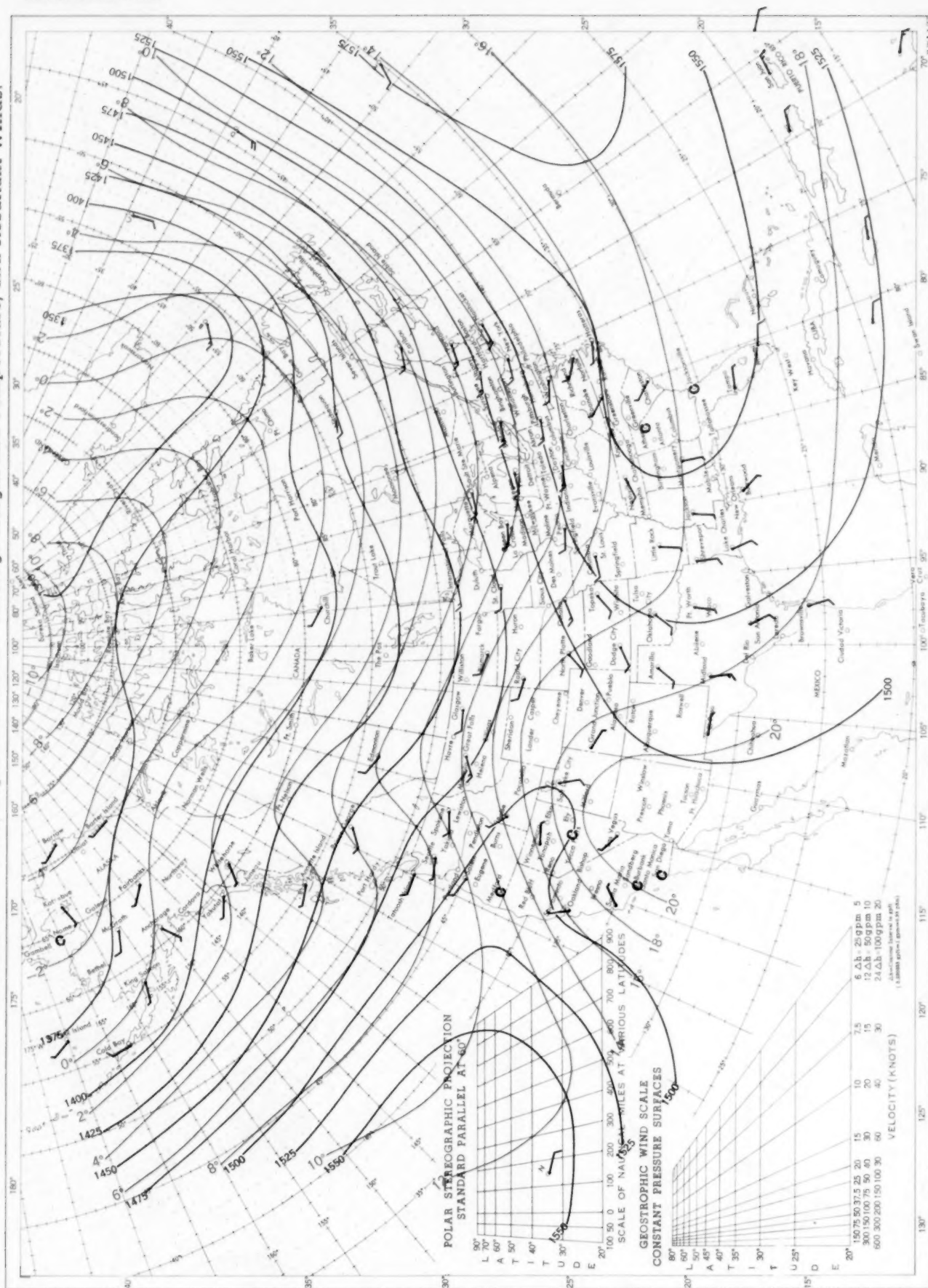Chart XII. 850-mb. Surface, 1200 GMT, September 1958. Average Height and Temperature, and Resultant Winds.

POLAR STEREOGRAPHIC PROJECTION
STANDARD PARALLEL AT 60°

SCALE OF NAUTICAL MILES AT VARIOUS LATITUDES

GEOSTROPHIC WIND SCALE
CONSTANT PRESSURE SURFACES

VELOCITY (KNOTS)

Height in geopotential meters (1 g.p.m. = 0.98 dynamic meters).   Temperature in °C.   Wind speed in knots; flag represents
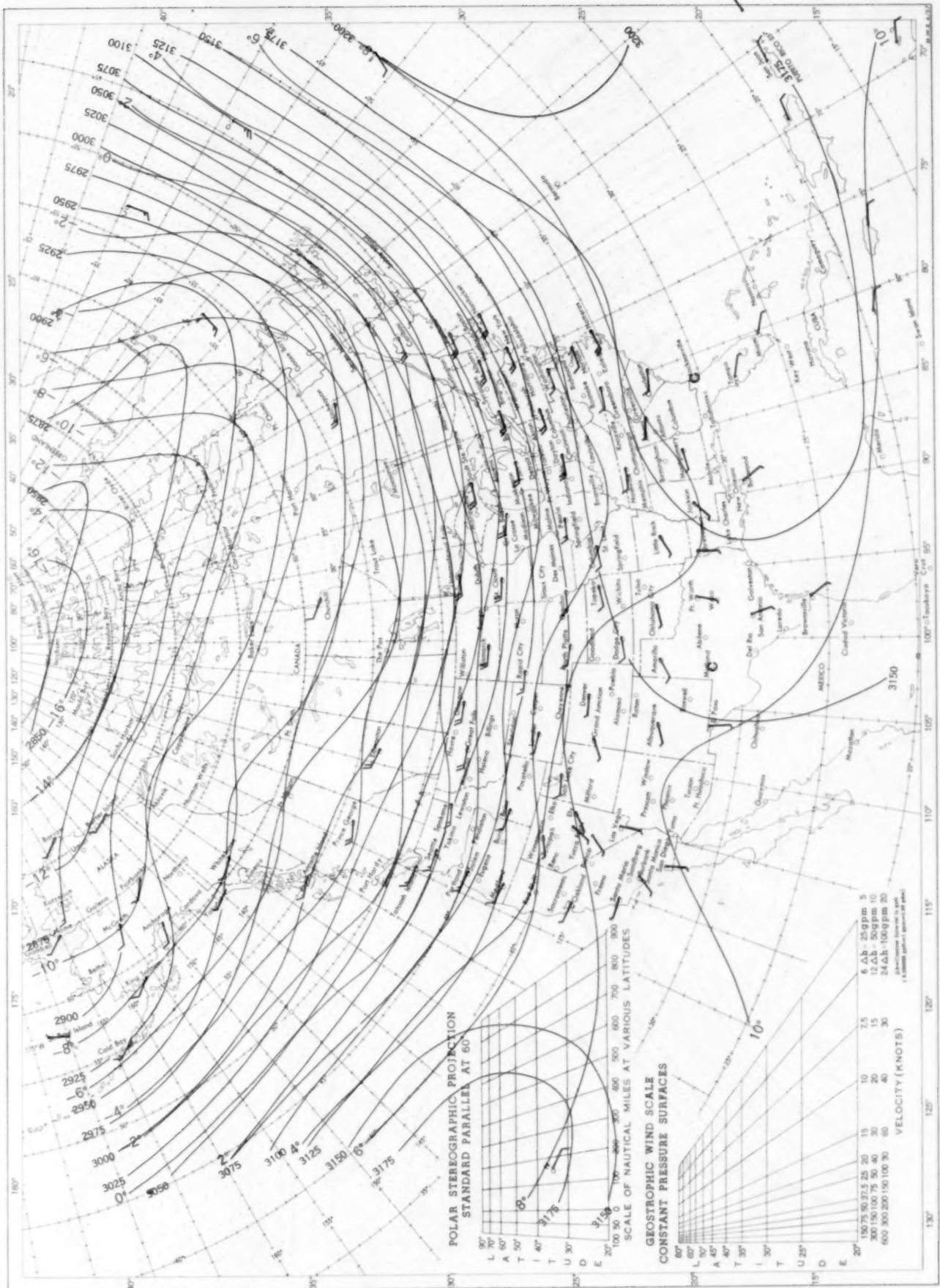50 knots, full feather 10 knots, and half feather 5 knots.   All wind data are based on rawin observations.

Chart XIII. 700-mb. Surface, 1200 GMT, September 1958. Average Height and Temperature, and Resultant Winds.

POLAR STEREOGRAPHIC PROJECTION
STANDARD PARALLEL AT 60°

SCALE OF NAUTICAL MILES AT VARIOUS LATITUDES

GEOSTROPHIC WIND SCALE
CONSTANT PRESSURE SURFACES

VELOCITY (KNOTS)

See Chart XII for explanation of map.

Chart XIV. 500-mb. Surface, 1200 GMT, September 1958. Average Height and Temperature, and Resultant Winds.

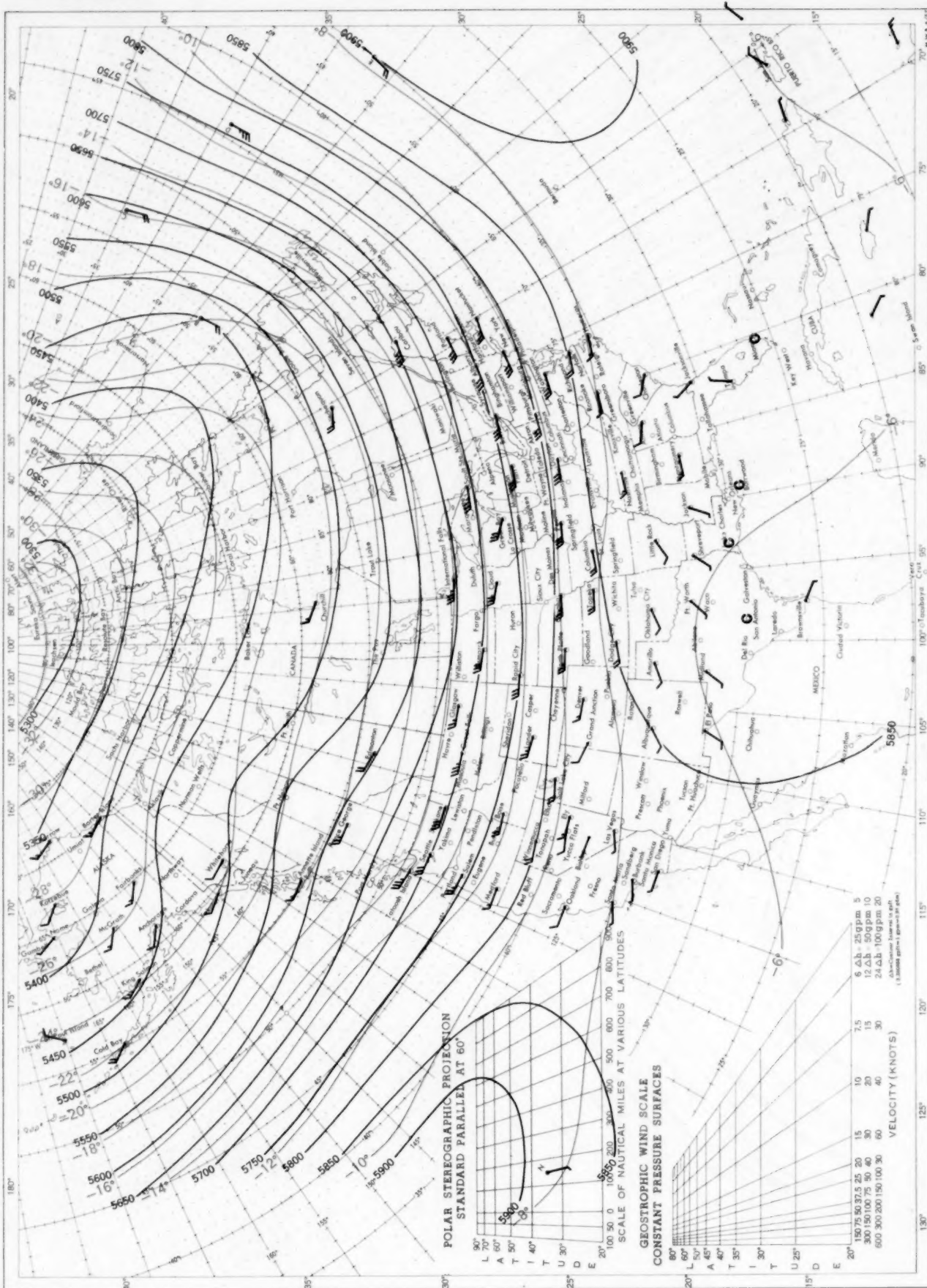POLAR STEREOGRAPHIC PROJECTION
STANDARD PARALLEL AT 60°

SCALE OF NAUTICAL MILES AT VARIOUS LATITUDES

GEOSTROPHIC WIND SCALE
CONSTANT PRESSURE SURFACES

VELOCITY (KNOTS)

See Chart XII for explanation of map.

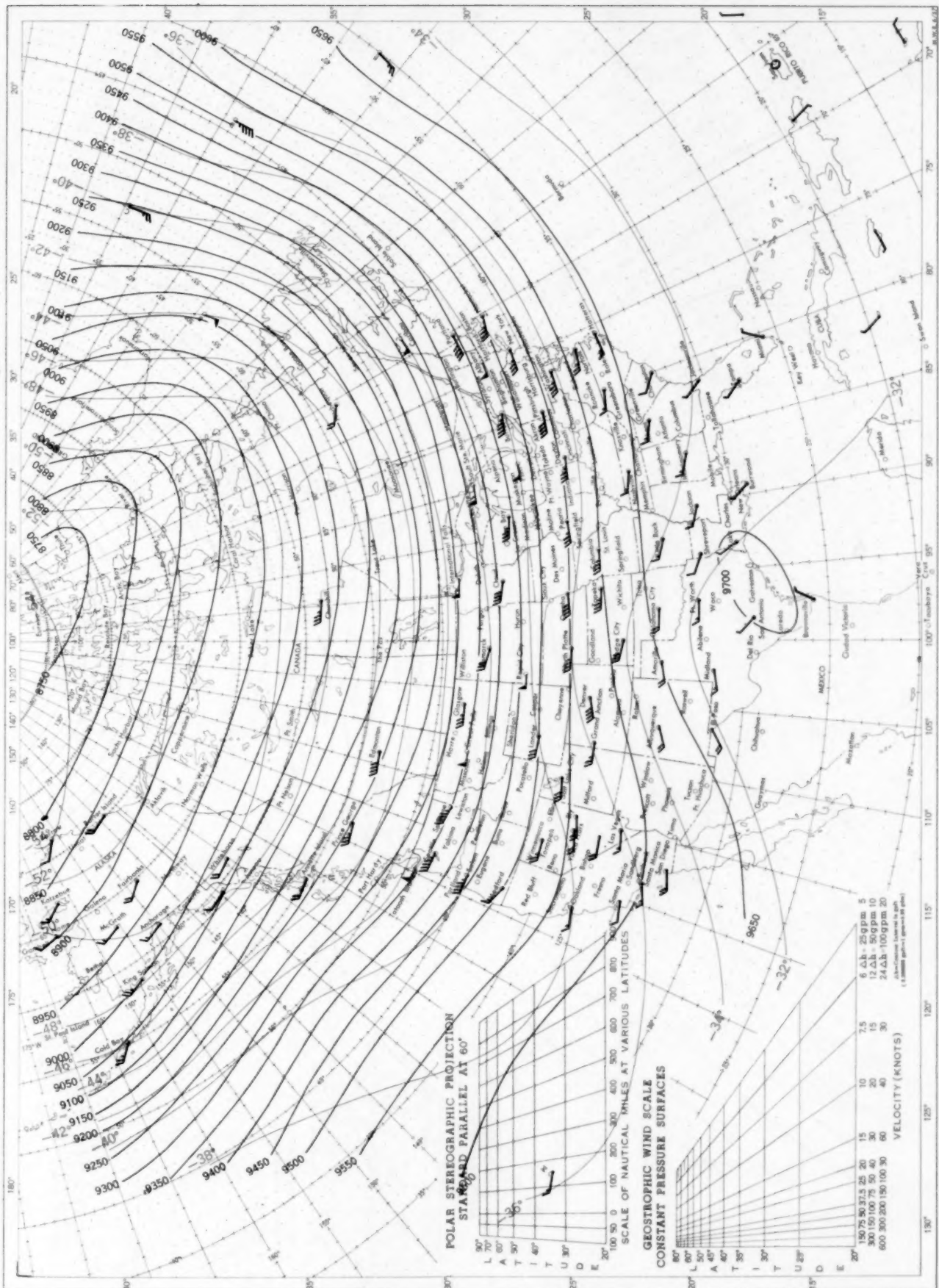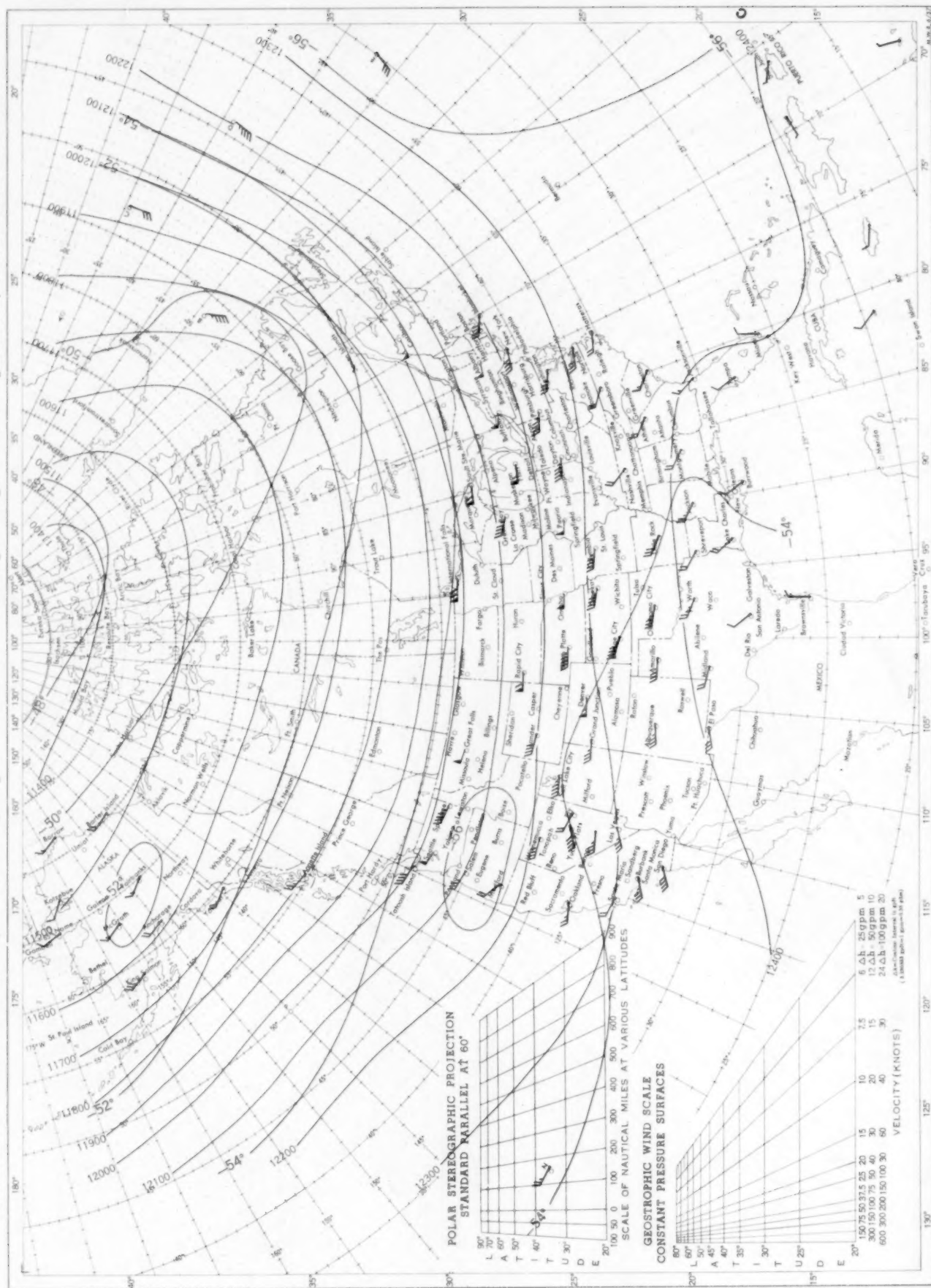Chart XV.   300-mb. Surface, 1200 GMT, September 1958.   Average Height and Temperature, and Resultant Winds.
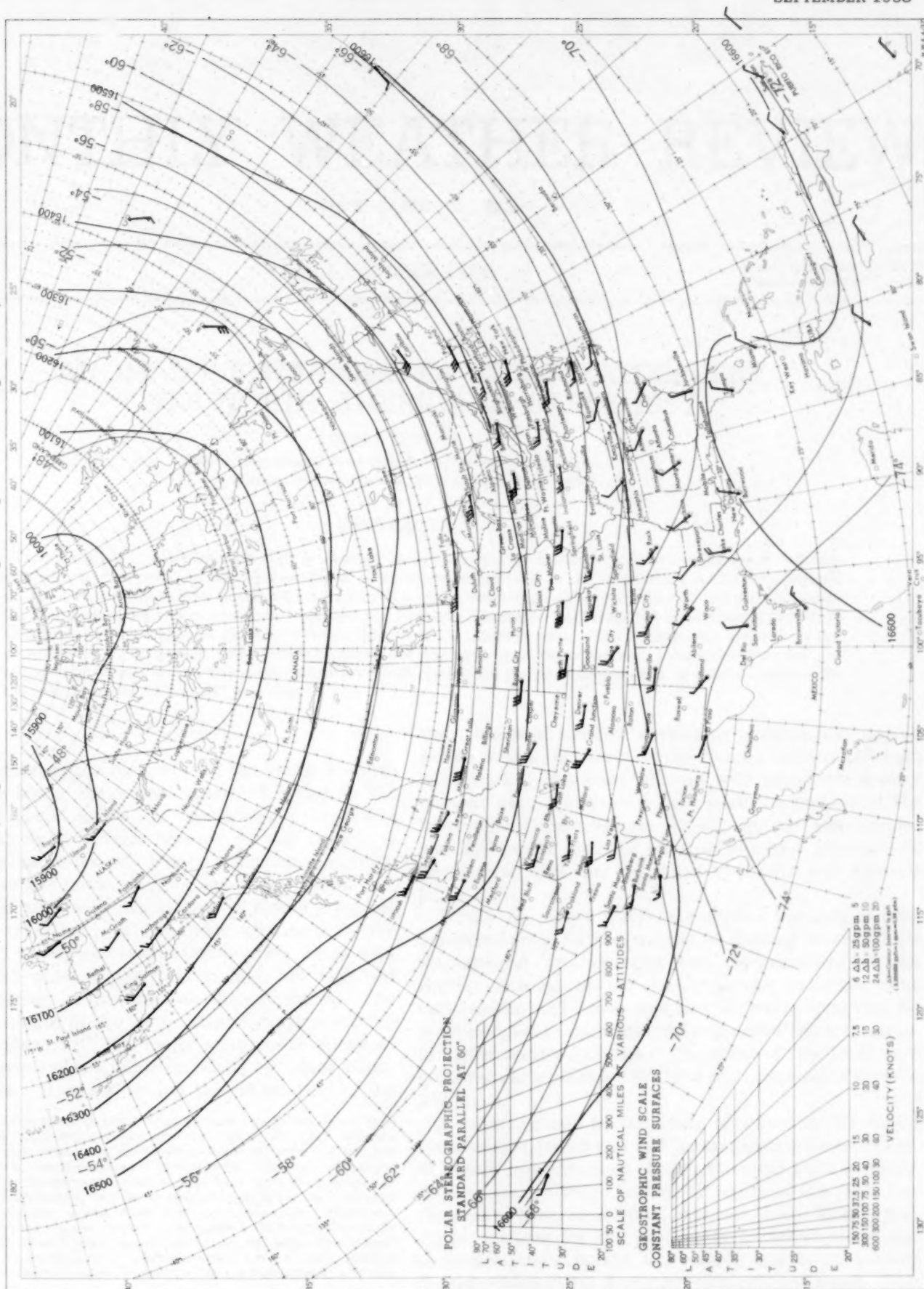

See Chart XII for explanation of map.

Chart XVI. 200-mb. Surface, 1200 GMT, September 1958. Average Height and Temperature, and Resultant Winds.

POLAR STEREOGRAPHIC PROJECTION
STANDARD PARALLEL AT 60°

SCALE OF NAUTICAL MILES AT VARIOUS LATITUDES

GEOSTROPHIC WIND SCALE
CONSTANT PRESSURE SURFACES

VELOCITY (KNOTS)

See Chart XII for explanation of map.

Chart XVII.   100-mb. Surface, 1200 GMT, September 1958.   Average Height and Temperature, and Resultant Winds.

See Chart XII for explanation of map.